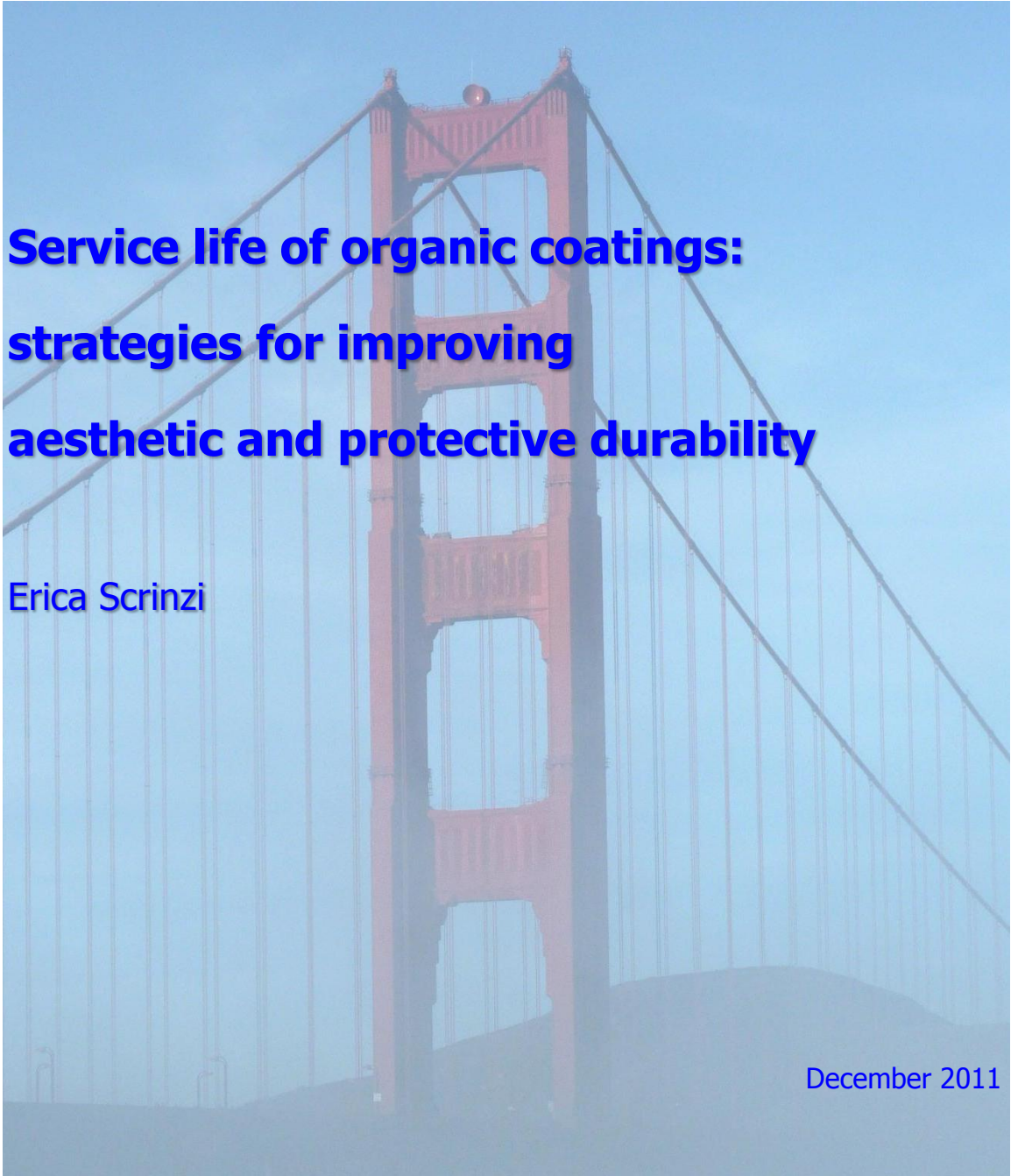




UNIVERSITY
OF TRENTO - Italy

Department of Materials Engineering
and Industrial Technologies

Doctoral School in Materials Science and Engineering – XXIV cycle

A photograph of the Golden Gate Bridge in San Francisco, California, viewed from a low angle looking up at one of the towers. The bridge is partially obscured by a semi-transparent blue overlay.

**Service life of organic coatings:
strategies for improving
aesthetic and protective durability**

Erica Scrinzi

December 2011

A zio Tomaso

Preface

This doctoral dissertation summarizes the research activity carried out during my Ph.D. studies in Science and Materials Engineering, at the University of Trento.

The thesis was structured into two sections. The first part of the investigation was performed in collaboration with industrial partners. In particular, the research activity focused on polyester powder coatings for architectural applications was developed in collaboration with Akzo Nobel Coatings S.p.A. (Romano d'Ezzelino, VI, Italy). The activity about the clear-coats for automotive applications was performed in collaboration with PPG Industries, Research Center (Allison Park, PA, U.S.).

The second part of the research activity was developed at the Coatings Research Institute, Eastern Michigan University (Ypsilanti, MI, U.S.) under the supervision of Prof. Jamil Baghdachi, and then completed at the University of Trento.

Acknowledgements

Firstly, I would like to thank my parents and Bernardo for their support, help and love.

I express my gratitude to my advisors, Flavio Deflorian and Stefano Rossi, for their support during my Ph.D. studies.

I gratefully acknowledge Akzo Nobel Coatings (Romano d'Ezzelino, VI) for the collaboration on architectural powder coatings, and in particular Dr. Roberto Paganica, for the useful and stimulating discussions.

I would also acknowledge PPG Industries (Research Center, Allison Park, PA) for the collaboration on automotive clear-coats, and especially Dr. Peter Kamarchik for the fruitful discussions.

Many thanks to Prof. Jamil Baghdachi (Eastern Michigan University) for the very constructive collaboration on advanced polyurethane coatings, and Prof. Vijay Mannari (Eastern Michigan University) for his suggestions on polyurethane coatings formulation.

I would also like to thank Prof. Graziano Guella, Prof. Luca Fambri, Prof. Claudio Migliaresi (University of Trento), Dr. Quynh-Huong Duong and Dr. Fanny Carlà (CSM Instruments, Peseux, Switzerland) for their collaboration.

Many thanks to Senthilkumar, Emma, Krishna and Sandy for the great time I spent in Michigan, for their help and friendship.

I gratefully acknowledge Luca Benedetti for his precious support in the Corrosion Control Laboratory.

Finally, many thanks to my friends and colleagues Caterina, Michele, Veronica, Dario, Sujie and Luiz for their friendship, help, and support.

Table of contents

Preface	i
Acknowledgements	iii
Table of contents	v
1. Introduction	1
1.1. References	9
2. Organic coatings for architectural applications: response to weathering stresses	10
2.1. Introduction	12
2.1.1. Weathering resistance	16
2.1.2. Corrosion issues	21
2.1.3. Surface pre-treatments	24
2.2. Materials and experimental procedures	25
2.3. Results and discussion	36
2.4. Conclusions	58
2.5. References	61
3. Clear coats for automotive applications: response to mar damage	65
3.1. Introduction	66
3.2. Methods of mar resistance assessment	74
3.3. Materials and experimental procedures	84
3.4. Results and discussion	90
3.4.1. Mar behaviour characterisation	90

3.4.2.	Analysis of the recovery properties	111
3.4.3.	Effects of UV weathering on mar resistance	121
3.5.	Conclusions	127
3.6.	References	129
4.	Protective properties of advanced polyurethane coatings	134
4.1.	Introduction	135
4.2.	Supramolecular polymers based on multiple hydrogen bonding	144
4.2.1.	2-Ureidopyrimidin-4-one (UPy) dimer	146
4.2.2.	UPy applications	148
4.2.3.	UPy introduction in crosslinked coatings	150
4.2.4.	Synthesis of UPy unit	153
4.3.	Materials and experimental procedures	154
4.4.	Results and discussion	162
4.5.	Conclusions	173
4.6.	References	175
5.	Concluding remarks and future work	181

CHAPTER 1

Introduction and overview

It is probably needless to mention that organic coatings are of paramount importance nowadays. Although the huge number of applications and their wide spread can suggest that organic coatings have now reached a level of maturity, they are still mysterious from a certain point of view [1]. The behaviour of these systems is not completely understood yet, especially as regarding the relationships between the chemical formulation and the manufacturing/applications technologies on one side, and the final properties on the other side. In this scenario, durability is regarded the most crucial point and finding satisfying design solutions is not straightforward.

Durability involves many factors simultaneously, concerning material properties, application, service environment and manufacturing (Fig. 1.1). It should be pointed out that durability must be intended in the most general meaning. Organic coatings must always ensure a mix of properties which are mainly related to the decorative and protective ambits [2, 3]. Accordingly, durability must be referred both to the aesthetic and protective properties. The decorative function relates to the appearance of the coating layer itself. It covers many features such as specular gloss and diffuse reflection, colour and texture, and more in

general all the aspects regarding the human perception. On the other hand, the protective function is in close interplay with the substrate, the barrier properties of the coating, and the interactions coating/substrate.

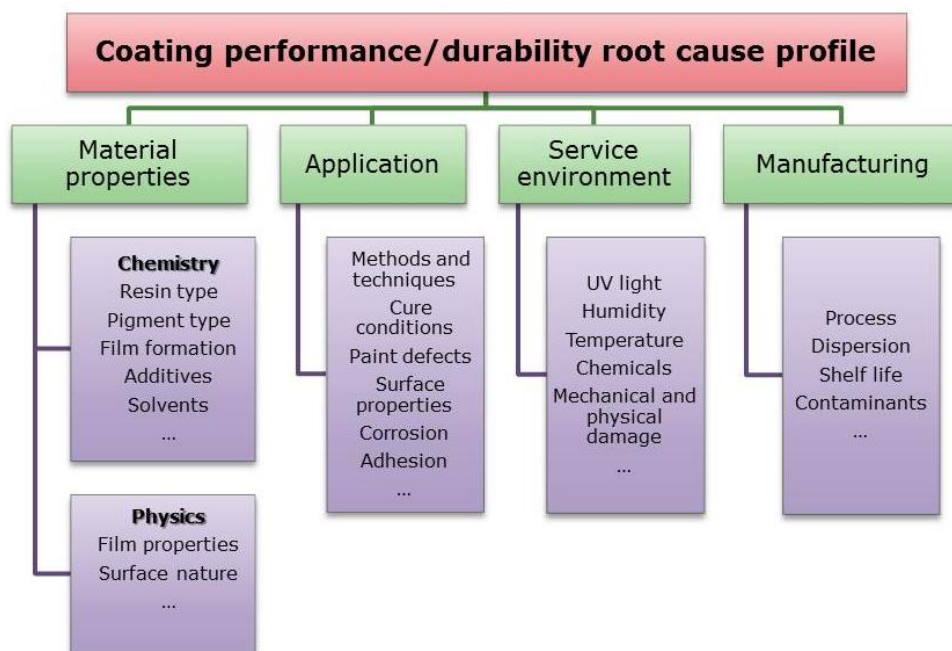


Figure 1.1 Main factors affecting the durability of organic coatings.

The substrate has to be sealed off from the environmental stresses such as light, humidity, chemicals, mechanical abrasion and the like. It should be noted that the aesthetic durability and protection one may gain different importance levels. Therefore, depending on the final application, the durability optimization have to be properly carried out.

Automotive and architecture are perhaps two of the most challenging areas where the durability is claimed at overcoming hurdles and satisfying increasing expectations. New strategies for facing the durability open issues are required. It should be remember that the development of novel strategies has to take into account also new driving factors, such as market demands, cost effectiveness, and environment concerning issues.

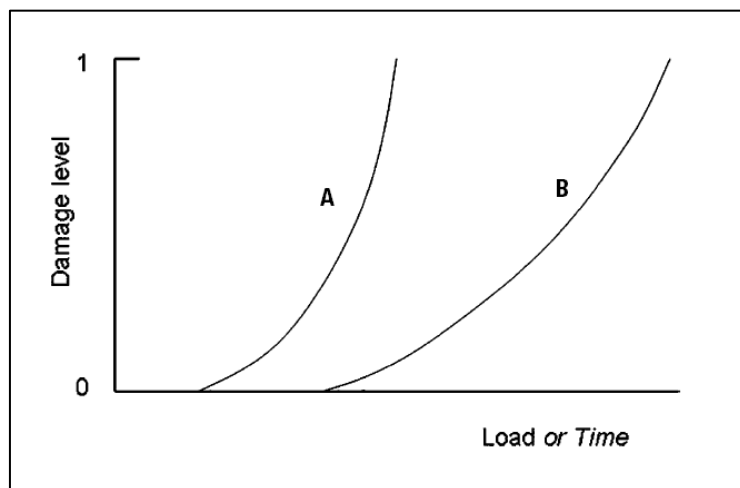


Figure 1.2 *Damage prevention concept (adapted from [4]). The curve for the reference material (A) represents the damage behaviour for the material exposed to a continuously increasing load or as a function of time for a constant load. At a certain load or time the first damage occurs but it does not lead to catastrophic failure. Beyond this point, the damage increases continuously, until the catastrophic failure occurs (damage level = 1) The damage curve for the improved material (B) shows both an improvement in the point of onset of damage as well as in the rate of damage formation.*

Traditional *damage prevention* concept still remains a very useful and effective design strategy and will play a crucial role in the development

of new materials in the future [4]. However, it may be not sufficient in those cases where durability open issues are particularly severe. *Damage prevention* concept, in fact, aims at delaying the loss of functional properties and extending the service life (Fig. 1.2). In any case, the formation of damage during service conditions can never be excluded and periodic inspection to monitor the damage development into the coating is needed, thus calling for actions and costs, sooner or later.

The above mentioned limit may be overcome by adopting a new design strategy where damage is not perceived as problematic if it is counteracted by subsequent self-repairing processes. This approach also known as *damage management* [4] aims at extending the life time by introducing self-healing capabilities in the organic coating (Fig. 1.3). From this point of view, if the organic coating is properly developed, even infinite lifetime can be ideally gained. Nowadays, the efforts are mainly spent in the determination of those formulations providing the best self-repairing capabilities. By contrast, the relationships between the formulation characteristics and durability in this new class of organic coatings are not completely assessed yet. The knowledge of these relationships is of paramount importance, especially as regards to the corrosion protection issues, being these ones usually related to the structures safety ambit.

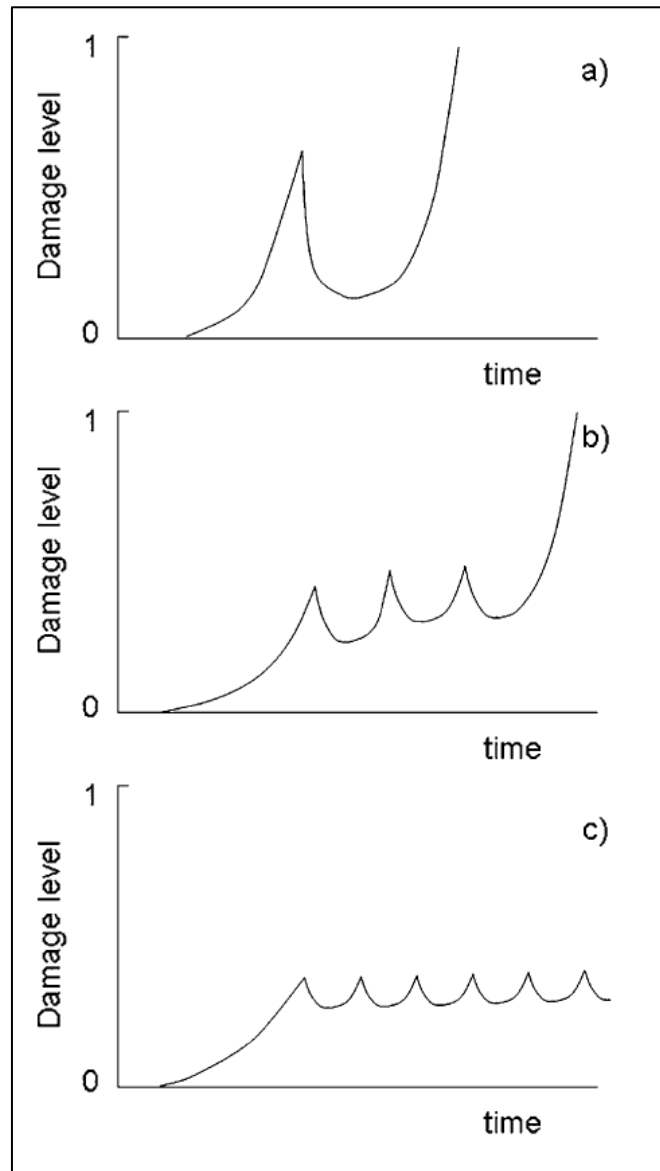


Figure 1.3 *Damage management concept [4]. In the material represented in curve (a) a single healing action takes place repairing the damage almost completely. The material shown in (b) is capable of showing multiple healing effects for some healing cycles. The material represented in (c) shows an ideal self-healing behaviour: the damage is removed many times and no damage accumulation to the failure threshold occurs.*

The present dissertation is aimed at contributing for filling the above mentioned gaps. The thesis is consequently structured into two parts. The wide spread and the importance of organic coatings in architecture and automotive industry addressed the first part of this research mainly onto these two fields. In these frameworks, novel strategies for attaining high performance organic coatings are explored. In order to validate the proposed strategies, the research has been carried out in collaboration with industrial partners operating in these areas, thus making it possible to produce and test real organic coatings. The second part of the investigation was specifically devoted to study the behaviour of self-repairing organic coatings from the corrosion protection point of view.

Organic coatings durability used in architectural applications is faced in the first part (Ch. 2). In this field, degradation phenomena concern both the aesthetic properties and corrosion protection in metallic structures, and are mainly related to the weathering stresses. Nowadays, whereas the aesthetic properties durability is ensured by a proper chemical formulation of the coating, the corrosion protection of the substrate is obtained by performing suitable surface pre-treatments. Paint manufacturers usually optimize their painting products considering the most effective substrate conditions, whereas those who focus the attention on corrosion protection do not always consider the aesthetic durability as important for organic coatings and point out the development of proper surface pre-treatments. In any case high

performance/durability of both the properties is never assured, except in the case of recourse to no environmentally friendly and expensive pre-treatments. It is apparent that this gap should be bridged in order to achieve enhanced performances of the overall systems. The investigation, carried out in collaboration with Akzo Nobel Coatings, concerned polyester powder coatings with different pigments applied onto pre-treated and untreated aluminium substrates. A proper experimental campaign was carried out for investigating the decrease of aesthetic attributes during artificial weathering tests, and the reduction in the protective properties, via electrochemical techniques and standard corrosion tests.

The issues inherent the organic coatings durability in automotive industry is handled in the third chapter of this thesis. Multilayer coating systems are typically used to ensure the protection from corrosion and the outer layer, the clear-coat, is claimed at providing the aesthetic appearance to the final coating. Glossy surface aspect and long-term aesthetic attributes are especially requested to clear-coats. In this scenario, the mar resistance of this layer plays a crucial role. Nowadays, the mar resistance is commonly improved by having recourse to organic-inorganic clear-coats. Although the novel hybrid clear-coats have led to very good results in terms of durability, it is believed that further enhancement may be attained if a proper combination of cross-linked binder-inorganic fillers is selected. Chapter three is devoted to give a contribution in this direction. Mar damage process is firstly

analysed, and the driving factors of the damage phenomena are distinguished. The mar behaviour of a 2-component polyurethane coating and a nano-silica filled polyurethane coating was then investigated by performing a proper experimental campaign, in collaboration with PPG Industries. Single-probe scratching test and field simulation testing were used for determining the relationships between the plastic capabilities and fracture properties of the coating and its formulation parameters. Based on the results obtained from the state of the art analysis and the experimental campaign, an enhanced cross-linking level consistent with embedded nano-silica particles showing excellent mar resistance was developed.

The second part of this dissertation (Ch. 4) is finally aimed at exploring the corrosion protection capabilities of self-repairing organic coatings. The attention is specifically focused onto the preemptive healing polyurethane coatings and their barrier properties. This choice was dictated by the fact that this coatings class may provide longer service life with respect to those based on micro-encapsulation approach [5] and by the poor knowledge of the role of hydrogen bonding in the water absorption characteristics, namely in the coating barrier properties. Based on the findings obtained by Sijbesma et al. [6], a new polyurethane binder in which covalent bonds are partially replaced by hydrogen bonds was firstly synthesized. The dependence of the barrier properties on the hydrogen bonding was subsequently assessed via

Electrochemical Impedance Spectroscopy for different ratios of covalent/hydrogen bonds ratio.

1.1. References

- [1] C. K. Schoff, "Organic coatings: the paradoxical materials," *Progress in Organic Coatings*, vol. 52, pp. 21–27, 2005.
- [2] R. A. T. M. v. Benthem, *et al.*, "Self Healing Polymer Coatings," in *Self Healing Materials. An Alternative Approach to 20 Centuries of Materials Science*, S. v. d. Zwaag, Ed., ed Dordrecht, The Netherlands: Springer, 2007, pp. 139-159.
- [3] J. Zeno W. Wicks, *et al.*, *Organic coatings: science and technology*, 2nd ed. New York, Chichester, Weinheim, Brisbane, Singapore, Toronto: Wiley-Interscience, 1999.
- [4] S. v. d. Zwaag, "An Introduction to Material Design Principles: Damage Prevention versus Damage Management," in *Self Healing Materials. An Alternative Approach to 20 Centuries of Materials Science*, S. v. d. Zwaag, Ed., ed Dordrecht, The Netherlands: Springer, 2007, pp. 1-18.
- [5] M. Samadzadeh, *et al.*, "A review on self-healing coatings based on micro/nanocapsules," *Progress in Organic Coatings*, vol. 68, pp. 159-164, 2010.
- [6] R. P. Sijbesma, *et al.*, "Reversible polymers formed from self-complementary monomers using quadruple hydrogen bonding," *Science*, vol. 278, pp. 1601-1604, 1997.

CHAPTER 2

Organic coatings for architectural applications: response to weathering stresses

Organic coatings are now widely used in architectural applications. They are able to satisfy the increasing demand of aesthetic appearance, and simultaneously protect the infrastructures against environmental stresses. Degradation phenomena still represent one of the most important issues affecting the aesthetic properties and corrosion protection in metallic structures. In this direction, the present chapter is aimed at inferring the above mentioned damage processes by analysing the aesthetic and protective durability of one of the most popular organic coatings classes in architectural applications.

In general, the performances of a painted metallic structure depend on the characteristics of the coating, the properties of the metallic substrate, and the interaction between the coating and the substrate. The durability of the aesthetic appearance is mainly related to the weathering resistance of the constituents of the coating, whereas the protective behaviour is linked both to the paint properties and metal surface. Nowadays, the use of a surface pre-treatment before the

application of organic coatings is of paramount importance for ensuring good corrosion protection. It is worthy to notice that very often paint manufacturer industry optimizes a painting product by considering the most effective surface pre-treatment (chromate conversion), and, on the other hand, those who focus the attention on corrosion protection do not always consider the aesthetic durability as important for organic coatings. The gap between these two approaches should be bridged. It should be remembered that chromate conversion is now prohibited and the alternative pre-treatments are still not so effective [1, 2]. It is therefore apparent that improving the coating performances is fundamental for obtaining the same high-level durability of the chromate conversion treated systems. The experimental research described in the present chapter aims at giving a contribution in this direction. The investigation concerned polyester powder coatings applied on aluminium substrate. An analysis of the aesthetic and protective durability of different pigmented coatings is reported. The substrate was pre-treated with chromate conversion treatment to analyse the best situation from the protective point of view. Afterwards, untreated aluminium was considered, thus deriving interesting results about the relationship between the aesthetic properties and the protective behaviour of the samples. The combined analysis has allowed to draw interesting conclusions about the durability issues of the overall system and the feasible strategies for further improvements.

2.1 Introduction

Nowadays, aluminium alloys are largely used in architectural field and their corrosion resistance is often significantly increased by painting [3]. In particular, powder coatings are widely employed, thus resulting in an overall painted system with good weathering resistance and green credentials. As a matter of fact, this system combines the recyclability of aluminium with the environmentally friendly technology of powder coating [4]. Moreover, this kind of coatings provides designers an almost unlimited range of colours and textures due to the increasingly improvements of the powders [3, 4]. Powder coated aluminium alloys find therefore several applications in building industry and construction, such as doors, frames, wall and ceiling panels, windows, louvers, street and garden furniture, satellite dishes and many others, with increasing perspectives for the future.

The advantages of using powder technology is summarized in the answer given by Bocchi [5] to the question: *why powder?* The popular “Four E’s”: Ecology, Excellence of finish, Economy and Energy. This technology represents one of the strategies, together with high-solids coatings and waterborne coatings, adopted to face the environmental issue of VOC (Volatile Organic Compounds). Solvents used in paints and varnishes are the source of this kind of compounds which, emitted directly into the atmosphere, cause the formation of ozone [6]. For this reason, restrictive rules have been set to limit the VOC’s emissions (e.g. Gothenburg Protocol in 1999 [7]).

In Table 2.1 some considerations about powder coatings World Market economics in comparison with other coatings systems are summarized. As clearly shown, this technology displays economic advantages, also considering the recent developments in application equipment (i.e. easier and faster change of colour, more reactive powders with lower curing temperatures), thus allowing higher line speeds with consequent energy saving [8].

Table 2.1 On-line cost comparison of four different coating systems [8]

Costs		Powder	High-Solids	Water borne	Conventional
Capital [\$]		165,000	204,000	240,000	550,000
Annual material [\$]	A	125,206	133,595	187,032	192,376
Labor, clean-up+main.[\$]	B	88,131	176,410	176,410	176,410
Energy [\$]	C	16,068	13,851	14,434	22,434
Total annual oper. [\$]	D	229,405	323,856	377,876	391,220
Rework + reject [\$]	E	4,588	25,908	30,230	31,298
Total annual [\$]	F	233,993	349,764	408,106	422,518
Applied costs/ft ² [\$]		0.09	0.14	0.16	0.17
Applied costs/m ² [\$]		0.97	1.51	1.72	1.83

Explanation: $D=A+B+C$
 $F=D+E$

As regarding outdoor applications the exterior durability is one of the fundamental requirements of the coatings. From Table 2.2 it can be observed the excellent properties, from this point of view, of the polyesters, in particular the TGIC (triglycidyl isocyanurate)/polyester system.

Table 2.2 Comparison of outdoor resistant powder coatings [8]

Property	Acrylic	Polyurethane	Polyester
Weathering resistance	+	+	++
Mechanical properties	-	+	++
Corrosion resistance	•	+	+
Storage stability	•	++	++
Decomposition products	+	-	++
Levelling	++	++	+ (1) ++ (2)
Edge covering	•	•-	++
Resistance to overcuring	+	•	++

++: Very good +: Good •: Average -: Bad. ⁽¹⁾ high gloss ⁽²⁾ semi-gloss or matt

In Europe polyester powder coatings have been largely used in building industry; in 2005 17% of the market was devoted to architectural applications. In American and Asian countries they have been less employed because this system showed some limits in particularly aggressive environments, such as tropical climates [9, 10]. Severe conditions as high ultraviolet irradiation, hot temperatures, and high humidity levels have evidenced a not sufficient weathering resistance. Recent efforts have led to the development of *super durable polyesters* with improved performances [11]. The innovation is based on the replacement of terephthalic acid (TPA) by isophthalic acid (IPA) in the polyester backbone (Fig. 2.1).

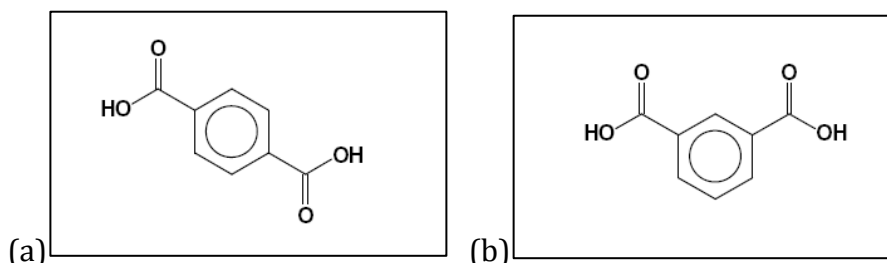


Figure 2.1 Lewis representation of (a) terephthalic acid (TPA), and (b) isophthalic acid (IPA).

The optimization of the paint for weathering resistance is investigated by applying the coating on a “perfect” substrate. In other words for improving the performances of the polymeric film, the best possible situation as regarding the metallic substrate is usually considered. Conversely, for enhancing the corrosion behaviour of the painted system, the attention is mainly focused on the barrier properties of the coating and the behaviour of the substrate (i.e. surface pre-treatments to increase corrosion resistance). A combined analysis could lead to interesting results correlating the aesthetic durability with the corrosion protection [12].

The present chapter is aimed at exploring the existence of a bridge between these two points of view. The analysis is carried out by studying the properties of standard and super durable polyester systems containing different pigments applied to two distinct substrates. The decrease in aesthetic attributes, measured as gloss loss and colour change, are firstly studied, and the decrease in protective properties, measured by electrochemical techniques and standard

accelerated laboratory corrosion tests are subsequently investigated. As regarding the choice of the substrates, chromate conversion treated aluminium, which has outstanding corrosion resistance, and subsequently untreated aluminium, where the durability properties are apparently less effective, are considered. It is worthy to highlight the fact that the recourse to chromate conversion pre-treating is now prohibited by environmental restrictions and the alternatives do not still provide the same effectiveness in terms of durability. From this point of view, enhancing the coatings durability is therefore of fundamental importance in order to achieve more long-lasting protective systems.

In the next paragraphs a survey on the main driving factors of the polyester coating degradation is reported. Moreover, the state-of-the-art was analysed by considering both the developments of the polymeric coatings and the aluminium pre-treatments aimed at obtaining a significant enhancement of the performances of the overall system.

2.1.1 Weathering resistance

Many environmental factors contribute simultaneously to the coatings degradation affecting their lifetime. Ultraviolet (UV) radiation, heat, humidity act cooperatively by changing the chemical structure of the polymeric film and its components, i.e. pigments and additives [13-15].

Surely one of the dominant factors for the coating degradation is the UV radiation [16]. The first macroscopic signals of the photodegradation concern the gloss and the colour of the surface. In general, in a pigmented coating erosion phenomena occur, thus resulting in a gloss reduction (Fig. 2.2).

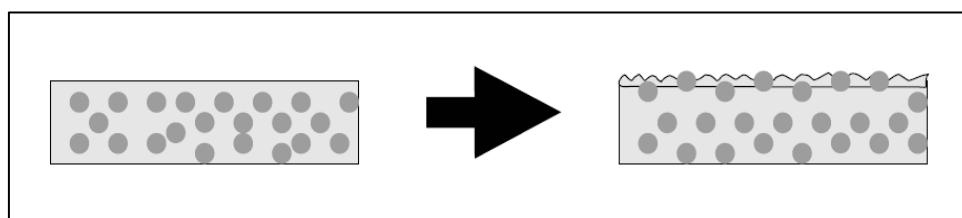


Figure 2.2 Polymer and pigments oxidation lead to erosion resulting in a gradual loss of gloss.

However, any change in appearance is related to chemical reactions which influence the physical properties with embrittlement, cracking, delamination, leading eventually to the loss of the protective function [17]. It should be remembered that weathering failures are mechanical in nature but controlled by chemistry.

Photodegradation evolves in three main stages:

1. chemical and photochemical reaction occurring at molecular level;
2. microscopic deterioration due to the binder (polymer) degradation and destruction of coating components;
3. macroscopic deterioration of the coating properties.

The mechanism of photodegradation was explained by Rabek [18]: “Photodegradation (chain scission and/or crosslinking) occurs by the activation of the polymer macromolecule provided by absorption of a photon of light by the polymer”. If the energy of the absorbed light is higher than the energy of the chemical bonds between macromolecules, photolysis occurs forming free radicals (initiation process), as shown in Fig. 2.3.

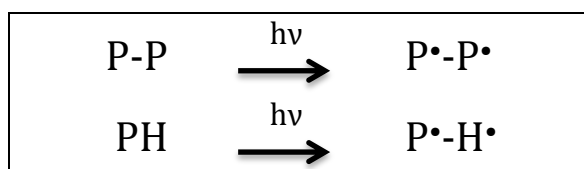


Figure 2.3 Initiation step of photodegradation.

In polymers containing chromophore groups the initiation step can take place in each repeating unit, whereas in polymers without chromophore groups, structural defects (carbonyls, double bonds, hydroperoxide) or impurities RH (catalyst, initiator,...) derived from synthesis or processing can absorb photons, form radicals and abstract a hydrogen atom from the polymer backbone (Fig. 2.4).

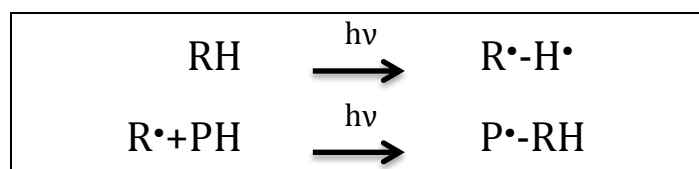


Figure 2.4 Initiation step of photodegradation triggered by impurities.

In the presence of oxygen, reactions of photooxidation take place (propagation step), thus resulting in polymer peroxy radical formation. This highly reactive intermediate abstracts hydrogen from the polymer backbone which propagates and dissociates into other compounds or low molecular weight polymer radicals (Fig. 2.5).

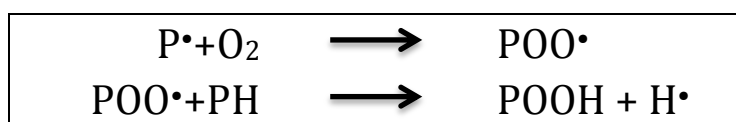


Figure 2.5 Propagation step.

Termination step involves different possible recombination steps which may lead to linear or crosslinked structures (Fig. 2.6).

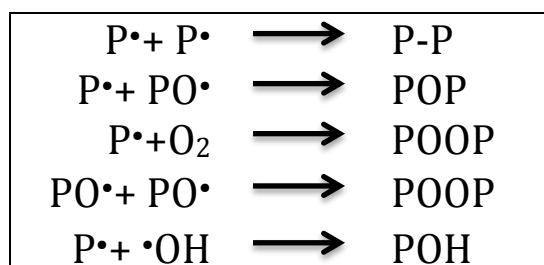


Figure 2.6 Termination steps.

It is known that polyesters containing isophthalic acid (IPA) show better weatherability properties than terephthalic acid (TPA) based polyesters [11]. Meatens [9] carried out an investigation on the differences in weathering degradation mechanism due to the replacement of TPA by IPA in the polyester backbone of powder

coatings. The weathering degradation in TPA displays the same evolution described in Fig. 2.2: an auto-catalytic chain scission de-protects pigments and fillers, thus affecting gloss and causing fading. It was proved that the degradation mechanism is due to a photo-induced oxidation generated by a photo-inductor R, as described in Fig. 2.7.

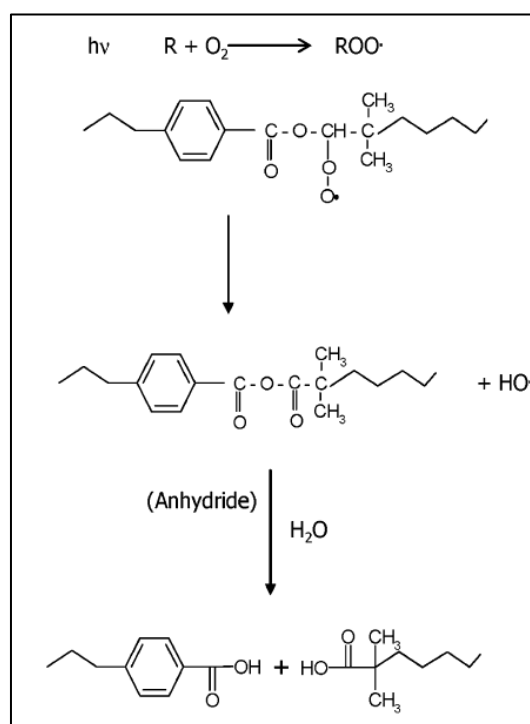


Figure 2.7. Photo-induced oxidation mechanism [9].

The strong oxidizing radical $ROO\cdot$ attacks preferably $-CH_2-$ in β position to the CO ester group. The peroxy intermediate is then converted into anhydride. In presence of water the anhydride is no more stable with consequent chain scission. TPA and IPA show the same mechanism but

the formation of anhydrides in IPA is much less . This could be related to lower concentration of the photo-inductors, or less active or less UV absorbing radicals.

2.1.2 Corrosion issues

The high reactivity of aluminium and its alloys promote the formation of a thin oxide layer which ensures corrosion resistance but, at the same time, affects the adhesion between the coating and the substrate in the case of painted aluminium [19]. Delamination processes lead to the corrosion phenomena affecting the functional properties of the coating, as well as the aesthetic appearance.

Filiform corrosion is a particular morphology of corrosion typical of painted aluminium alloys. Firstly described by Sharman in 1944 [20], it is a cosmetic corrosion because in most cases it affects only the surface aesthetics with the formation of thread-like filaments. In architectural aluminium it was first observed in 1980-82 in buildings exposed to marine and industrial environments [21].

The typical filaments are produced by differential aeration resulting in separate anodic and cathodic sites. The head front of the filament, where metal dissolves, is the anode of the process, the tail, where the oxygen is reduced, is the cathode. Filiform corrosion is activated by the presence of chloride ions and acidic environment, and promoted by high relative humidity. In Fig. 2.8 a sketch of a filament and the relative electrochemical reactions are displayed.

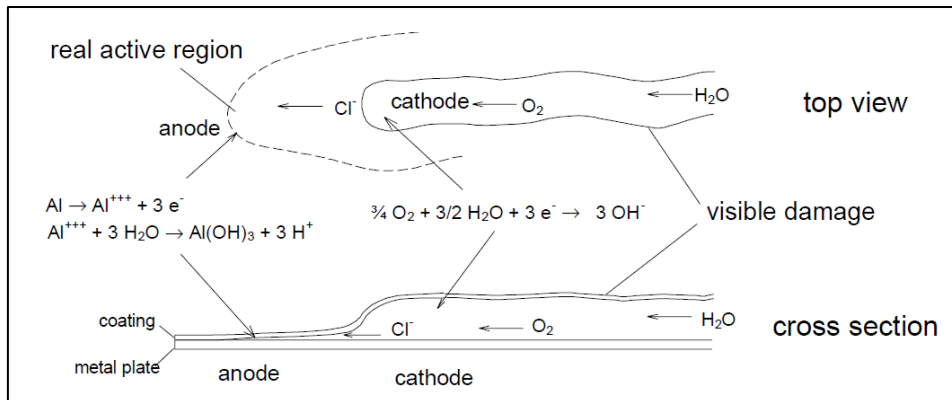
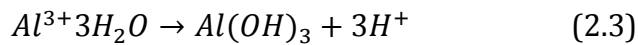
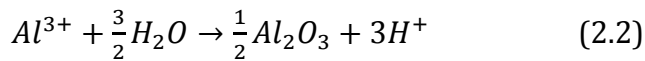
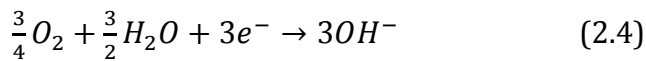


Figure 2.8 Sketch of a filament and electrochemical reactions [22].

Aluminium, uncovered by a defect in the organic coating, oxidized and forms Al_2O_3 and/or $Al(OH)_3$, according to the following steps [23]:



The correspondent reduction reaction, reported in (2.4), occurs preferably behind the detachment front, where availability of oxygen is higher.



The oxidation and reduction reactions taking place at different locations create two distinct zones: the detachment front of the coating

which becomes more acidic (reactions 2.2 and 2.3) and the tail area which becomes more alkaline (reaction 2.4). The true anode is actually far beyond the visible head of the filament which is more aerated than the real active region [22].

In Fig. 2.9 the potential-pH plot for the system Al-H₂O is reported. In the head the pH is more acidic and the potential lower, while in the tail the pH is more alkaline, with higher potential.

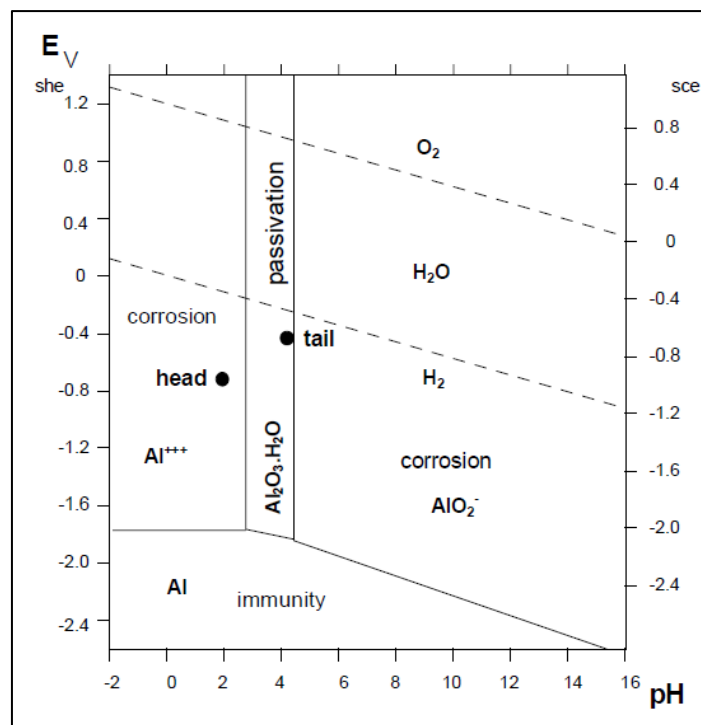


Figure 2.9 *E-pH diagram in heads and tails of filaments [22].*

The sensitivity to filiform corrosion depends on several factors related to the metal substrate, the surface pre-treatments, the adhesion

between the coating and the substrate, and the characteristics of the coating [3, 19, 21-31].

2.1.3 Surface pre-treatments

Generally, the use of surface pre-treatments of aluminium and aluminium alloys before the application of an organic coating is mandatory in order to obtain an overall system with acceptable corrosion protection properties [32]. Chromium conversion treatments have been used for long time for their outstanding performances. The immersion in chromic acid containing Cr^{6+} species baths leads to the formation of a passivation layer, a mixture of chromium compounds acting as a barrier to moisture/air and as corrosion inhibitor by releasing chromate ions [6, 33]. Moreover, the adhesion between the paint and the substrate is promoted by this passivation layer [6]. However, the health and environmental issues caused by the use of hexavalent chromium has led to restrictions banning this kind of pre-treatments. For this reason, in the last two decades, the efforts aimed at replacing chromate conversion treatments have developed many different kinds of pre-treatments [6]. These “environmentally friendly” pre-treatments may use the same protection mechanism of Cr^{6+} treatments as in case of passivating agent such as molybdates, permanganates, vanadates, and tungstates or other mechanisms. Rare earth based conversion treatments, Cr^{3+} conversion layers, fluo-titanate, and fluo-zirconate conversion treatments are some

examples. Phosphate conversion treatment provides a surface with many anchor points and a barrier to the spread of corrosion under paint [6, 34]. Metal alkoxides and/or organically modified metal alkoxides are another emerging strategy with many advantages [35]. Hybrid organic-inorganic compounds such as silanes induce strong (covalent) chemical bonds both with the substrate and with the polymeric layer, thus ensuring a stable adhesion also in humid environments due to the resistance of these bonds to hydrolysis [35, 36].

2.2 Materials and experimental procedures

The experimental work described in this chapter has been carried out in collaboration with Akzo Nobel Coating S.p.A, Romano d'Ezzelino (VI, Italy), which kindly provided the powder coated samples. The durability of different polyester powder coatings was investigated, firstly on chromate conversion treated aluminium, and then on untreated aluminium. A durable version (based on TPA and a small percentage of IPA) and a super durable version (based exclusively on IPA) were compared. The coatings systems were crosslinked by using β -hydroxylalkilamide to avoid the use of triglycidyl isocyanurate (TGIC). The replacement of TGIC is one important issue in powder coatings technology and one of the reason promoting the developments in this field. The toxicity and mutagenicity of this kind of crosslinker is

leading to new toxicologically-safe coatings systems with the same or improved properties [37, 38].

The polyester coatings were applied by powder technology on 150x75 mm² panels of 3003-H14 aluminium alloy (composition in wt%: Si 0.6, Fe 0.7, Cu 0.2, Mn 1.2, Zn 0.1, Al bal.) with a chromate conversion (CC) treatment and without any pre-treatment. The coatings were cured at 180°C for 20 minutes. In Table 2.3 the list of the studied samples is reported, as well as the main constituents and the coatings thickness measured by a Phynix Surfex FN coating thickness gauge.

Table 2.3 Investigated samples

Sample	Binder	Pigments	Additives	Thickness
R - STD	TPA/IPA	Standard Red	-	73.6±3.2 µm
R - SD	IPA	Super durable Red	UVAs + HALS	74.4±5.0 µm
G - STD	TPA/IPA	Standard Green	-	79.9±3.9 µm
G - SD	IPA	Super durable Green	UVAs + HALS	79.5±5.2 µm
W - STD	TPA/IPA	Standard White	-	66.7±4.5 µm
W - SD	IPA	Super durable White	UVAs + HALS	102.6±6.7 µm
Y - STD	TPA/IPA	Standard Yellow	-	77.6±6.9 µm
Y - SD	IPA	Super durable Yellow	UVAs + HALS	76.2±5.6 µm

The main differences between the standard durable version (STD) and the super durable version (SD) are related to the composition of the binder, the addition of anti UV agents (Benzotriazole and Triazine combined with Hindered Amine Light Stabilizers) and more durable pigments. In samples STD the composition of the carboxyl polyester resin is based on terephthalic acid and a small percentage of isophthalic

acid, in samples SD terephthalic acid is not used. Different commercial formulations were chosen with four pigments systems: red, green, white, and yellow (R, G, W and Y). Every colour was obtained by an appropriate combination of different pigments both organic and inorganic. The difference between a standard pigment system and a super durable pigment system depends on the colour. For red, green and white samples the super durable pigments do not exhibit great differences in the Pigment Volume Concentration (PVC) or in the chemistry of the used pigments between STD and SD versions. Conversely, in the case of yellow samples the organic component of the pigment system is markedly higher in SD version than in STD one. The pigment base of the STD coatings shows brighter colours (higher saturation), while in SD coatings the base has duller colours (lower saturation) requiring a higher amount of organic pigments to achieve the same colour characteristics.

Gloss was evaluated by using Picogloss 20°-60°-85° mod. 503 Erichsen glossmeter at an angle of 20°, according to ASTM D523 Standard. The measurement area of the glossmeter was 10x10 mm². The mean gloss and the standard deviation were obtained from 10 measurements. The initial gloss values are reported in Fig. 2.10.

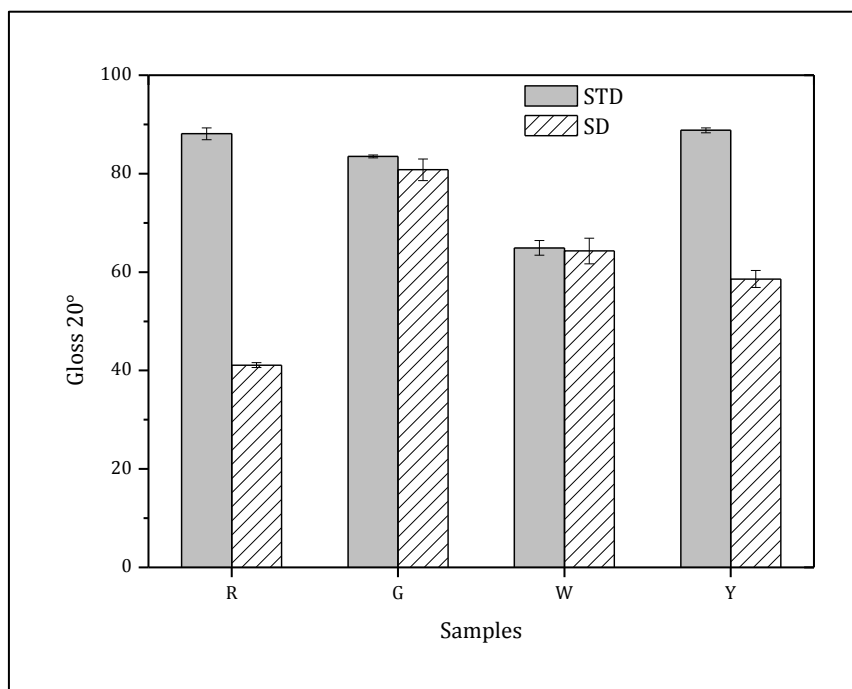


Figure 2.10 Initial gloss of the samples measured at 20°.

All the samples have high gloss surfaces with values higher than 40. Samples R-STD and Y-STD show the lowest values due to a specific market demand of the commercial products. In the other two cases the differences between the durable and super durable version are negligible.

The glass transition temperature of the samples was measured by Differential Scanning Calorimetry (DSC) by Q100 – *TA Instrument*. The powder samples were quickly heated until 100°C for removing a *pseudo-crystallinity* which can form in the material during storage due to relaxation processes in the polymeric binder, and may affect the T_g

measurement. The samples were then cooled down at room temperature and reheated for determining the T_g . Subsequently the samples were maintained at 180°C for 20 min (cure time) and a further cool/heat cycle was performed to assess the T_g of the crosslinked system.

In Figs. 2.11 and 2.12 the glass transition temperature derived from the DSC curves is plotted for the powders and the crosslinked coatings, respectively.

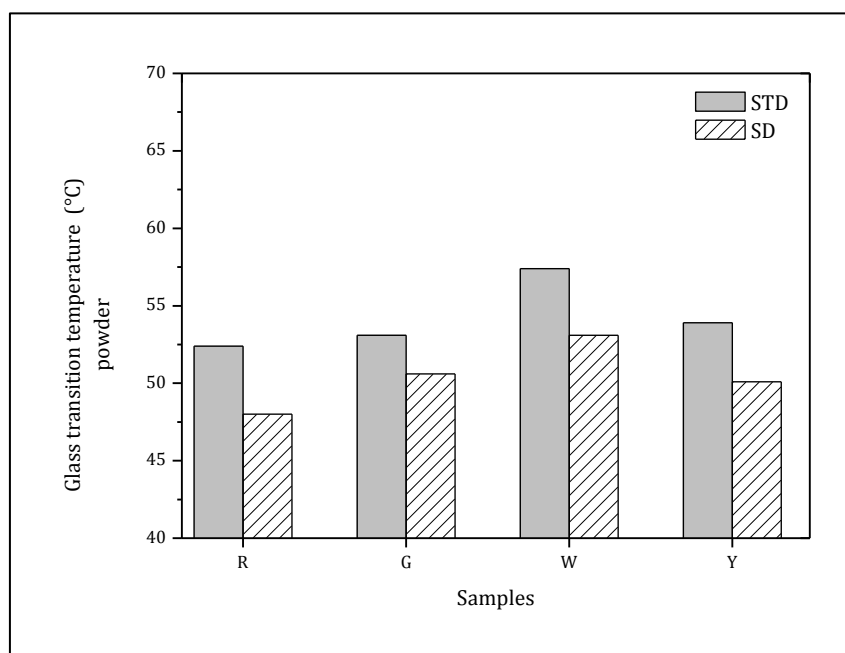


Figure 2.11 Glass transition temperature (T_g) of the powders.

IPA based powders display a lower T_g values; in the crosslinked systems the trend is the same, except in the case of green samples,

although the difference between the standard and super durable version is almost negligible. The fact that TPA based coatings show higher T_g is confirmed by literature findings [39, 40]. As regarding the differences among the pigment systems, the highest values of T_g belong to the white samples.

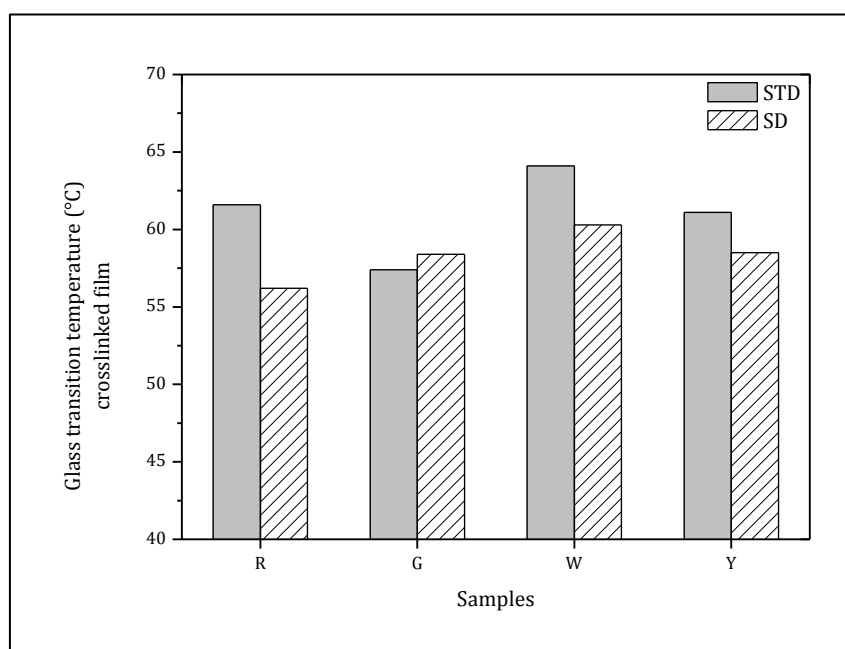


Figure 2.12 Glass transition temperature (T_g) of the crosslinked samples.

The rheological behaviour of the powders was characterized by viscosity measurements carried out with ARES-TA Instruments Rheometer. The initial heating from 40°C to 180°C was performed at 10°C/min, the remaining test time was performed in isothermal conditions (180°C).

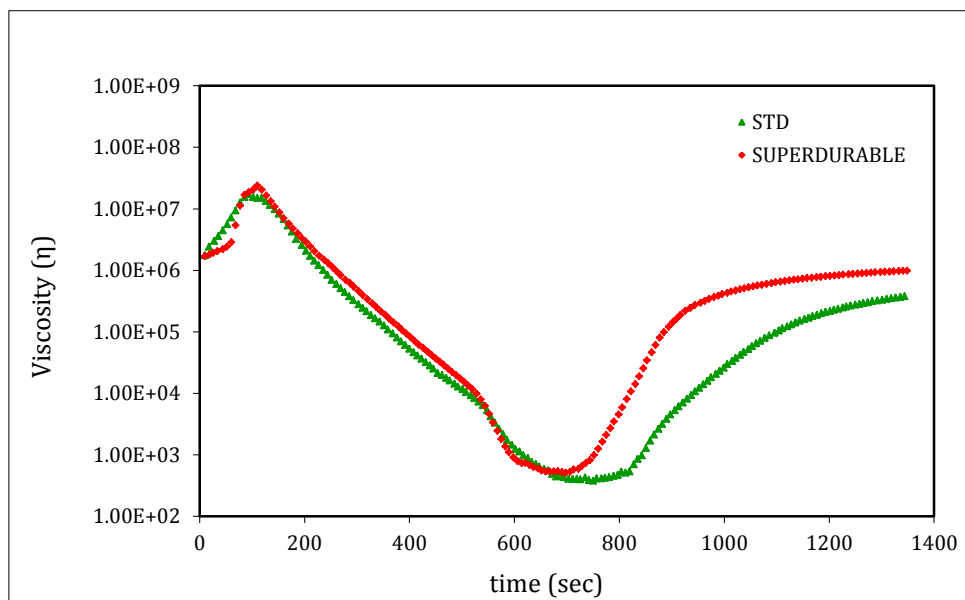


Figure 2.13 Rheological curves - Samples R.

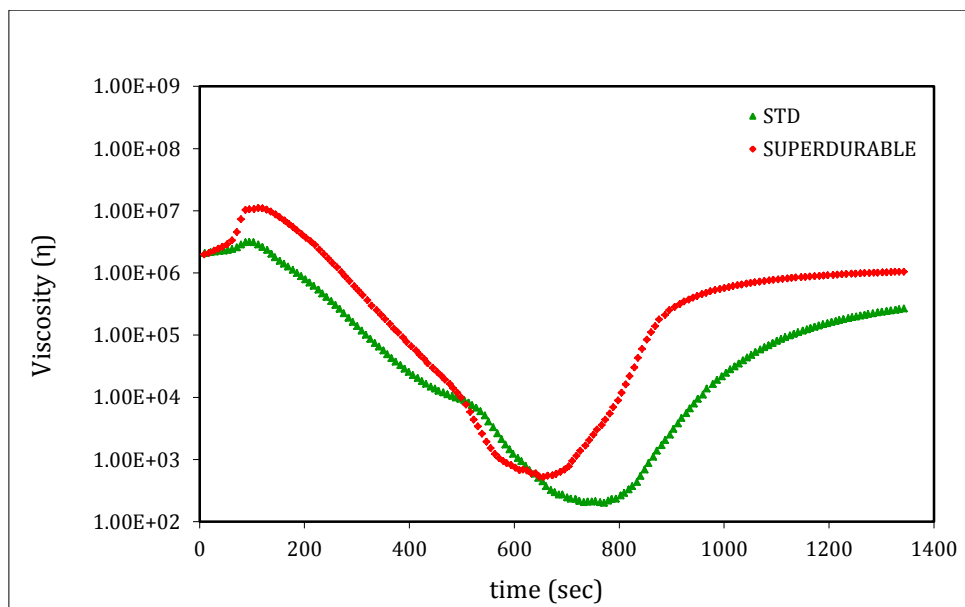


Figure 2.14 Rheological curves – Samples G.

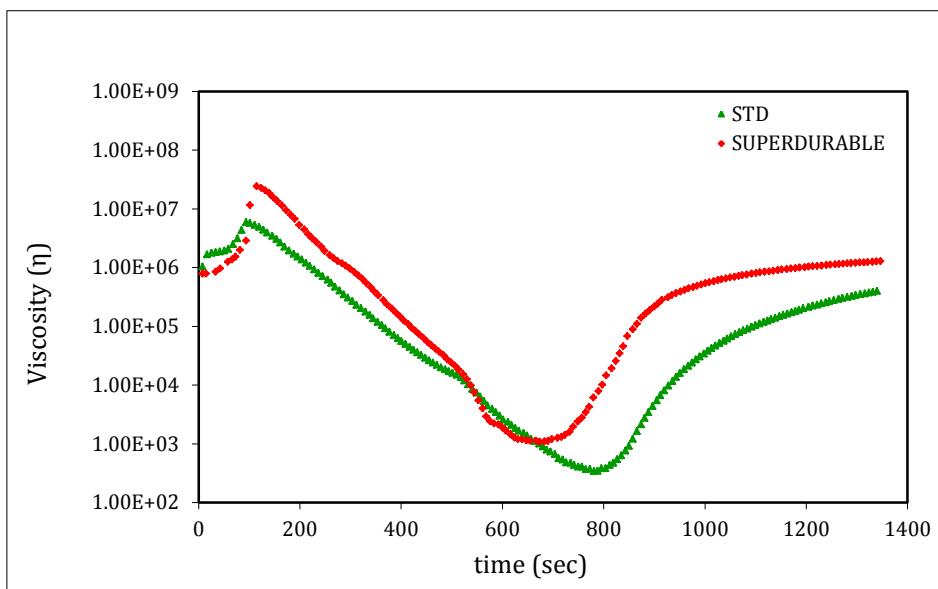


Figure 2.15 Rheological curves – Samples W.

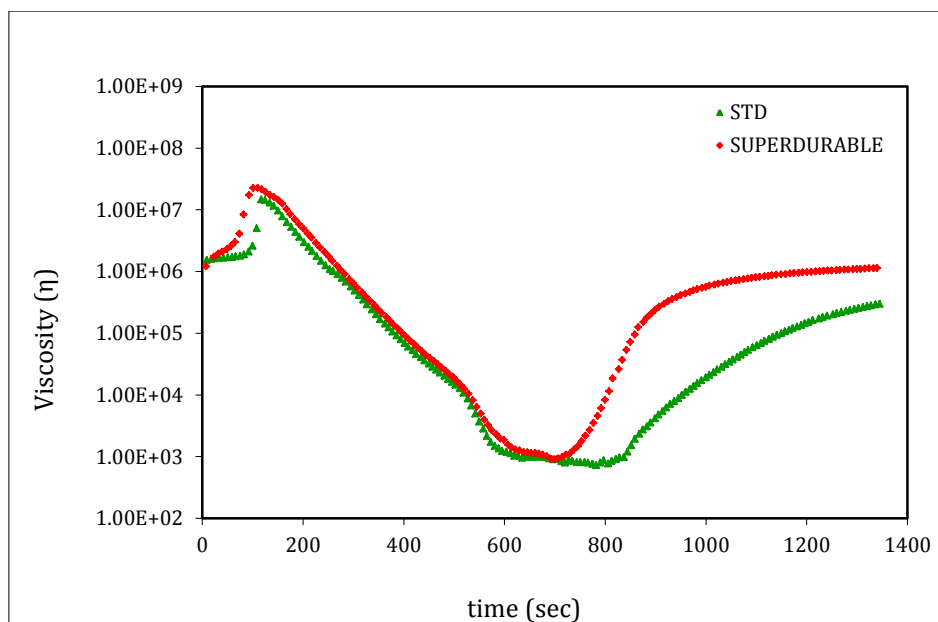


Figure 2.16 Rheological curves – Samples Y.

Figs. 2.13 – 2.16 display the rheological curves obtained for the samples. The trend is characterized by a decrease in the viscosity, and then an increase as a result of the polymer's crosslinking. The so-called *flow window* is described by the lowest viscosity attained and the length of time [41]. This window influences the flowing and levelling ability of the coatings. Wider window means higher wettability of the powders. It is apparent that the IPA based coatings show a narrower flow. This was found for every couple of coatings. The comparison between the pigment systems does not reveal significant differences in rheological behaviour.

UV exposure

The samples were artificially weathered by exposure to ultraviolet radiation (UV-A, according to ASTM G154) for 2000 hours.

The aesthetic degradation was studied by gloss and colour change measurements. The decrease of gloss was expressed as percentage residual gloss referring to the initial value.

Colour variation was measured by using the spectrophotometer CM-2600d Konica Minolta with a D65/10° illuminant/observer. Both SCI (Specular Component Included) and SCE (Specular Component Excluded) modes have been used. The colour change is reported as ΔE^*_{ab} calculated as expressed in Eqn (2.5):

$$\Delta E^*_{ab} = \sqrt{\Delta L^2 + \Delta a^2 + \Delta b^2} \quad (2.5)$$

where L is the lightness (0 is black, and 100 is white), a is the red-green variation (positive values are red, negative values are green, and 0 is neutral), and b is the yellow-blue variation (positive values are yellow, negative values are blue, and 0 is neutral), according to ASTM E308 Standard.

The chemical degradation of the coating was evaluated by Fourier Transform Infrared Spectroscopy (FT-IR measurements using Varian 4100 FTIR (Excalibur series), with a resolution of 4 cm^{-1} over the range of $4000\text{--}500\text{ cm}^{-1}$).

Corrosion tests

The scribed samples were exposed to acetic acid-salt spray fog (fog obtained by 5% NaCl solution at $\text{pH} = 3$ by adding acetic acid), according to ASTM G85 for 1000 hours. After the test the panels were examined by visual inspection by comparing the delaminated area from the scratch, and the possible presence of blistering phenomena.

The filiform corrosion resistance of the samples was studied according to UNI EN 3665 Standard. Two 1 mm wide scratches were produced in longitudinal (100 mm in length) and transverse directions (50 mm in length). The samples were placed in a corrosive environment (HCl vapours) for 1 hour to initiate the corrosion process of the aluminium alloy. Subsequently they were exposed to controlled temperature ($40 \pm 2\text{ }^\circ\text{C}$) and relative humidity ($82 \pm 3\%$). The test finished after 120 hours of exposure for the untreated samples and after 30 days for the pre-treated samples.

Electrochemical impedance spectroscopy measurements were performed on the samples in continuous immersion in Harrison's solution (3.5 g/l $(\text{NH}_4)_2\text{SO}_4$, 0.5 g/l NaCl, pH =6). The measurements were carried out using a potentiostat and a frequency response analyser PARSTAT 2773. The frequency range was from 10^5 to 10^{-2} Hz and the signal amplitude 20 mV. A platinum electrode was used as counter-electrode, and an Ag/AgCl (+207 mV SHE) as reference electrode. The tested area was 15.9 cm^2 . At least two EIS measurements on different samples were carried out to confirm the obtained results. EIS results were fitted (using ZSimpWin 3.22 Software) by the equivalent electrical circuit represented in Fig. 2.17, where R_{el} is the resistance of the electrolyte, C_c the coating capacitance and R_c the coating resistance.

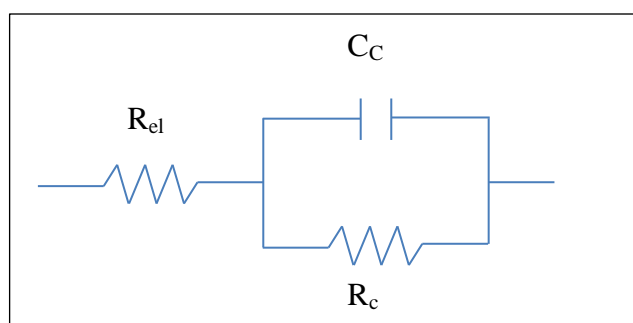


Figure 2.17 Equivalent electrical circuit used for fitting EIS raw data.

2.3 Results and discussion

In Fig. 2.18 and 2.19 the percentage residual gloss during the UV exposure is reported. In particular, Fig. 2.18 displays the results for the standard version of the samples.

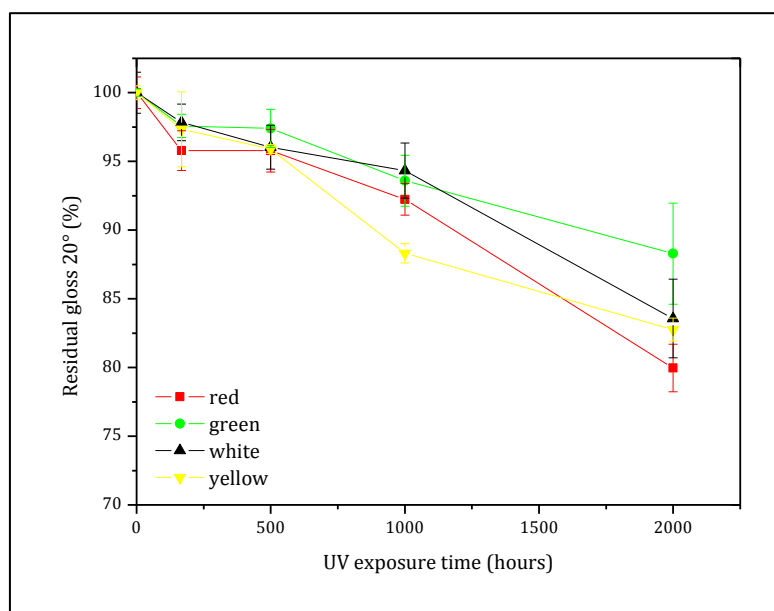


Figure 2.18 Residual gloss measured at 20° during UV exposure (standard samples).

The behaviour of the green sample is slightly better than the other samples with a residual gloss equal to 88.3% at the end of the test. The differences between the other samples are negligible. The super durable IPA-based coatings show a better behaviour than TPA/IPA-based samples. After the first 500 hours of exposure the gloss of all the samples does not show any change, in the later time some differences

are appreciable. Green samples are confirmed to be the more withstanding as regarding the gloss reduction (98.6% residual gloss). White samples seem to have the worst behaviour with a loss of gloss of 14.9% respect to the red and yellow samples (10.9% and 9.2% of gloss loss).

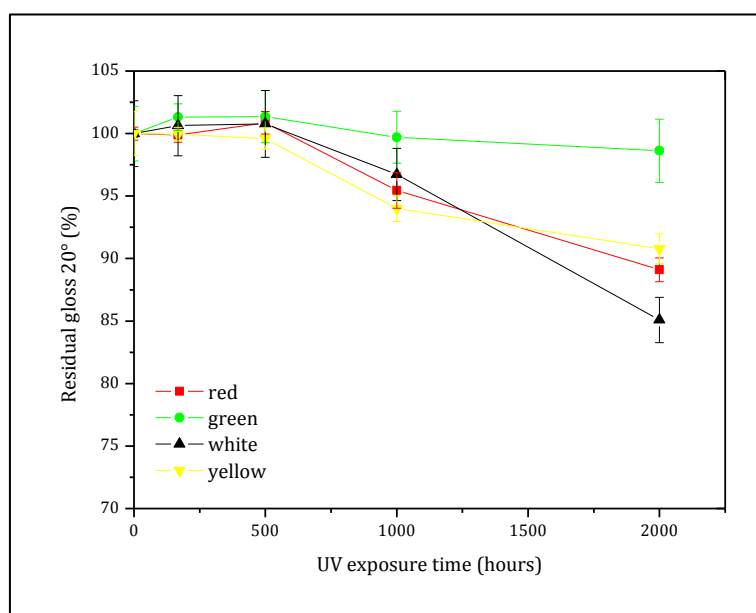


Figure 2.19 Residual gloss measured at 20° during UV exposure (super durable samples).

In Fig. 2.20 a comparison between the TPA/IPA and IPA based coatings is reported by analysing the percentage residual gloss at the end of UV exposure for each pigment system. It can be clearly observed that the super durable version shows lower gloss reductions. The difference in white samples is less pronounced. As concerning the gloss trends, it is

possible to conclude that the chemical composition of the binder plays a fundamental role.

Moreover, it is worthy to notice that 2000 hours of UV exposure represent a significantly severe test conditions, thus highlighting the excellent properties of these coatings.

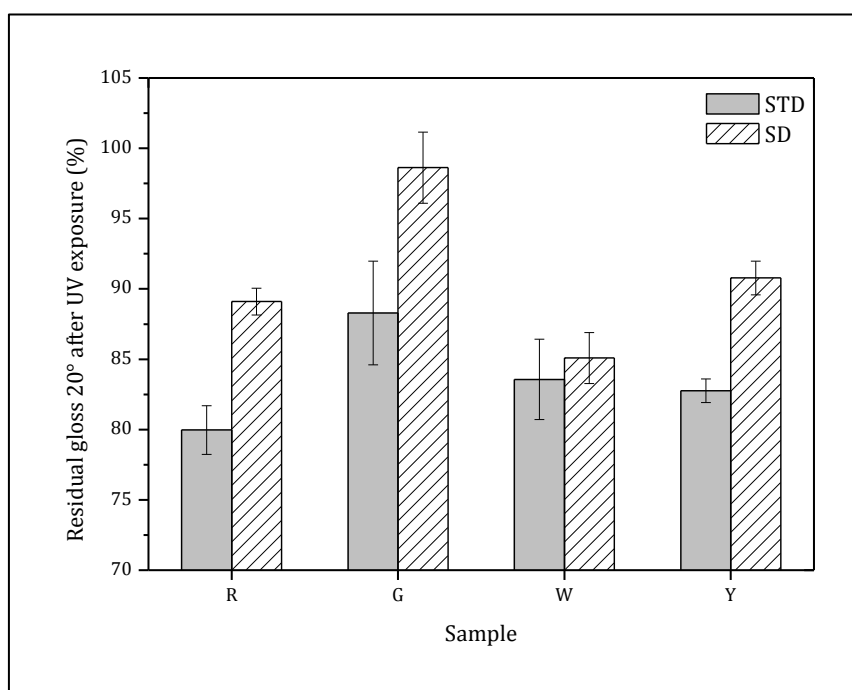


Figure 2.20 Comparison between standard and super durable version for each pigment system.

Figs. 2.21 - 2.24 report the FT-IR spectra of the samples after UV exposure, in the range 4000-500 cm^{-1} . It is apparent that the polyester coatings based exclusively on IPA show a very limited degradation in all

Chapter 2

the samples, confirming the results obtained by gloss measurements and proving the better UV resistance of this kind of coatings.

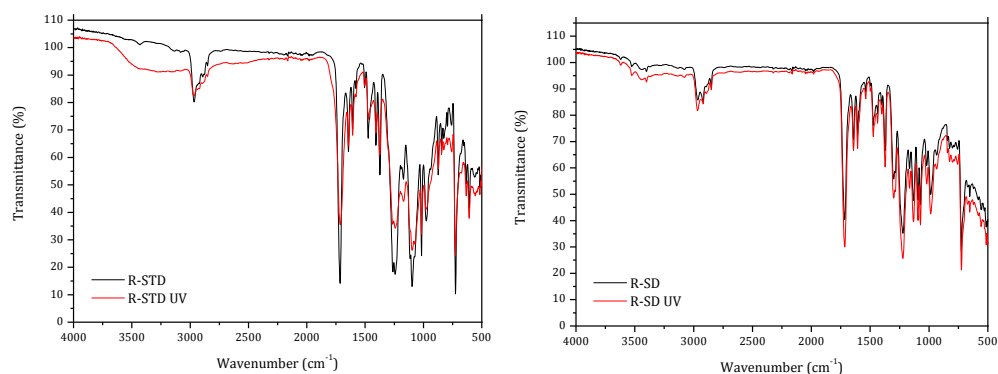


Figure 2.21 FT-IR spectra of the samples before and after UV exposure - Samples R.

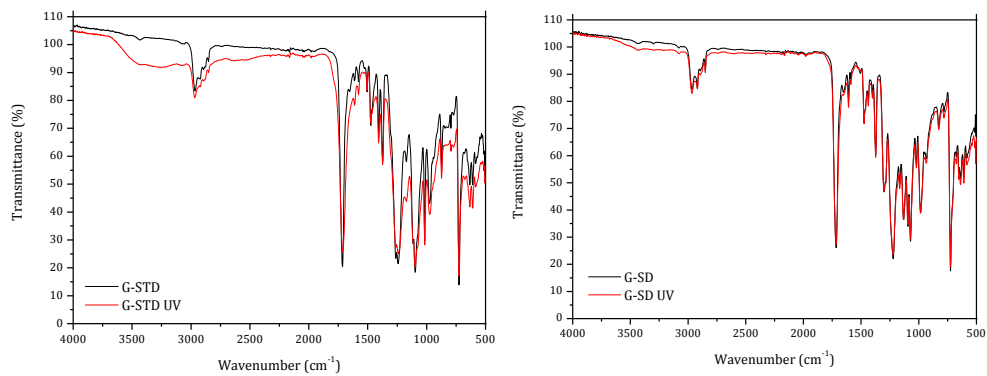


Figure 2.22 FT-IR spectra of the samples before and after UV exposure - Samples G.

Chapter 2

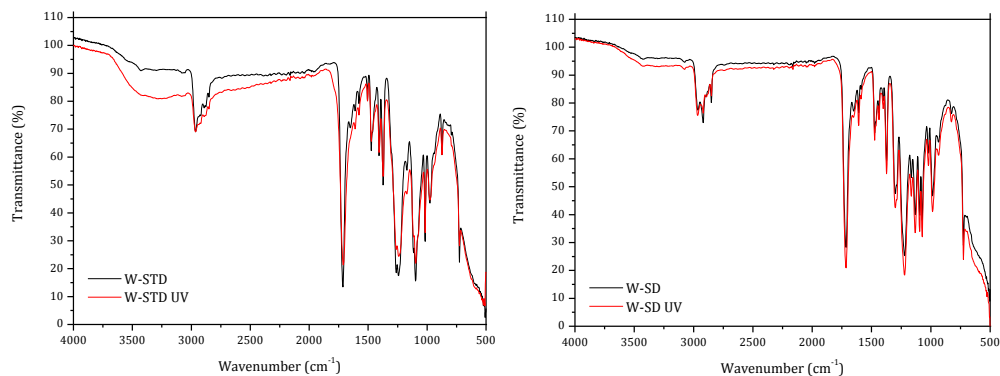


Figure 2.23 FT-IR spectra of the samples before and after UV exposure - Samples W.

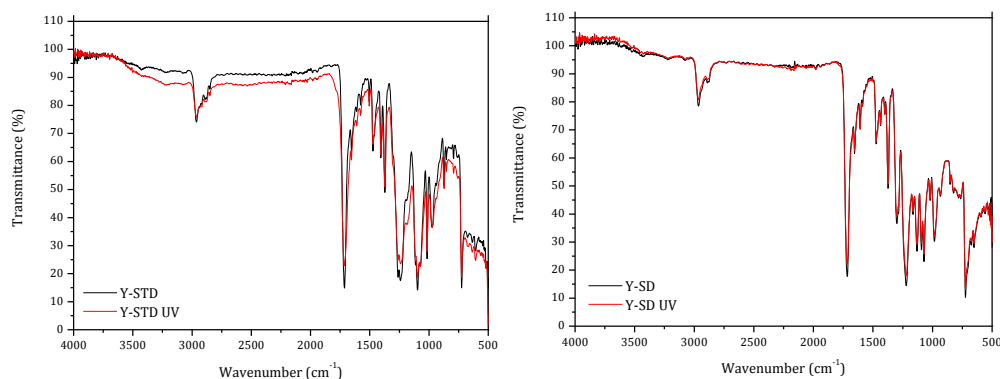


Figure 2.24 FT-IR spectra of the samples before and after UV exposure - Samples Y.

Fig. 2.25 shows two details that more clearly represent the chemical degradation of the bonds. As an example, FT-IR spectra of samples R-STD and R-SD are reported. The most evident changes are visible in hydroxyl region and CH₂-CH₃ region (3600-2800 cm⁻¹), and carbonyl region (1800-1650 cm⁻¹). The durable version (R-STD) shows significant changes in these regions, on the contrary the super durable

version based entirely on IPA (R-SD) does not show any remarkable difference from the initial spectrum.

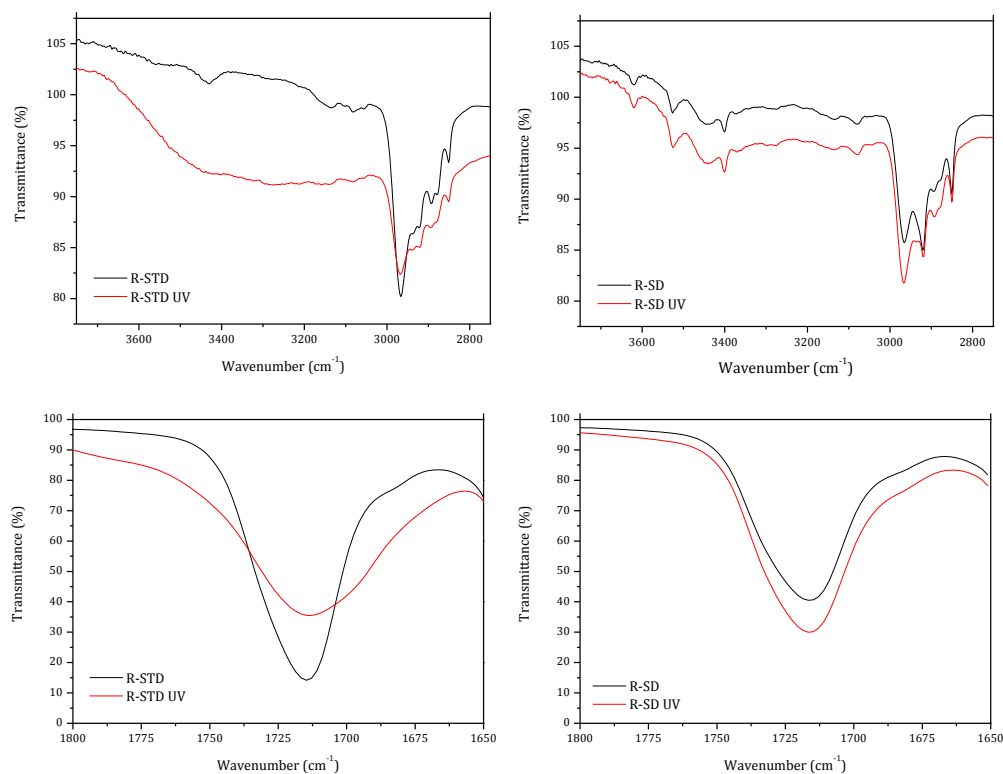


Figure 2.25 FT-IR spectra of the samples R before (R-STD, R-SD) and after UV exposure (R-STD UV, R-SD UV) (regions of OH, CH₂, CH₃ and C=O bonds).

Figs. 2.26 and 2.27 show the colour variation at the end of the UV test for the standard and super durable samples, respectively. The total colour change is reported as ΔE^*_{ab} in both SCI and SCE modes. In SCI mode the measurement includes the diffuse reflectance and the specular reflectance, while in SCE mode the light reflected in specular direction is excluded. The former is indicated for studying the colour as

the actual physical properties of the sample, the latter is useful to measure the surface appearance as it looks like to the human eye. In fact, it covers all the surface characteristics that influence the colour perceived by our eye: colour, gloss, texture, and finish.

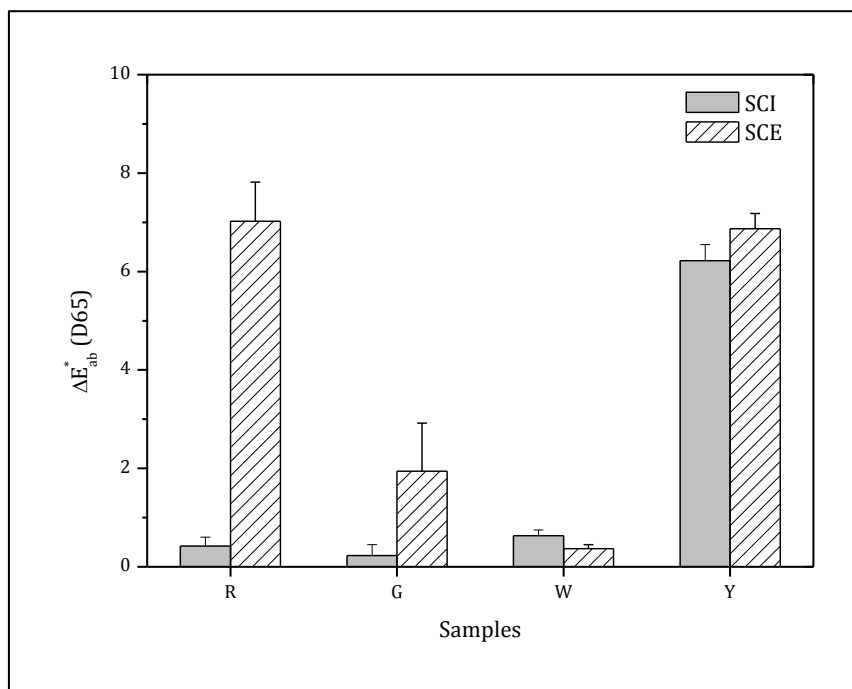


Figure 2.26 ΔE^*_{ab} after UV exposure – standard samples.

As regarding the standard samples (Fig. 2.26), ΔE^*_{ab} in SCI mode is lower than 1 for all the samples, except for the yellow one which shows a remarkable colour change. The measurements in SCE mode highlight the critical feature of the red and yellow pigment systems. Therefore, from these results yellow samples are proved to be the most critical

system. The UV radiation directly acts on the pigment characteristics and on the binder structure modifying the appearance attributes. Also red samples appear to be negatively affected by the UV action but the pigment seem to be more withstanding, as derived from the SCI mode measurements. The colour properties of the white and green samples are less influenced by the test, in particular the white one shows an excellent resistance from this point of view.

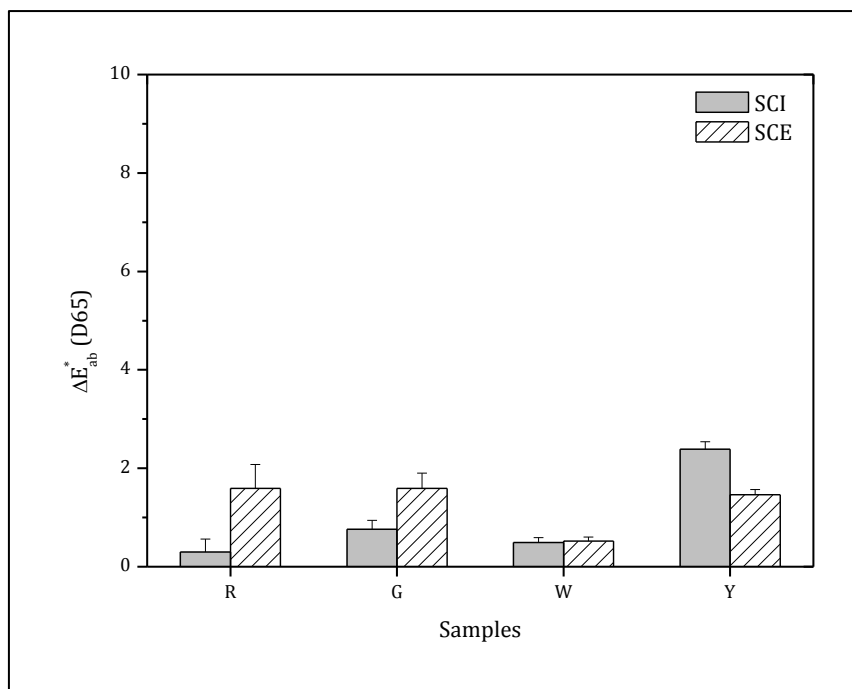


Figure 2.27 ΔE^*_{ab} after UV exposure – super durable samples.

Fig. 2.27 displays the results for the super durable version of the samples. In this case, the colour change is significantly lower. The

differences between the pigment systems are almost negligible, only the most sensitive yellow shows a higher ΔE^*_{ab} . The introduction of UV absorbers additives combined with more resistant pigments and binder, determines a remarkable enhancement in the durability of the aesthetic attributes.

Figs. 2.28-2.31 show the elaborated data derived from the EIS measurements performed on the STD and SD samples applied on CC aluminium substrate. From the fitting of the raw data, the values of coating capacitance C_c are derived. C_c is given by the formula expressed in Eqn. (2.6):

$$C_c = \frac{\varepsilon \varepsilon_0 A}{d} \quad (2.6)$$

where ε is the dielectric constant of the coating, ε_0 is the permittivity of vacuum, A is the tested area, d is the thickness of the coating.

In the graphs of Figs. 2.28-2.31 the trend of the dielectric constant coating is plotted as a function of the immersion time. It is possible to notice some difference in the increase of ε during the immersion time. In particular, for all the standard samples the ε rise seems to be more pronounced. To better appreciate the difference between the STD and SD versions and among the differently pigmented systems, the water uptake was calculated for each sample.

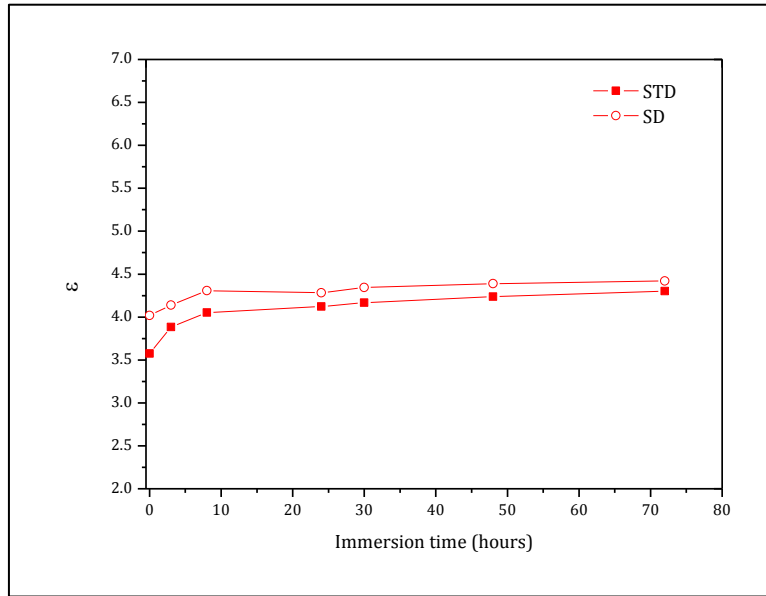


Figure 2.28 Dielectric constant of R samples as a function of the immersion time.

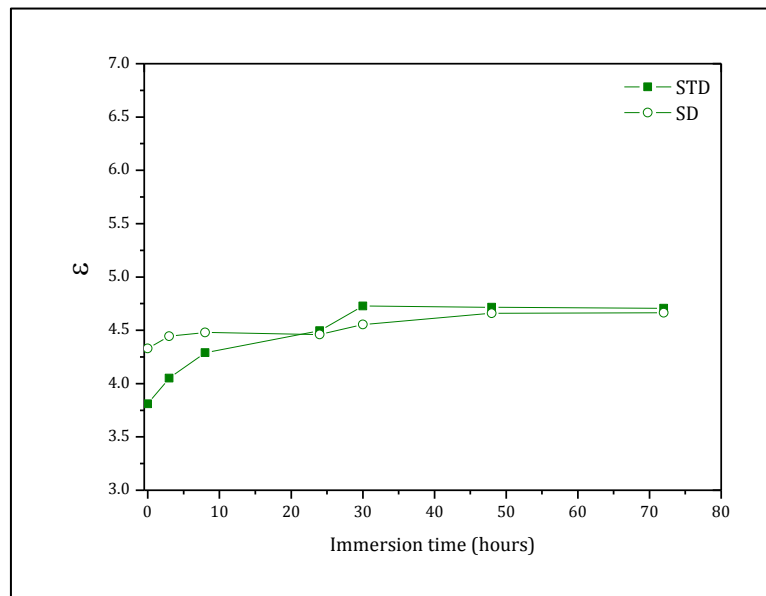


Figure 2.29 Dielectric constant of G samples as a function of the immersion time.

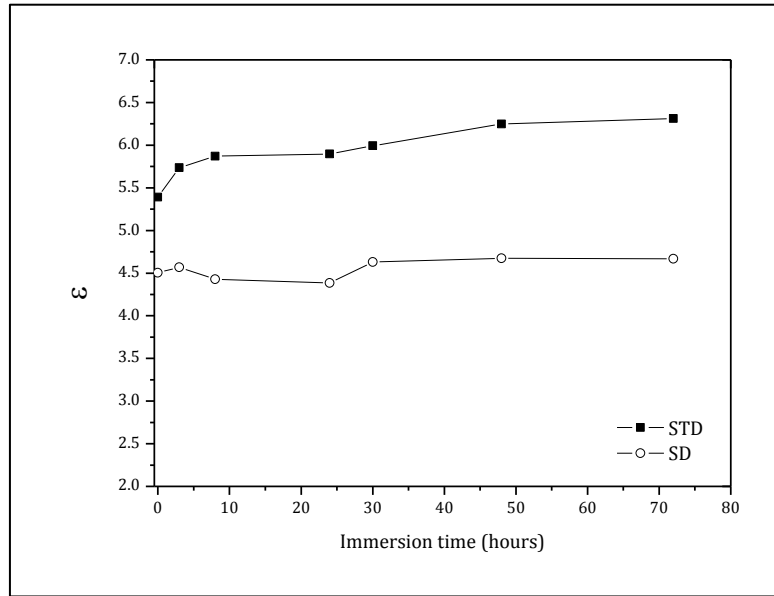


Figure 2.30 Dielectric constant of W samples as a function of the immersion time.

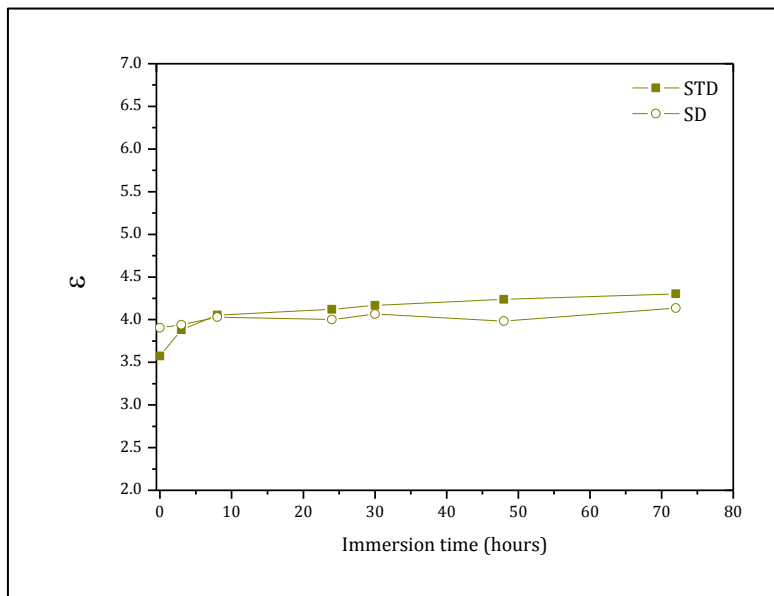


Figure 2.31 Dielectric constant of Y samples as a function of the immersion time.

From the increase of ε , corresponding to an increase of coating capacitance, a numerical value for the water uptake is computable by using Brasher and Kingsbury equation (Eqn. 2.7) [42]:

$$X_V = \frac{\log\left(\frac{C_c}{C_0}\right)}{\log \varepsilon_w} \quad (2.7)$$

where X_V is the water uptake volume fraction, C_0 is the initial coating capacitance, C_c is the coating capacitance at a generic time and ε_w is the dielectric constant of water (=80) [42, 43]. To obtain the values of water uptake volume fraction represented in Fig. 2.32, the values of C_c after 72 hours of immersion were considered.

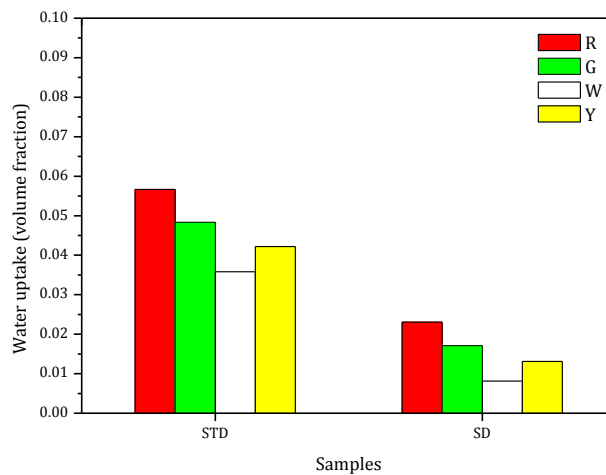


Figure 2.32 Water uptake volume fraction for samples applied on CC Al substrate.

In general the IPA based coatings show a lower water uptake with respect to the TPA/IPA based samples. Moreover, some differences are noticeable among the different pigment systems. It is interesting to observe that these differences are present in STD and SD versions with the same ranking. These results could suggest a potential different behaviour in the corrosion tests.

Figs. 2.33a-b show the samples at the end of acetic salt spray test, after 1000 hours of exposure. On the left side the standard samples are displayed, on the right the super durable version. It is apparent that the CC treated samples show an excellent behaviour in response to this test. No delaminated areas from the X scratches are noticeable without any observable difference among the systems, either with respect to the binder composition, or with respect to the used pigment system.

Figs 2.34a-b display the STD (on the left) and SD (on the right) samples after the filiform corrosion test. Also in this case, after 30 days of test, only few marks of filiform corrosion departing from the artificial scratch are visible in samples W-STD and Y-SDT and Y-SD.

This result confirms the outstanding performances of CC samples but highlights the fact that by investigating the behaviour of different powder coatings applied on this kind of substrate, does not allow to emphasize the differences among the samples. The role played by the pre-treatment is dominant and resets the possibility to detect the role of the coating barrier properties.

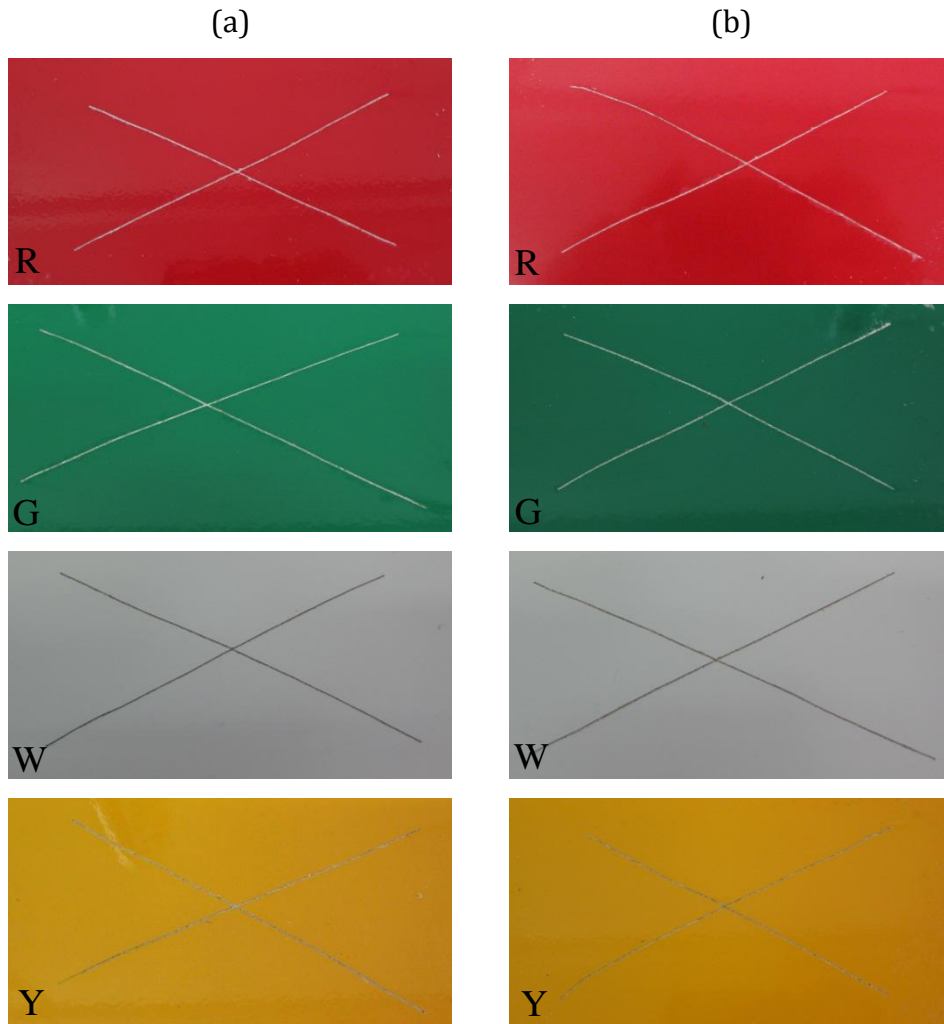


Figure 2.33 CC treated samples after acetic salt spray exposure:
(a) STD samples; (b) SD samples.

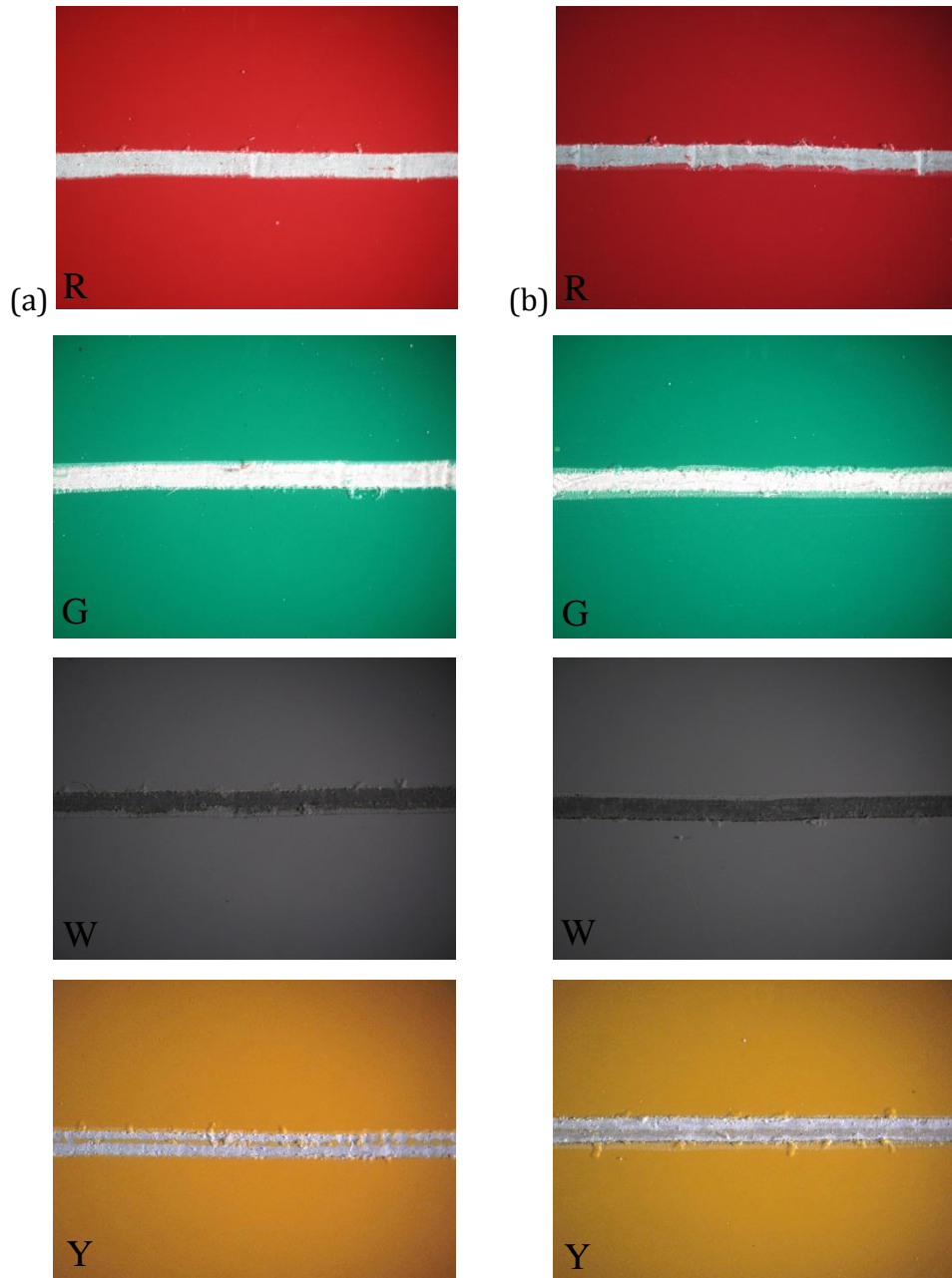


Figure 2.34 CC treated samples after filiform corrosion test (30 days):
(a) STD samples; (b) SD samples.

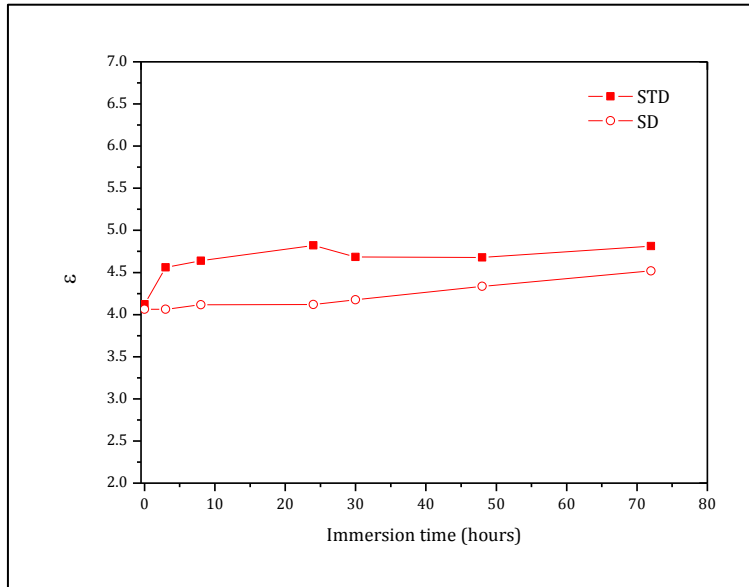


Figure 2.35 Dielectric constant of the R samples applied on untreated Al as a function of the immersion time.

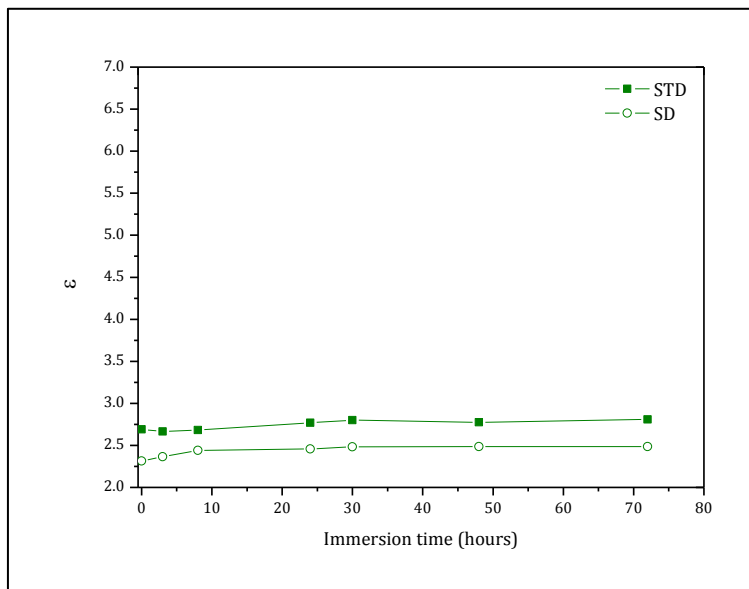


Figure 2.36 Dielectric constant of the G samples applied on untreated Al as a function of the immersion time.

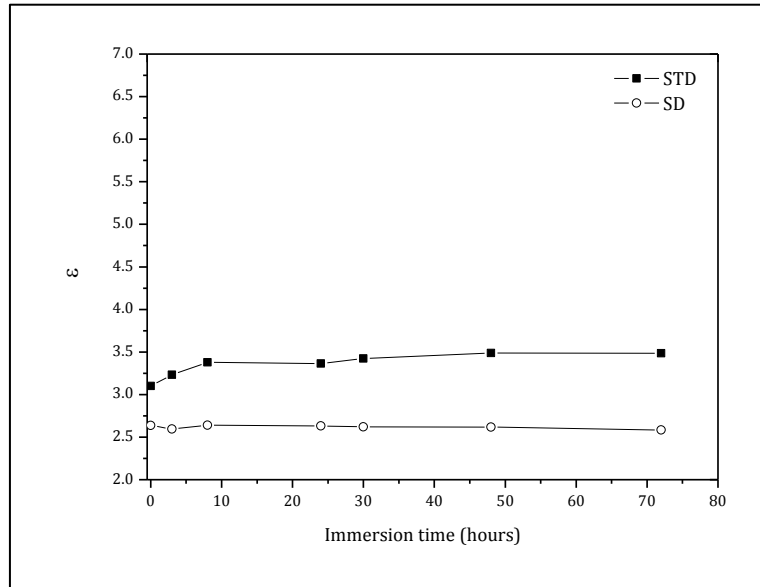


Figure 2.37 Dielectric constant of the W samples applied on untreated Al as a function of the immersion time.

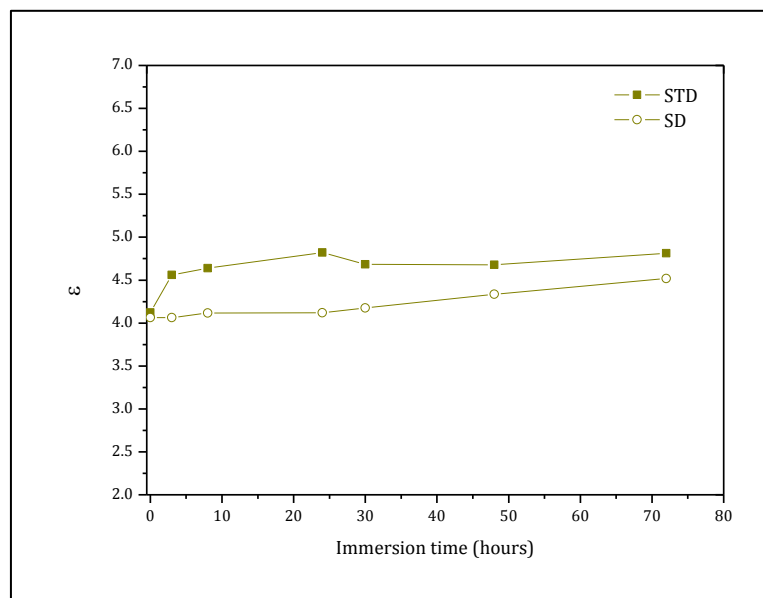


Figure 2.38 Dielectric constant of the Y samples applied on untreated Al as a function of the immersion time.

The EIS measurements performed on the coatings applied on untreated aluminium gave the results represented in Figs. 2.35-2.38. The trends of the dielectric constant are plotted as a function of the immersion time. The elaboration of the data and the calculated water uptake values are displayed in Fig. 2.39. It can be noticed that the trends among the coatings of the same binder composition founded in the CC treated samples are not confirmed but the fact that the IPA based coatings show a lower water uptake finds a confirmation in this set of measurements, except for the green samples. For W-SD samples any water uptake is not computable (the coating capacitance remains almost unchanged).

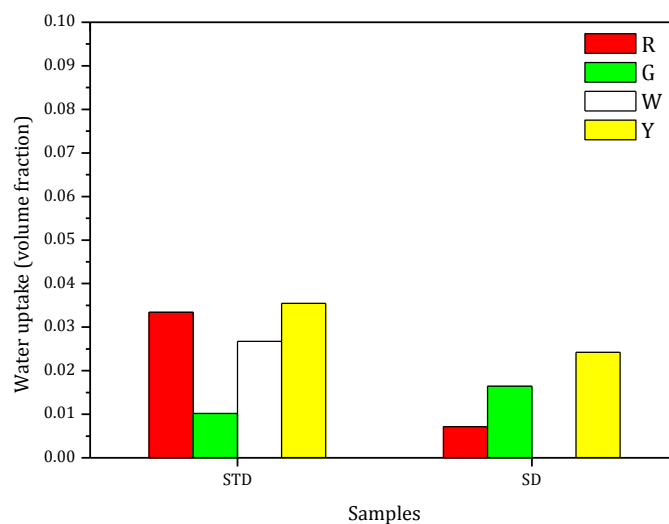


Figure 2.39 Water uptake volume fraction for samples applied on untreated Al substrate.

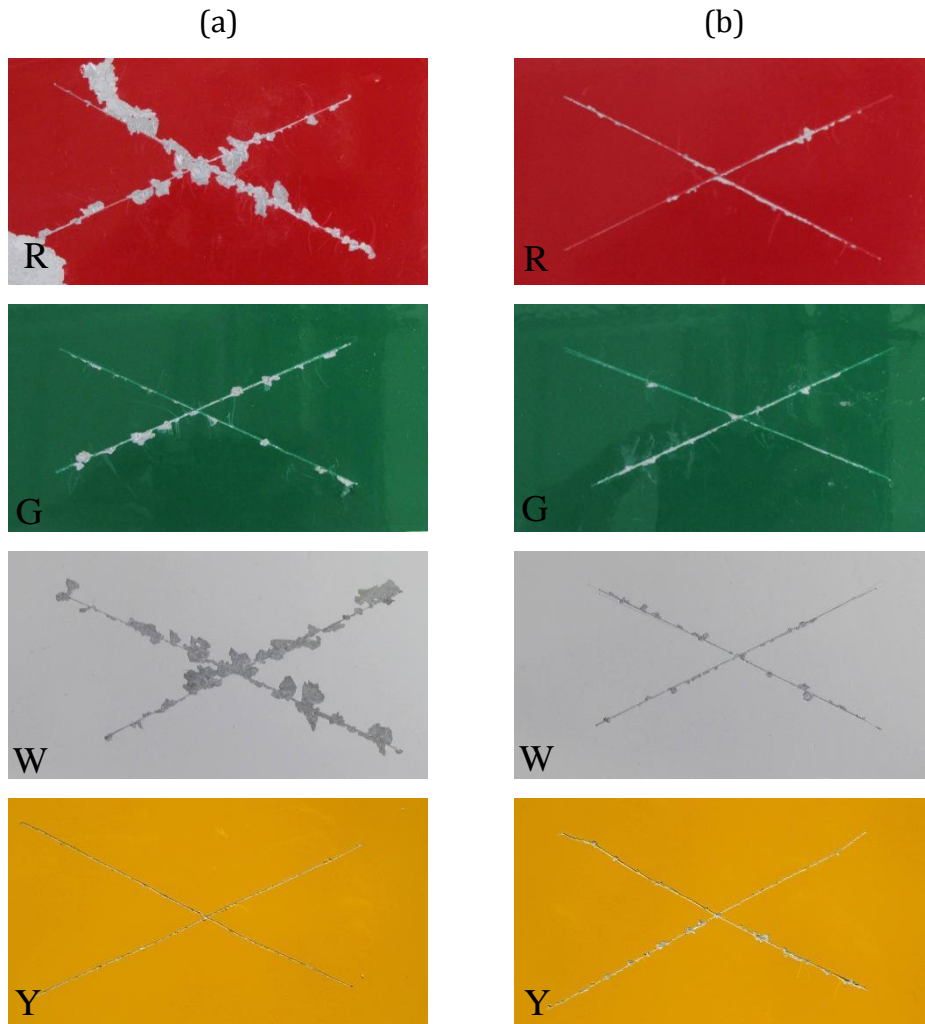


Figure 2.40 *Untreated Al samples after 1000 hs of acetic salt spray exposure: (a) STD samples, (b) SD samples on the right.*

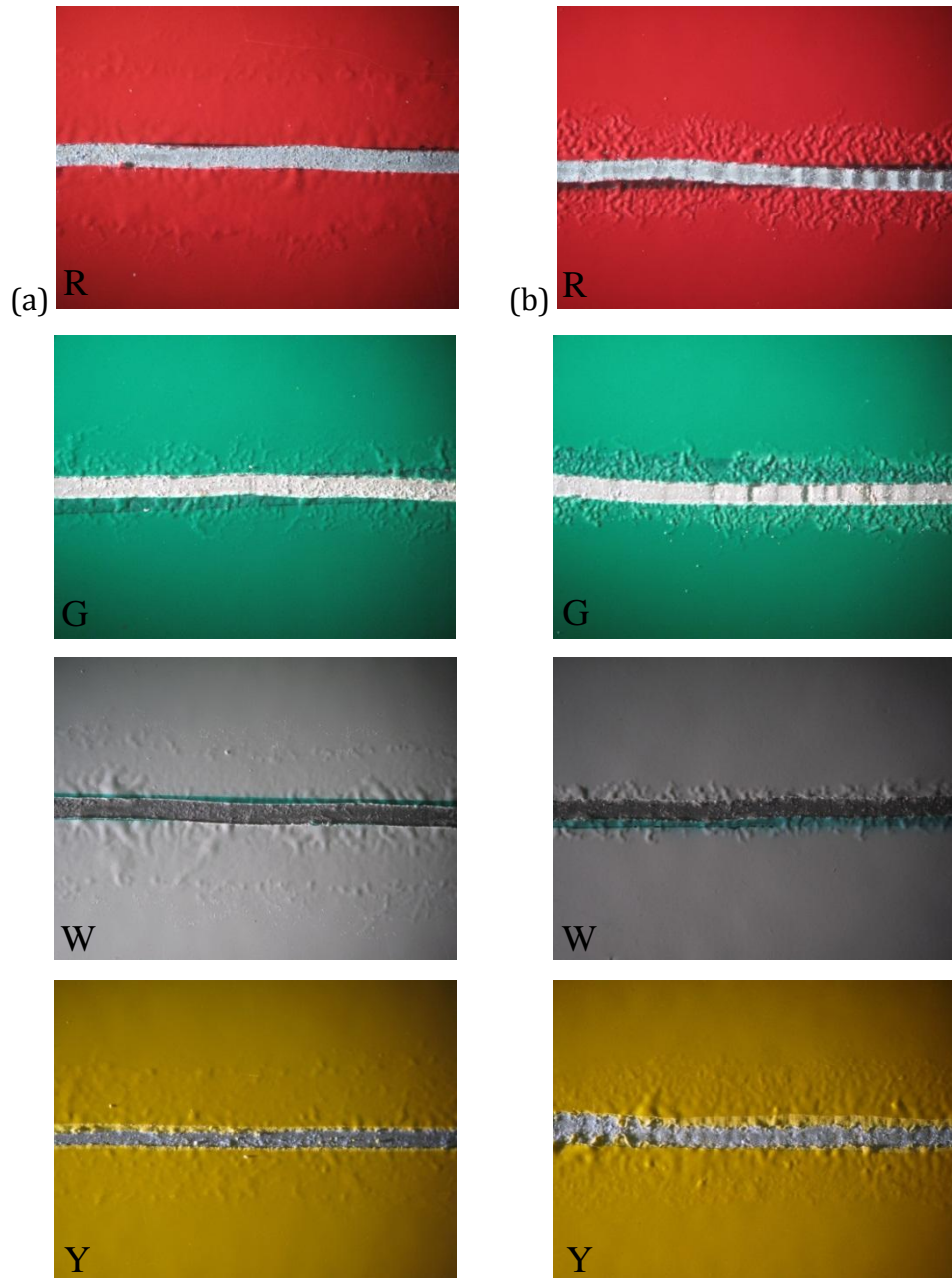


Figure 2.41 Untreated Al samples after filiform corrosion test:
(a) STD samples, (b) SD samples.

Fig. 2.40 shows the samples after the acetic salt spray exposure (1000 hours). In the durable version some differences are noticeable among the four pigments systems. The red and white coatings exhibit an apparently greater delamination areas, in addition blistering phenomena developing far from the scratch, in correspondence of the panels' edges, are observable. For these samples the difference between STD and SD is evident. Also in the case of green samples the SD displays a slightly worse behaviour. As concerning the yellow samples the STD and SD coating seem to exhibit the same results, perhaps slightly better in STD version.

In Fig. 2.41 the samples after the filiform corrosion test are shown. Unlike the CC treated samples the pictures have been taken after 5 days of test. The typical filaments of filiform corrosion are clearly recognizable. Red samples display a significant more extended corrosion in STD version, the same occurs for the white samples. The green and yellow seem to have more or less the same damage in both versions. Moreover, comparing the STD samples, the green one presents the lowest extent of the filaments; comparing the SD samples, the white one shows the best behaviour. Where the corrosion is more extended, i.e. R STD, W-STD, Y-STD and Y-SD, the filaments are still visible near the artificial scribe, but a further detachment is clearly noticeable at a certain distance from the scratch.

The results obtained for the coatings applied on untreated aluminum have emphasized different protective behaviors among the samples, unlike the results obtained on the CC samples. The less effective system

has allowed to discriminate between the standard and the super durable formulation and among the four different pigment systems. For summarizing and comparing the results, on the base of acetic salt spray test, filiform corrosion test, and EIS test a ranking among the samples was assigned (• = very good; ••••• = bad). In Tables 2.4-2.6 the rankings for the three tests are reported.

Table 2.4 Ranking – Acetic salt spray test

	STD	SD
R	•••••	•
G	••	•
W	••••	•
Y	•	••

Table 2.5 Ranking – Filiform corrosion test

	STD	SD
R	•••••	•••
G	••	••
W	••••	•
Y	••••	••••

Table 2.6 Ranking – Water uptake measurements

	STD	SD
R	•••••	•
G	•	••
W	•••	•
Y	•••••	•••

For the red pigmented coatings, the standard version shows worse protective performance than the superdurable version in both corrosion tests, and this result is confirmed by a higher water uptake. In the case of green pigmented samples the performances are good in standard and superdurable formulations, thus demonstrating the “green formulation constituents” the most durable among the investigated samples. The white pigmented samples show higher water uptakes and worse performances in acetic salt spray test and filiform corrosion test in standard version, whereas the properties are appreciably improved in the super durable formulation. Finally, in the case of the yellow pigmented samples the improvements in super durable version seen in the other samples are not confirmed. The water uptake values are quite high in both the formulations, the behaviour in filiform corrosion test is comparable, and in acetic salt spray exposure the delamination is very limited in STD and SD coatings. From this point of view, the higher content of organic pigments, even greater in super durable coatings, can play some role also in corrosion protection behaviour.

2.4 Conclusions

The use of powder coated aluminium alloys in architectural applications is nowadays widespread owing to its capability of meeting the demanding aesthetic requirements, as well as the protective function. However, improved durability is still a goal to achieve due to

the increasingly demanding market expectations, and the environmental restrictions concerning the use of toxic and dangerous substances and technologies.

The investigation, carried out in collaboration with Akzo Nobel Coatings, concerned polyester powder coatings with different pigments applied on pre-treated (chromate conversion) and untreated aluminium substrates. Two different binders were especially studied: polyester based on terephthalic-isophthalic acid (durable) and isophthalic acid (super durable). The experimental campaign was carried out for determining the decrease in aesthetic attributes during artificial weathering tests, and the reduction in the protective properties, via electrochemical techniques and standard accelerated laboratory corrosion tests. As regarding the aesthetic durability the super durable formulation was demonstrated to be significantly more effective. 2000 hours of UV exposure represented significantly severe test conditions, thus emphasizing the outstanding properties of these coatings. The improvements in the binder composition, pigments properties and additives have led to a remarkably increased durability from this point of view. With respect to corrosion protection, the results confirmed that the use of chromate conversion pre-treatment allows to obtain an excellent durability level which is barely influenced by the formulation of the coating. However, it was also probed that this pre-treatment makes hard to distinguish the contributions of the organic coatings in the protective capabilities of the coating-substrate system. Experimental findings obtained from the tests performed on untreated

substrates revealed that the formulation parameters related to the aesthetic properties (pigments) affect noticeably the barrier properties of the coating, and thus the corrosion protection. In particular, in the durable formulation, red, white and yellow pigment systems revealed some criticalities in the corrosion tests. Conversely, green pigments showed better performances. In the super durable version, in general the protective properties are proved to be enhanced but, for the yellow coatings, this is not confirmed. The negative/positive contributions in the protective properties could therefore depend both on binder chemistry, pigments types and all the other formulation parameters related to a specific colour of the coating. This investigation suggests that proper binder-pigments-additives combinations have to be designed for obtaining high performance durability organic coatings. Moreover, these results take a different meaning in the current scenario. Environmental restrictions do not allow the recourse to chromate conversion for surface pre-treating. Unfortunately, chromate conversion alternative surface treatments do not still provide the same effectiveness in terms of durability. From this point of view, organic coatings having enhanced durability must be developed for attaining the same durability level of coatings applied on chromate conversion treated metals. It is apparent that the development of novel formulations inspired by this strategy could represent the main topic of future works.

2.5 References

- [1] A. Forsgren, *Corrosion Control through Organic Coatings*. Boca Raton: CRC Press, 2006.
- [2] A. Tiwari and L. H. Hihara, "High performance reaction-induced quasi-ceramic silicone conversion coating for corrosion protection of aluminium alloys," *Progress in Organic Coatings*, vol. 69, pp. 16-25, 2010.
- [3] L. Fedrizzi, *et al.*, "Effect of powder painting procedures on the filiform corrosion of aluminium profiles," *Progress in Organic Coatings*, vol. 59, pp. 230-238, 2007.
- [4] R. Deane, "Powder coatings and sustainability," *Akzo Nobel website: www.akzonobel.com* Access date: October 31 2011, 2008.
- [5] G. J. Bocchi, *Modern Paints and Coatings*, vol. 76, p. 44, 1986.
- [6] M. Fedel, "Environmentally friendly hybrid coatings for corrosion protection: silane based pre-treatments and nanostructured waterborne coatings," Ph.D. thesis, Department of Materials Engineering and Industrial Technology, University of Trento, 2010.
- [7] *The 1999 Gothenburg Protocol to Abate Acidification, Eutrophication and Ground-level Ozone* www.unece.org/env/lrtap/multi_h1.html Access date: October 31, 2011.
- [8] P. G. d. Lange, *Powder Coatings - Chemistry and Technology*. Hannover, Germany: Vincentz Network, 2004.
- [9] D. Maetens, "Weathering degradation mechanism in polyester powder coatings," *Progress in Organic Coatings*, vol. 58, pp. 172-179, 2007.
- [10] B. W. Johnson, *et al.*, "An evaluation of the effect of light stabilisers on the exterior durability of polyester powder coatings for the architectural market " *Surface Coatings International Part B: Coatings Transaction*, vol. 82, pp. 134-141, 1999.
- [11] E. Dumain, "Use of analytical techniques to predict and correlate powder coating weatherability," in *Powder Coating 2004 Formulator's Technology Conference*, Charlotte, NC, USA, 2004.

Chapter 2

- [12] E. Scrinzi, *et al.*, "Influence of natural and artificial weathering on aesthetic and protective properties of organic coatings," *Corrosion Reviews* vol. 29, pp. 275-285, 2011.
- [13] G. Wypych, *Handbook of Material Weathering*, 3rd ed. Toronto: ChemTec Publishing, 1993.
- [14] G. Wypych, *Weathering of plastics testing to mirror real life performance*. Norwich, NY: William Andrew Publishing/Plastics Design Library, 1999.
- [15] L. F. E. Jacques, "Accelerated and outdoor/natural exposure testing of coatings," *Progress in Polymer Science*, vol. 25, pp. 1337-1362, 2000.
- [16] R. D. Armstrong, *et al.*, "An investigation into the UV breakdown of thermoset polyester coatings using impedance spectroscopy," *Corrosion Science*, vol. 37, pp. 1615-1625, 1995.
- [17] P. Malanowski, "Weathering of aromatic polyester coatings," PhD thesis, Eindhoven University of Technology, 2009.
- [18] J. F. Rabek, *Polymer photodegradation - mechanisms and experimental methods*, 1st ed. ed. London, UK: Chapman and Hall, 1995.
- [19] F. Deflorian, *et al.*, "Improvement of corrosion protection system for aluminium body bus used in public transportation," *Materials & Design*, vol. 27, pp. 758-769, 2006.
- [20] C. F. Sharman, "Filiform Underfilm Corrosion of Lacquered Steel Surfaces," *Nature*, vol. 153, pp. 621-622, 1944.
- [21] A. Bautista, "Filiform corrosion in polymer-coated metals," *Progress in Organic Coatings*, vol. 28, pp. 49-58, 1996.
- [22] A. Pourbaix, "Filiform corrosion: mechanisms and some possible consequences," *Rapports techniques CEBELCOR*, 2003.
- [23] J. L. Delplancke, *et al.*, "Filiform corrosion: interactions between electrochemistry and mechanical properties of the paints," *Progress in Organic Coatings*, vol. 43, pp. 64-74, 2001.
- [24] A. T. A. Jenkins and R. D. Armstrong, "The breakdown in the barrier properties of organic coatings due to filiform corrosion," *Corrosion Science*, vol. 38, pp. 1147-1157, 1996.

- [25] M. Fedel, *et al.*, "Correlations between the Volta potential and filiform corrosion on painted AA2024 aluminum alloy," *Surface and Interface Analysis*, vol. 42, pp. 199-204, 2010.
- [26] L. Fedrizzi, *et al.*, "Effect of chemical cleaning on the corrosion behaviour of painted aluminium alloys," *Electrochimica Acta*, vol. 47, pp. 2159-2168, 2002.
- [27] M. G. Olivier, *et al.*, "EIS evaluation of the filiform corrosion of aluminium coated by a cathoporetic paint," *Progress in Organic Coatings*, vol. 52, pp. 263-270, 2005.
- [28] H. K. Leth-Olsen, *et al.*, "Filiform corrosion of aluminium sheet. III. Microstructure of reactive surfaces " *Corrosion Science*, vol. 40, pp. 2051-2063, 1998.
- [29] X. Zhou, "The influence of surface treatment on filiform corrosion resistance of painted aluminium alloy sheet," *Corrosion Science*, vol. 45, pp. 1767-1777, 2003.
- [30] P. Kalenda and M. Petrasek, "Study of the resistances of organic coatings to filiform corrosion," *Macromolecular Symposia*, vol. 187, pp. 387-396, 2002.
- [31] L. Fedrizzi, *et al.*, "Study of aluminium filiform corrosion by using electrochemical techniques," *Electrochemical Methods in Corrosion Research Vi, Pts 1 and 2*, vol. 289, pp. 485-497, 1998.
- [32] S. Wernick, *et al.*, *The Surface Treatment and Finishing of Aluminium and its Alloys*. London: Finishing Publications, 1989.
- [33] T. Bellezze, *et al.*, "Electrochemical study on the corrosion resistance of Cr III-based conversion layers on zinc coatings," *Surface and Coatings Technology* vol. 155, pp. 221-230, 2002.
- [34] J. B. Bajat, *et al.*, "The influence of aluminium surface pretreatment on the corrosion stability and adhesion of powder polyester coating," *Progress in Organic Coatings*, vol. 69, pp. 316-321, 2010.
- [35] F. Deflorian, *et al.*, "Silane pre-treatments on copper and aluminium," *Electrochimica Acta*, vol. 51, pp. 6097-6103, 2006.
- [36] L. Fedrizzi, *et al.*, "Corrosion behaviour of fluotitanate pretreated and painted aluminium sheets," *Electrochimica Acta*, vol. 42, pp. 969-978, 1997.

Chapter 2

- [37] J. Ring, "TGIC: Latest Developments & Update of Progress in Global Substitution", in *PCE 2002*, Nuremberg, 2002.
- [38] T. A. Misev and R. v. d. Linde, "Powder coatings technology: new developments at the turn of the century," *Progress in Organic Coatings*, vol. 34, pp. 160-168, 1998.
- [39] E. G. Belder, *et al.*, "Cure characterization of powder coatings," *Progress in Organic Coatings*, vol. 42 pp. 142-149, 2001.
- [40] R. v. d. Linde, *et al.*, "Effect of physical aging and thermal stress on the behavior of polyester/TGIC powder coatings," *Progress in Organic Coatings*, vol. 40, pp. 215-224, 2000.
- [41] J. Zeno W. Wicks, *et al.*, *Organic coatings: science and technology*, 2nd ed. New York, Chichester, Weinheim, Brisbane, Singapore, Toronto: Wiley-Interscience, 1999.
- [42] D. M. Brasher and A. H. Kingsbury, "Electrical measurements in the study of immersed paint coatings on metal. I. Comparison between capacitance and gravimetric methods of estimating water-uptake," *Journal of Applied Chemistry*, vol. 4, pp. 62-72, 1954.
- [43] S. Mirabedini, "Corrosion performance of powder coated aluminium using EIS," *Progress in Organic Coatings*, vol. 46, pp. 112-120, 2003.

CHAPTER 3

Clear coats for automotive applications: response to mar damage

Automotive field can be surely considered one of the most severe contexts for the durability of the aesthetic appearance of organic coatings. In this framework, clear coats play a fundamental role and new strategies are continuously needed to satisfy increasingly demanding market expectations. From this point of view, the resistance to mar damage probably represents one of the most crucial point. Nowadays, the developed strategies aim to prevent the mar damage by increasing the plastic resistance of the paint systems. Hybrid clear coats, and especially nano-silica filled systems, can be considered the most representative solutions based on the *damage prevention* concept. Although very good results in terms of durability have been obtained with these innovative solutions, it is believed that excellent performances can be attained if a proper cross-linking is combined to the introduction of nano-silica particles.

The present chapter is devoted to give a contribution in this direction. To this purpose the mar damage process is firstly described and analysed, thus making it possible to establish the driving factors of the

damage phenomena. In this preliminary step the methodologies for assessing the mar resistance of organic coatings are also taken into account. A proper experimental campaign aimed at investigating the mar behaviour of common clear coats was then carried out in collaboration with PPG Industries. The mar behaviour of a 2-K polyurethane coating and nano-silica filled polyurethane coating were especially studied. Based on the results obtained from the state of the art analysis and the experimental campaign, an innovative clear coat embedding nano-silica particles and having an enhanced crosslinking level was developed. Experimental characterization of the mar behaviour of the proposed clear-coat confirmed the increased durability performances.

3.1 Introduction

The quality of a product is often associated with its appearance [1, 2], and this is especially true for the products with a high added value of the OEM area (Original Equipment Manufacturer Market). From this point of view, the needs of the market are continuously growing in automotive field [3]. Therefore, organic coatings in this field must satisfy increasingly important aesthetic requirements due to the consumers' higher expectations [4-7]. Multilayer coating systems are typically used to ensure the protection from corrosion phenomena and to give the aesthetic appearance to the final coating. Every layer has its

specific characteristics designed to guarantee high performances of the entire coating system [8]. Automotive basecoat/clearcoat paint systems were introduced into the market in the 1980s to improve the initial and long-term appearance of vehicles [4, 9]. The function of clear coats is especially giving a glossy surface aspect and guarantee long-term aesthetic attributes. The ability of the clear coats to retain the initial properties by withstanding the weathering stresses, chemical and physical degradation, is a key point in automotive coating industry [4-6, 9, 10]. Durability of appearance means colour and gloss stability and resistance to mar/scratch damage. The latter is one attribute that has consistently come to the forefront of customer satisfaction surveys. Customers desire a permanent, scratch-free finish on their car [4].

The scratch damage may occur at different scales from very small scratches which do not refract the light to large grooves which fracture the clear coat appearing white to our eyes [11]. The difference between scratch and mar lays essentially in the extent of the damage. The terms mar/marring are related to a light surface damage, shallow and narrow defects of few micrometres in size. On the other side, scratches abrasion may go deeply into the coating [12]. Several causes could produce this kind of damage: brushes of the automatic car washing, stone, sand or salt particles on the road, tree branches, keys, fingernails and many others. It is apparent that different types of scratches can be produced affecting the appearance of the surface, and in the worst cases, the protective properties of the coating system. A more detailed description

of the damage processes occurring at increasing applied force is given by Shen et al. [13] and reported in Fig. 3.1.

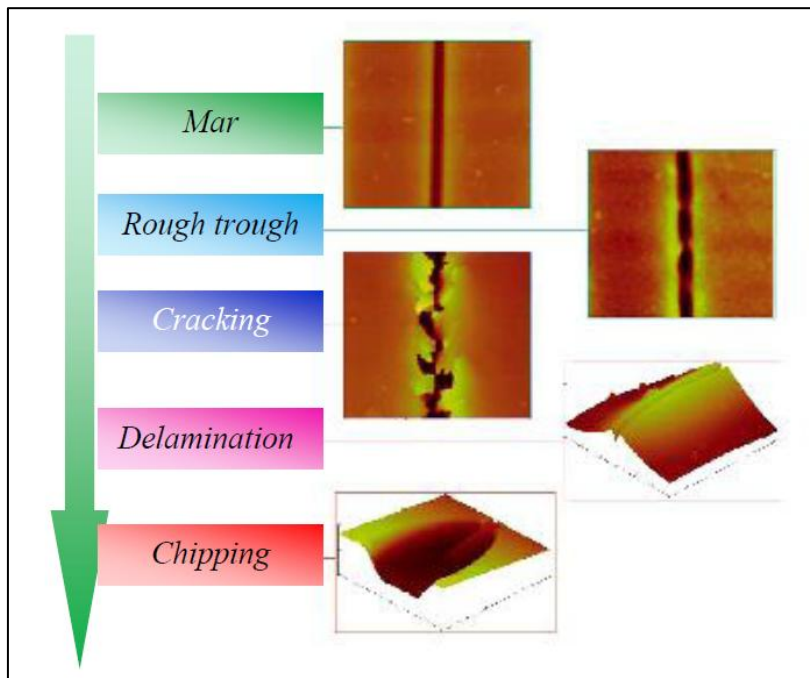


Figure 3.1 Five scratching modes under an increasing normal force [13].

A single mar is hardly detectable but more marring events are recognizable as a reduction of the gloss. More severe damages are clearly visible and fracture scratches have the potential to grow into the coating and reach eventually the substrate reducing the protective properties of the coating against the corrosion of the underlying metal. It is therefore apparent that mar/scratch resistance is a key property for the appearance attributed and their durability over time. Moreover,

it is worthy to notice that the visibility of mar/scratches on the surface is not a trivial issue due to the complexity of the involved variables [14]. These parameters concern the basecoat colour, lighting, orientation, duration of inspection and subjective factors regarding the observer as well as the dimensions and morphology of the scratch [15].

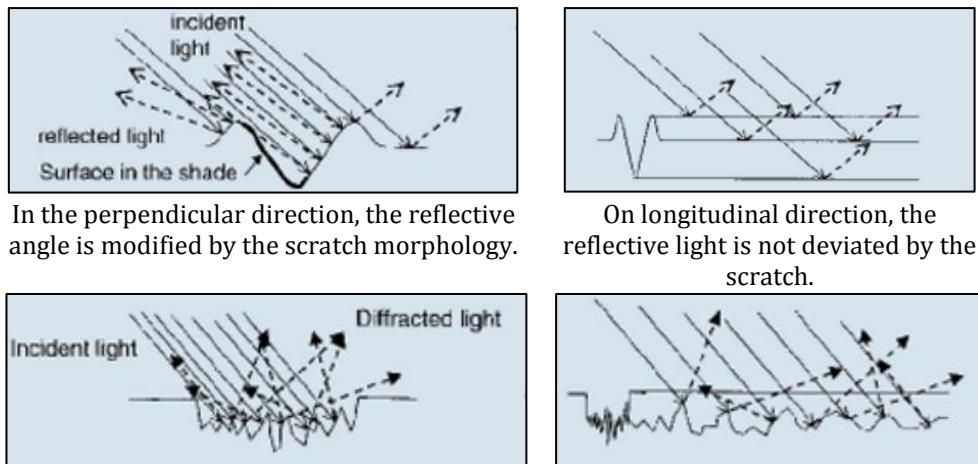


Figure 3.2 *Cross section views of two kinds of scratches. Impact of the morphology on the visibility [14].*

As described in Fig. 3.2, the visibility of fractured scratches is independent on the incident light and observation direction. On the other hand, the ductile and regular scratches are visible only under certain lighting conditions. If the scratch direction and the observation and lighting directions are coincident, the scratch is not visible [14].

The mechanisms of scratch and mar damages have been widely investigated in order to understand the driving factors and propose effective strategies for enhancing the resistance to this kind of mechanical damage, and consequently improving the aesthetic durability of clear coats. In the real field, the damage may consist of a single scratch but, more frequently, of a pattern of mars/scratches different in size and morphology. Understanding the damage mechanism is therefore quite hard. Conversely, by analysing the phenomena occurring during a single scratch applying a progressively increasing force, it is possible to investigate the response of the material. In Figs. 3.3 and 3.4 the damage mechanism of mar/scratch is schematically represented [16-18].

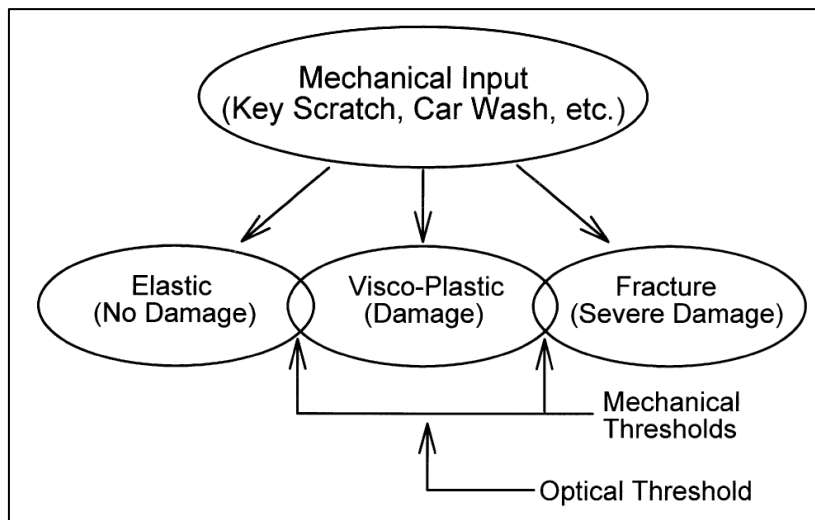


Figure 3.3 Damage mechanism of scratch and mar [15].

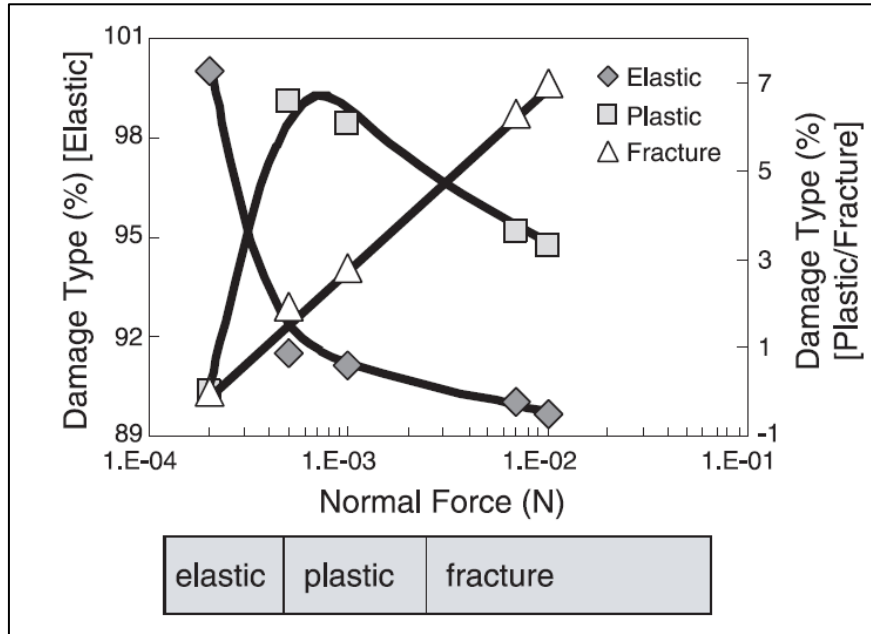


Figure 3.4 Change of damage structure and type with increasing normal loads [16].

At very low applied forces, the way of response is elastic, in this case a complete recovery occurs, and no visible damage will remain. At higher loads, plastic deformation takes place. The cross-section of the scratch is characterized by two shoulders on both sides of the ditch (Fig. 3.5a), built up by the displacement of material from the ditch during the marring. The extent of this pile-up represents an index of the material resistance to plastic deformation. The key parameter governing the plastic deformation resistance is the scratch hardness [19]. With further increasing in the applied force, another way of response might occur: fracture-type deformation. In this case the morphology of

damage is characterized by cracks along the scratch, the shoulders resulting from the previous plastic deformation, are fractured by tensile cracking phenomena (Fig. 3.5b). If the damage is particularly severe, mass losses occur, and, in extreme cases, detachment phenomena might take place involving also the adhesion between the coating and the substrate.

The passage from plastic response to fracture response is defined by the so-called *critical load*, i.e. the applied force at which the first fracture-type damage occurs. This parameter is governed by the elastic and fracture resistance properties, namely by the ratio between the elastic modulus and fracture energy [20].

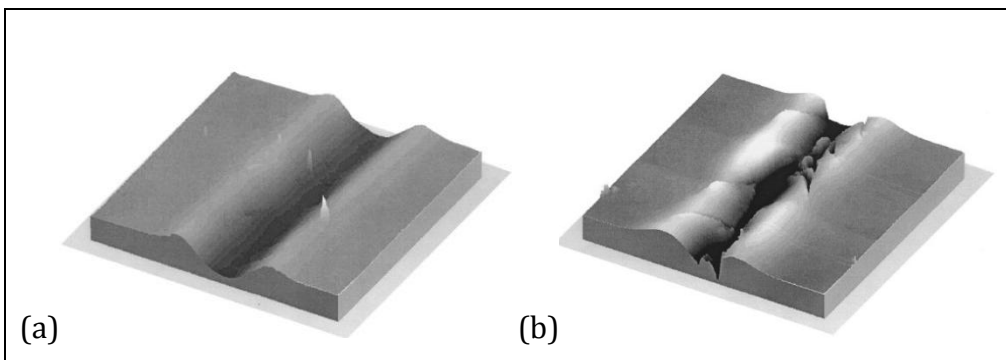


Figure 3.5 AFM images of (a) plastic deformation-type scratch and (b) fracture-type scratch [15].

As regards mar/scratch damage, another aspect should be considered: while fracture damage is accumulative, plastic flow damage can potentially be repaired by heating (e.g. reflow under a hot sun or a

period of thermal cycling) [12]. Due to the viscoelastic nature of the organic coatings this phenomenon can be exploited to increase the mar resistance by optimizing this *self-healing* behaviour. The glass transition temperature of the coating plays a fundamental role in this sense [21, 22].

By considering the abovementioned damage mechanisms, different strategies have been found to improve mar/scratch resistance. Coatings with high crosslinking density, introduction of fillers, hybrid materials with organic and inorganic domains, coatings with low glass transition temperature are some of the adopted strategies [23]. Coatings with increased crosslink density show an increased resistance to plastic deformation due to the yield strength of the network. The drawback concerns an increased brittleness, thus reducing toughness, with a lowering of the critical load. Embedding nano-particles is another possibility for enhancing the mar/scratch resistance without affecting the transparency of the clear coat [24-28]. Coatings with low glass transition temperature are aimed at exploiting the reflow properties and the ability to heal the scratches over time or typically after a thermal treatment.

Another important parameter that has to be considered is the influence of weathering on the mar/scratch resistance. The consumers' expectations concern the short-period but also the long-term performances in terms of resistance to mechanical damage. It is well

known that weathering factors influence the physical properties of the coatings [6], and consequently the mar resistance [5].

The aim of the work reported in the present chapter was to study a new possible strategy for further improvements in the mar resistance of polyurethane clear coats. Nano-silica filled samples and unfilled samples were compared and a novel clear coat with nano silica particles and an enhanced crosslinking was studied. Nano scratch experiments have allowed to analyse the material response and quantify the resistance to plastic deformation and fracture. As above explained, the main effect of mars concerns the aesthetic appearance, and field simulation test are needed to prove the actual improvement in the mar resistance. Taber test and falling abrasive test were performed for assessing the mar resistance by measuring gloss reduction, a property directly related to the surface appearance.

In the next paragraph a brief summary of the test methodologies for assessing the mar/scratch resistance is reported. Single-probe scratching tests and field simulation tests are described.

3.2 Methods of mar resistance assessment

As regards the mar/scratch resistance evaluation of organic coatings, many test methodologies have been developed [29-31]. Depending on the characterization to be performed, testing methods can be grouped into two categories: field simulation tests and single-scratch tests. The

former class is aimed at reproducing the real damage encountered by coatings, and subsequently analysing the coatings response on macro-scale. Although these approaches permit to explore the coating behaviour during the service conditions and derive important information, e.g. the trend of surface gloss as a function of the damage level, the material parameters driving the damage phenomena are usually hard to be distinguished. By contrast, the latter group focuses the attention onto the coating response during a single scratch. These methodologies allow to understand the damage phenomena on micro- or nano-scale, and unlike the field simulation tests, make it possible to distinguish the factors governing the damage process and enhance the coating properties for minimizing the damage effects. As it will be clear later, both kinds of analyses have to be accounted for developing high-performances clear coats. Depending on the coating properties to be optimized, the most suitable testing procedures must be firstly selected. To this purpose, the most common field simulation and single-scratch tests are presented. Advantages and drawbacks of each testing procedure are highlighted and the most effective testing analyses for the aims of the present investigation are finally selected.

Field simulation tests

Car wash test can be surely regarded one of the most effective testing procedures for evaluating the scratch/mar resistance of clear coats in automotive field [6, 11, 29, 31]. A typical car washing testing apparatus

is represented in Fig. 3.6. Damage process is produced by mean of a rotating brush put in contact with the sample moving back and forth. The brush is simultaneously sprayed with water containing quartz powder. Surface damage induced by this kind of test is characterized by a distribution of scratches preferably oriented along the brush movement. Both *plastic-type* and *fracture-type* scratches may be generated during the test due to the action of the brush and the presence of a third body [16, 31]. Mar resistance is estimated by measuring the gloss before and after the test, and is expressed as the percentage residual gloss with respect to the initial gloss value.

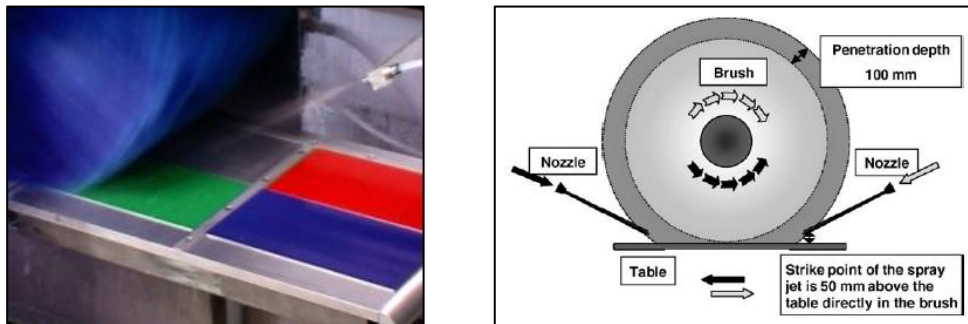


Figure 3.6 Car wash lab apparatus (Amtec Kistler GmbH) [29, 32].

The test method is able to truly reproduce the conditions undergone by clear coats during an automatic car wash, and, for this reason, it is widely used by automotive and coatings industries to determine the scratch resistance of clear coats. However, no information about the factors affecting the nucleation and morphologies of the scratches are

provided by this test. The major drawback of this testing procedure relies mainly in the lack of correlation between coating parameters, as the chemical formulation or the constitutive behaviour, and the damage evidences.

Scratch resistance of clear coats can also be estimated via the crockmeter test [6, 29]. Damage is promoted into the coating by subjecting the sample to linear rubbing (Fig. 3.7), and is characterized by the presence of a distribution of scratches mainly oriented along the rubbing direction.



Figure 3.7 *Crockmeter test* [33].

Both kinds of scratches regimes, ductile and brittle, can be produced during the test. In this test too, percentage retained gloss represents the measurement of the mar resistance. However, crockmeter test may be used also for measuring colour fastness and abrasion resistance. Despite of the differences between the straining processes inducing the damage in the car wash tests, good correlations between car wash and crockmeter test are found as regards to the measurement of the scratch

resistance [31]. Unfortunately, as already highlighted for the car wash test, the same drawbacks characterize the crockmeter test. No direct correlations between the damage morphology and coating properties can be derived from the experimental findings, but the final results of a specific damage process expressed in terms of residual gloss only.

The mar behaviour of paints systems can alternatively be measured via Taber testing, according to ASTM D6037 Standard. The experimental set-up is based on the use of two abrasive grinders pressed against the sample to be tested (Fig. 3.8) [34]. Surface damage is promoted by enforcing a rotation motion to the sample. The applied load on the grinders may be varied within the range of 250g till to 1000g, whereas the rotational speed of the sample is maintained constant (60 rpm) during the test. Taber test can be performed also in presence of free-abrasive dry means or slurries containing abrasive particles, thus allowing the study of third body abrasion of the system under investigation [35-37].

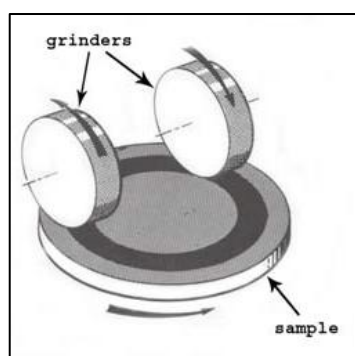


Figure 3.8 *Taber test configuration.*

Damage is uniformly located on an annular area and consists of a random distribution of ductile and brittle scratches having a typical “X shape” morphologies (Fig. 3.9). Scratches are generated by the abrasive particles embedded into the abrasive wheels or into the means if third body abrasion occurs. Mar resistance is measured as the percentage retained gloss with respect to the initial gloss [35-37].

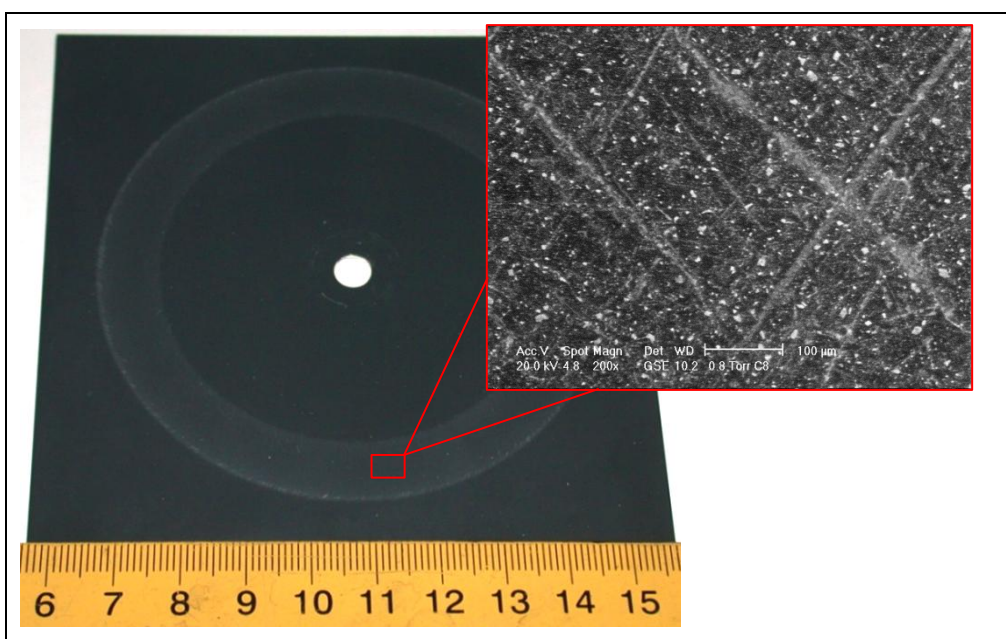


Figure 3.9 *Taber test: damage morphology.*

Although Taber test does not truly reproduce the damage processes occurring in paints systems during service conditions, the large number of experimental parameters (applied load, rotational speed, and the

characteristics of the grinding wheels and potential media between the grinders and the tested surface) which can be modified, and the relative wide ranges within which they can vary, make the Taber testing a powerful method for exploring different damage processes. However, it should be taken into account that this approach is characterized by the same limitations of the above presented methodologies.

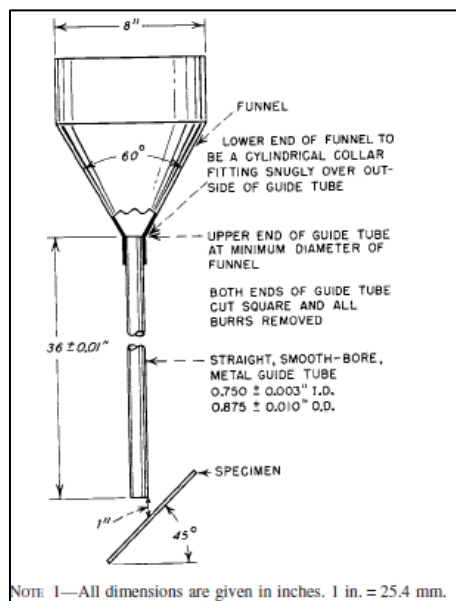


Figure 3.10 Falling abrasive test configuration [Standard ASTM D968].

Although falling abrasive test cannot be considered as a suitable method for inferring the mar behaviour of paint systems, it may provide interesting outcomes about the paint performances during the service conditions. The erosion-wear mechanisms induced by the falling

abrasive test, in fact, greatly differ from those corresponding to the described field testing methodologies [35, 38]. However, during the operating conditions of any paints, the occurrence of erosive-wear damage mechanisms cannot be neglected a priori.

Fig. 3.10 illustrates the basic principles behind the falling abrasive test. The experimental apparatus consists of a funnel at the upper part connected to a guide tube by which the abrasive agent flows by gravity. The sample is maintained at 45° respect to the guide tube, leaving a gap of 25 mm from the sample surface to the end of the tube. Surface damage is characterized by a uniform distribution of small craters having few micrometres as characteristic dimensions (Fig. 3.11) [35].

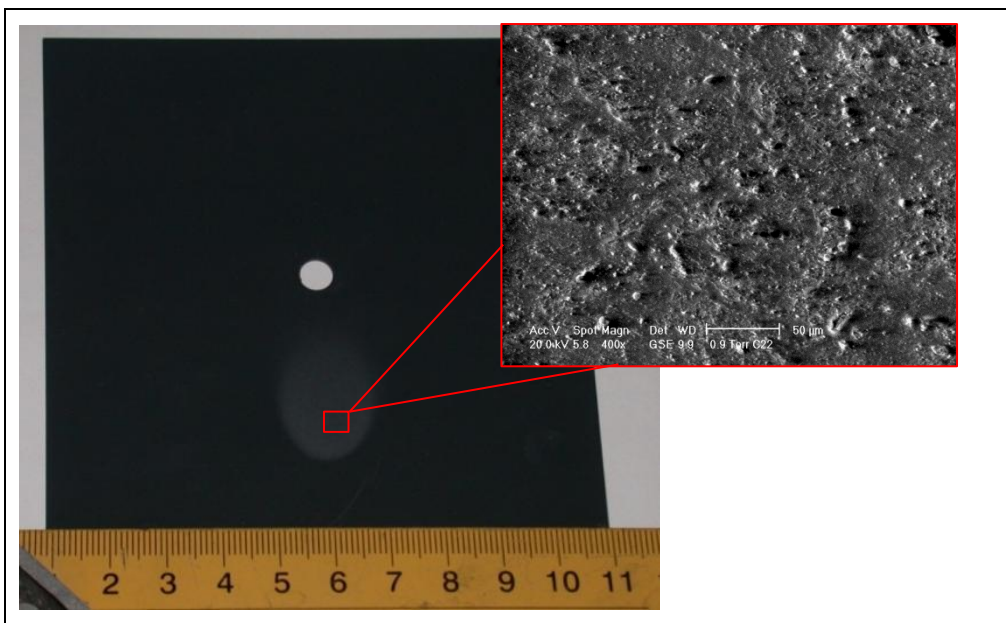


Figure 3.11 *Falling abrasive test: damage morphology.*

Single-probe scratching tests

The previous field simulation methodologies allow to evaluate the scratch/mar resistance by scratching the sample surface with multiple contact cuttings, and subsequently by measuring the percentage residual gloss. It has been recognized that the visibility of the scratches is mainly related to the morphology of the scratches [14]. From this point of view, single-scratch tests aimed at exploring the paint response at micro- and nano-scale represent the only way for investigating the correlations between mar resistance and coating characteristics. In this direction, many single-scratch procedures have been developed [13, 15, 16, 20, 22, 39-41], and the effort spent in this sense has led to standardized single-scratch tests [ASTM D5178, ASTM D7187]. According the Standard ASTM D7187, the scratch-test consists of the generation of scratches with a sphero-conical indenter drawn at a constant speed across the system to be tested. The indenter is pressed against the surface by applying a force which can be maintained constant or progressively increasing during the test (Fig. 3.12). For progressive loading, the critical load (L_c) is defined as the smallest load at which a recognisable failure occurs. For the constant loading mode, the critical load corresponds to the load at which a regular occurrence of such failure along the track is observed. The basic idea of this method is to measure the scratch/mar resistance of paints by quantitatively measuring the damage produced by an external known input. The estimation is performed by determining the relationship between the

damage shape and size and the external input (force applied to the indenter).

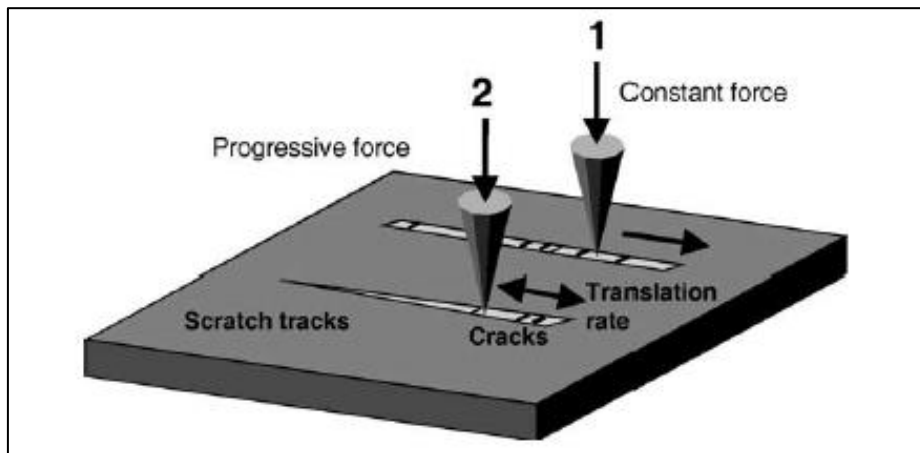


Figure 3.12 Principle of single-scratch test [29].

In more detail, the correlation between the damage characteristics and the applied load is expressed by mean of the magnitude of residual depth (RD), the plastic resistance (PR) and the critical load above which the plastic deformation process is replaced by the surface tensile cracking. According to the Standard, the magnitude of residual depth represents the permanent plastic deformation, whereas the plastic resistance is defined as the ratio between the normal load applied to the indenter and the magnitude of the residual depth.

3.3 Materials and experimental procedures

The investigation reported in the present chapter was carried out in collaboration with PPG Industries Research Center, Allison Park, PA (U.S.). The painted samples have been kindly provided by PPG.

Steel panels treated with standard phosphate pre-treatment have been coated with a four-layers coating system as represented in Fig. 3.13: a standard cationic electrocoat (20 μm), a spray primer (thickness about 15 μm), a basecoat (15 μm), and a clear coat (40-45 μm).

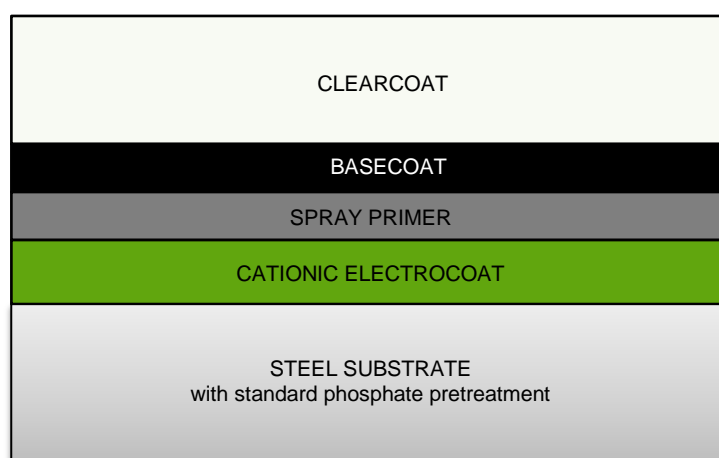


Figure 3.13 *The four-layers coating system.*

Three different 2-component isocyanate/polyol clear coats were considered (Table 3.1). Sample R does not contain any filler, samples NS

and NS-C have nano-silica particles in the surface layer but different crosslinking levels. In sample NS-C the crosslink density is increased owing to a secondary crosslink reaction which creates a separate structure. The silica is added as a surfactant stabilized colloidal dispersion. The size of the silica particles is lower than 50 nm.

Table 3.1 *The clear coat systems*

Sample	Characteristics of the clear coat
R	2K isocyanate/polyol (reference)
NS	2K isocyanate/polyol with nano silica
NS-C	2K isocyanate/polyol with nano silica and enhanced crosslinking

Fig. 3.14 shows a transmission electron micrograph of a cross section of sample NS. The total thickness of the layer is 40 μm , in the image the first 2 micrometres of the film are visible. Particles of about 15 - 20 nm in diameter are observable, they are crowded together at the surface, the boundary is about 2 particles thick and they almost touch each other in the boundary layer. In the remaining thickness of the film the particles are separated from each other by around 30 to 100 nm. The average distribution of particles at a distance of 100 nm from the surface looks about the same as the distribution at deeper distances.

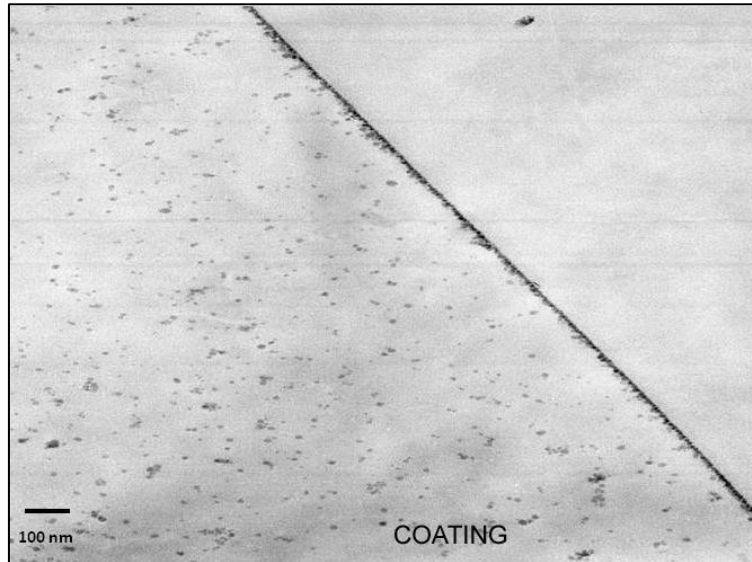


Figure 3.14 *Transmission electron micrograph of microtomed cross section of sample 2 (from PPG).*

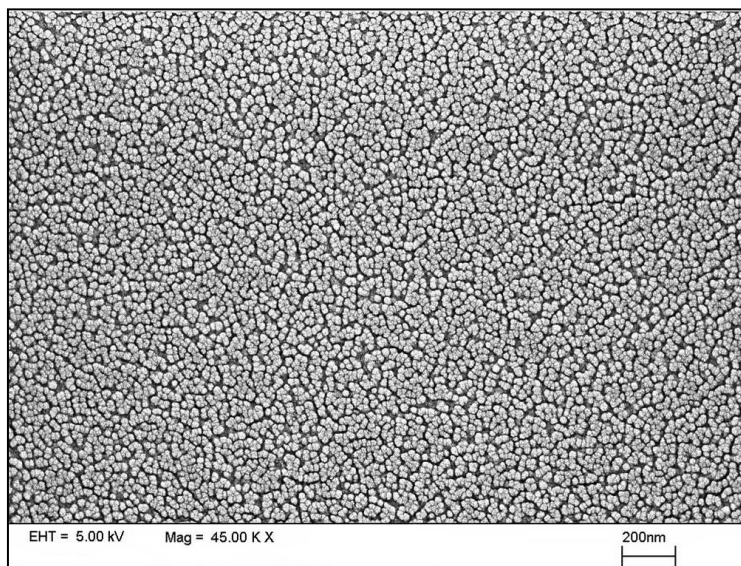


Figure 3.15 *Scanning electron micrograph of plasma ashed surface of sample 2 (from PPG).*

Fig. 3.15 shows a scanning electron micrograph of the plasma ashed surface of sample NS. It shows the near approach of the particles to each other in the surface layer. It is not possible to say that there is no compacting of one layer onto the one below during the processing, but the conditions of ashing were chosen so that this was not very likely.

The aesthetic properties of the coatings were assessed by gloss measurements, using a Picogloss 20°-60°-85° mod. 503 Erichsen glossmeter at 20° angle because of the high gloss surfaces of the samples (ASTM D523). The measuring area of the glossmeter was 10 x 10 mm². Table 3.2 reports the initial gloss of the three samples. The values are very similar, thus proving that the introduction of silica nano-particles does not affect the optical properties of the clear coat.

Table 3.2 Gloss values measured at 20°

Sample	Gloss 20°
R	90.7±0.3
NS	88.8±1.9
NS-C	89.9±1.0

A Mettler DSC30 differential scanning calorimeter was used to measure the glass transition temperature. The calorimetric test was performed in a temperature range between 0°C and 220°C at a heating rate of 10°C/min, under a nitrogen flow of 100 mL/min. A significant difference is noticeable in the glass transition temperature: the introduction of nano-silica particles leads to an increase in the T_g of

about 20°C, whereas the secondary crosslinking introduced in the sample NS-C creates a separate structure that does not affect the dominant polymer structure and does not influence the glass transition temperature.

Table 3.3 Glass transition temperature T_g

Sample	T_g (°C)
R	71
NS	89
NS-C	89

Three nano scratch tests have been performed on each sample using the CSM Nano Scratch Tester (NST). In Table 3.4 the experimental parameters of the test are reported.

Table 3.4 Nano scratch test parameters

Indenter Type	Spherico-conical
Indenter Radius	2 μm
Loading Type	Progressive
Scanning Load	0.2 mN
Initial Load	0.2 mN
Final Load	40 mN
Loading Rate	39.8 mN/min
Scratch Length	3 mm
Speed	3 mm/min

The scratches morphology was examined by Atomic Force Microscopy (AFM). The images (25x50 μm^2 scan area, 256x512 pixels) were acquired with a NT-MDT scanning probe microscopy solver P47H

equipped with a Smena scanner (scanning by probe). The measurements were performed in contact mode, with a Si cantilever (spring constant of 0.03 N/m) and a tip radius of 10 nm, at a scanning rate of 1Hz. The first portion (50 μm) of each scratch was analysed. After a thermal treatment at 60°C for two hours [4], the scratches were examined again to quantify the recovery induced by the temperature. In order to examine the same region of the scratch, the scan area was delimited by four micro-indentations.

The abrasion tests were carried out with a Taber Abraser 5131 according to ASTM D6037 Standard, using CS10 wheels and an applied load of 250 g. Every 10 cycles gloss was measured. The entire test consisted of 50 cycles. The falling abrasive test (Elcometer 1700 Falling Sand Tester) was carried out with Ottawa (silica) sand as abrasive agent. The gloss measurements were performed after a certain amount of abrasive was passed through the device, in increments of 25 ml. The worn surfaces were examined using optical microscope (ZEISS Stemi 2000-C) and environmental scanning electron microscope TMP ESEM FEI (ESEM Philips XL30) to highlight the morphology of the damage and correlate it to the changes of gloss.

The samples subjected to 20 cycles of Taber test and a fall of 25 ml of abrasive were thermally treated (60°C for two hours) and the gloss changes were then measured.

Nano scratch experiments, Taber test and falling abrasive test were repeated for weathered samples after 1000 hours of ultraviolet (UV-A)

exposure. In this way, the influence of UV radiation exposure on the mar resistance of the samples was investigated.

3.4 Results and discussion

In the next paragraphs the results of mar characterization of the three samples, the recovery effects of the thermal treatment and the influence of UV weathering will be described and discussed. Nano scratch test results are firstly reported followed by the data obtained in the field simulation tests, i.e. Taber test and Falling Abrasive test [42].

3.4.1 Mar behaviour characterisation

The results obtained for the three investigated coatings from nano scratch experiments are summarized in Figs. 3.16-3.18. For sake of clarity, the experimental curves obtained from one test are reported for each coating typology. The penetration depth and the residual depth are plotted as function of the scratch length with the normal force applied to the indenter during the test. According to ASTM D7187 Standard, the penetration depth is calculated as reported in Eqn. 3.1:

$$PD = C_3 - C_1 \quad (3.1)$$

where C_3 is the displacement of the indenter during the scratch and C_1 is the displacement during the pre-scan, while the magnitude of residual depth is given by Eqn. 3.2:

$$RD = C_2 - C_1 \quad (3.2)$$

where C_2 is the displacement of the indenter during post-scan and C_1 is the displacement during the pre-scan.

Finally, the plastic resistance is defined as the ratio between the normal load applied to the indenter F_N and the residual depth RD (Eqn. 3.3):

$$PR = \frac{F_N}{RD} \quad (3.3)$$

It is apparent that the estimation of the plastic resistance must be performed in the plastic regime of the scratch process, namely at force values lower than the critical load.

By analysing the curves (Figs. 3.16-3.18), it is possible to distinguish the presence of the plastic and brittle regimes. The large fluctuations in the trend of the residual depth and penetration depth curves denote the occurrence of tensile cracking.

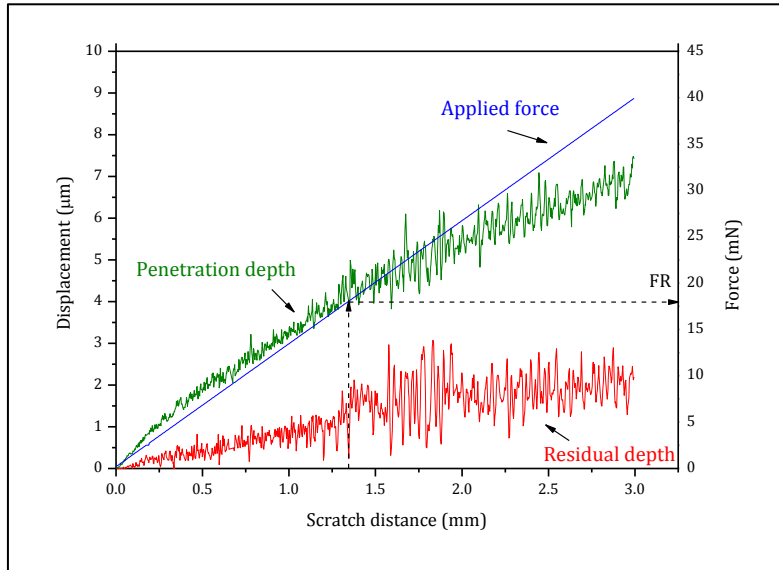


Figure 3.16 Data from nanoscratch experiment – Sample R.

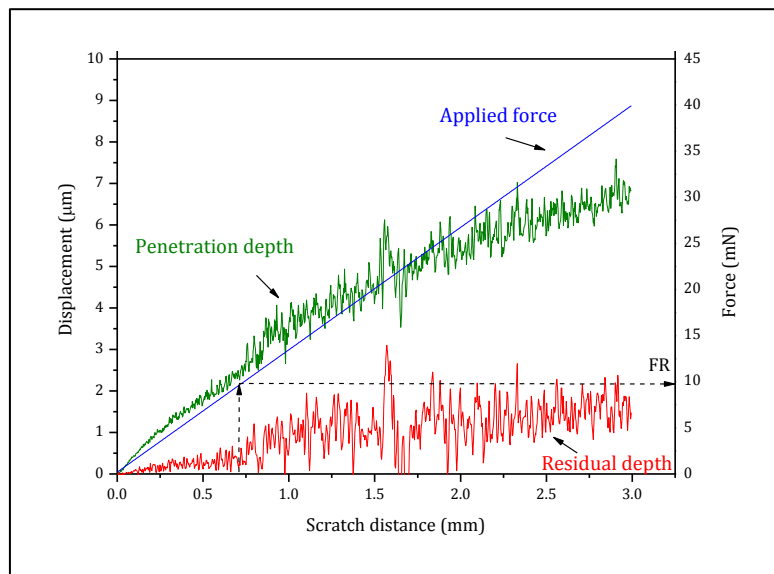


Figure 3.17 Data from nanoscratch experiment – Sample NS.

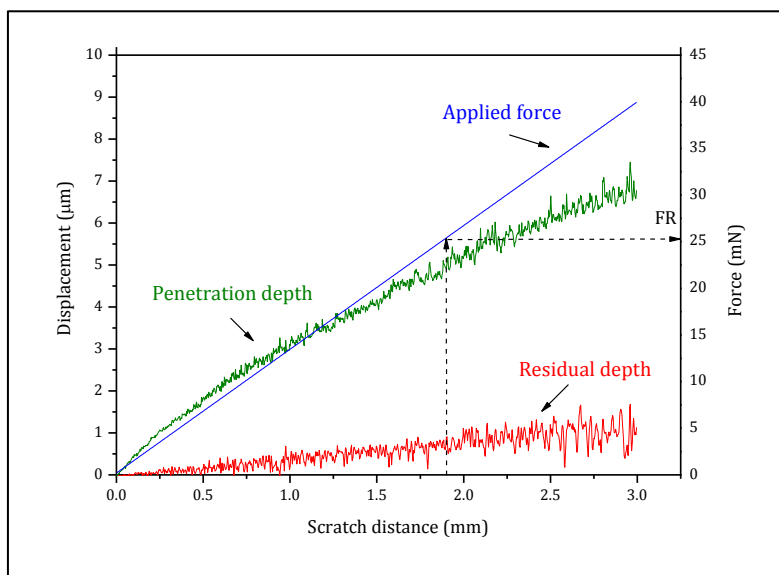


Figure 3.18 Data from nanoscratch experiment – Sample NS-C.

The optical observations of the scratches produced by the indenter allow to establish the exact point where the first fracture occurs. Fig. 3.19 shows these points for the investigated coatings. For sample R (Fig. 3.19a) the first fracture occurred at 1.3 mm approximately from the beginning of the scratch, whereas for samples NS and NS-C at distances of 0.75 and 1.9 mm, respectively. In terms of critical loads FR (Fig. 3.20), these distances correspond to average values of 18.45 ± 1.17 , 9.73 ± 0.48 , and 23.89 ± 2.07 mN, respectively. It should be noted that the introduction of nano-silica particles promotes a decrease in the critical load of about 50%. However, if a proper crosslinking is considered in combination with nano-particles, the critical load increases remarkably more than twice.

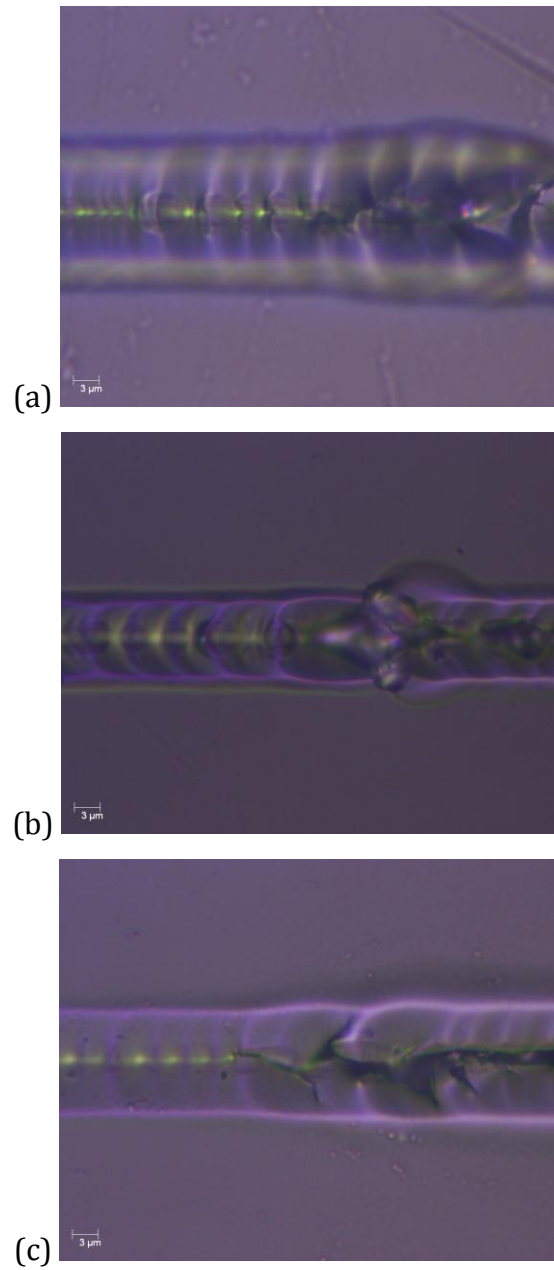


Figure 3.19 *Optical micrographs of the first brittle failure: (a) sample R; (b) sample NS; (c) sample NS-C.*

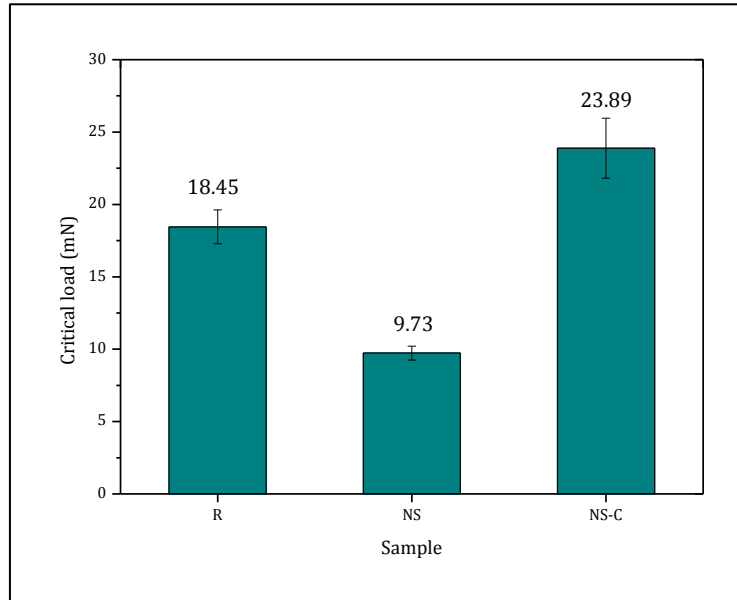


Figure 3.20 Critical load (optically evaluated).

Besides the determination of the ductile-brittle transition, the residual depth curve permits to infer the plastic capabilities of each sample. Fig. 3.21 illustrates a detail of the residual depth curves trend till to the critical load obtained for the three samples. Although the experimental data are characterized by an appreciable scatter, they seem to fall close to a line passing through the origin of the axes. This line was used to estimate the plastic resistance. Average slopes of 0.82, 0.54 and 0.36 mN/mm for R, NS and NS-C, respectively, were found to be quite representative of the observed responses. As suggested by the Standard, a normal force of 5 mN was chosen for computing the plastic resistance.

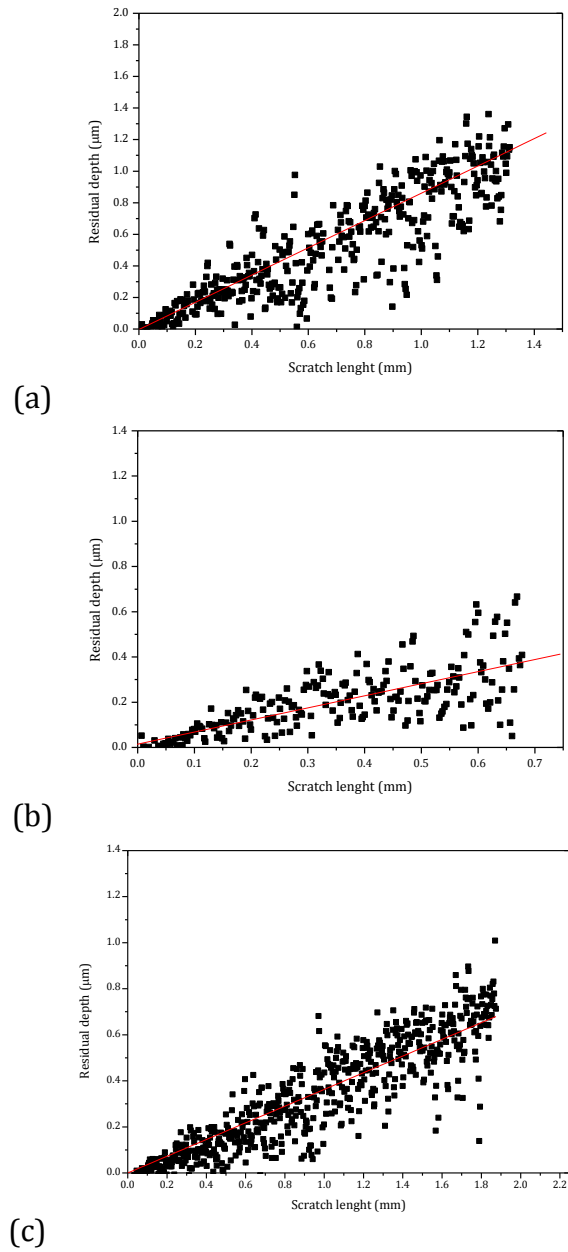


Figure 3.21 Residual depth curves till to the critical load for (a) sample R, (b) sample NS, (c) sample NS-C.

The results summarized in Fig. 3.22 show that the sample NS have an increased plastic resistance with respect to the reference sample. However, the innovative sample NS-C displays a further increment in the plastic resistance.

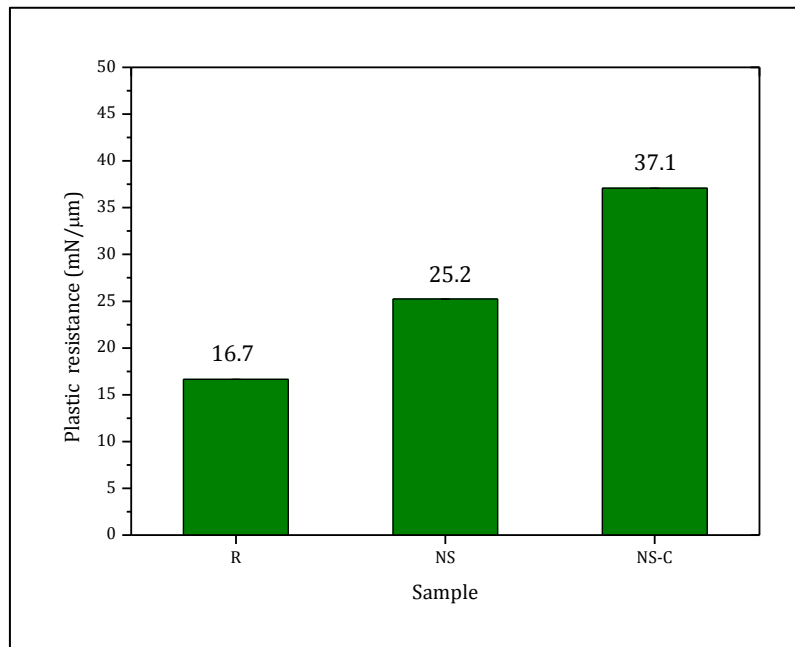


Figure 3.22 *Plastic resistance calculated by considering a normal applied force of 5 mN.*

A more detailed comprehension of the deformation phenomena can be derived from the investigation of the damage morphology. By analysing the scratch profile, useful information can be obtained as reported by John et al. [18] and Shen et al. [22] (Fig. 3.23). The authors proposed this model for calculating the responses of the coating to marring

stresses. The percentage elastic deformation, plastic deformation and fracture are computable as following (Eqn. 3.4-3.6):

$$\% \text{ elastic deformation} = \frac{(A_{ind} - A_{dit}) \times 100}{A_{ind}} \quad (3.4)$$

$$\% \text{ fracture} = \frac{(A_{dit} - A_{shs}) \times 100}{A_{ind}} \quad (3.5)$$

$$\% \text{ plastic deformation} = \frac{(A_{shs}) \times 100}{A_{ind}} \quad (3.6)$$

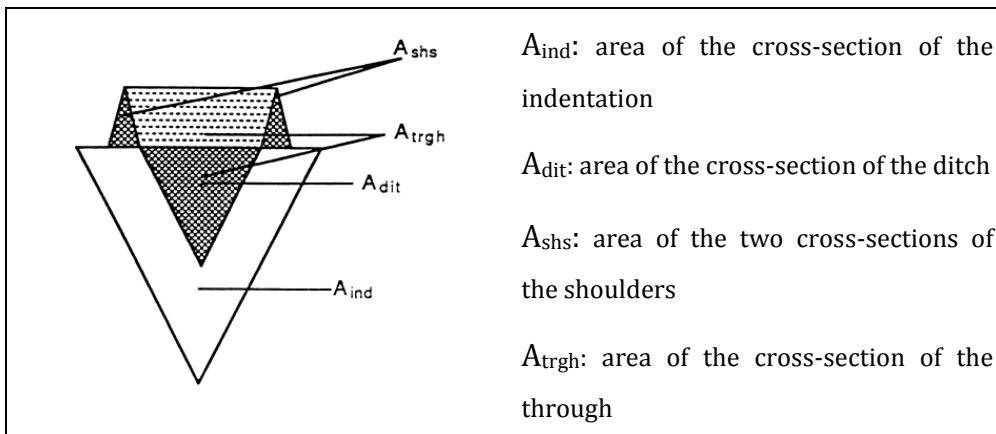


Figure 3.23 Cross-section areas used in calculating responses of a coating to marring stress [18].

On the base of this model, the morphology of the scratch in the plastic regime was analysed.

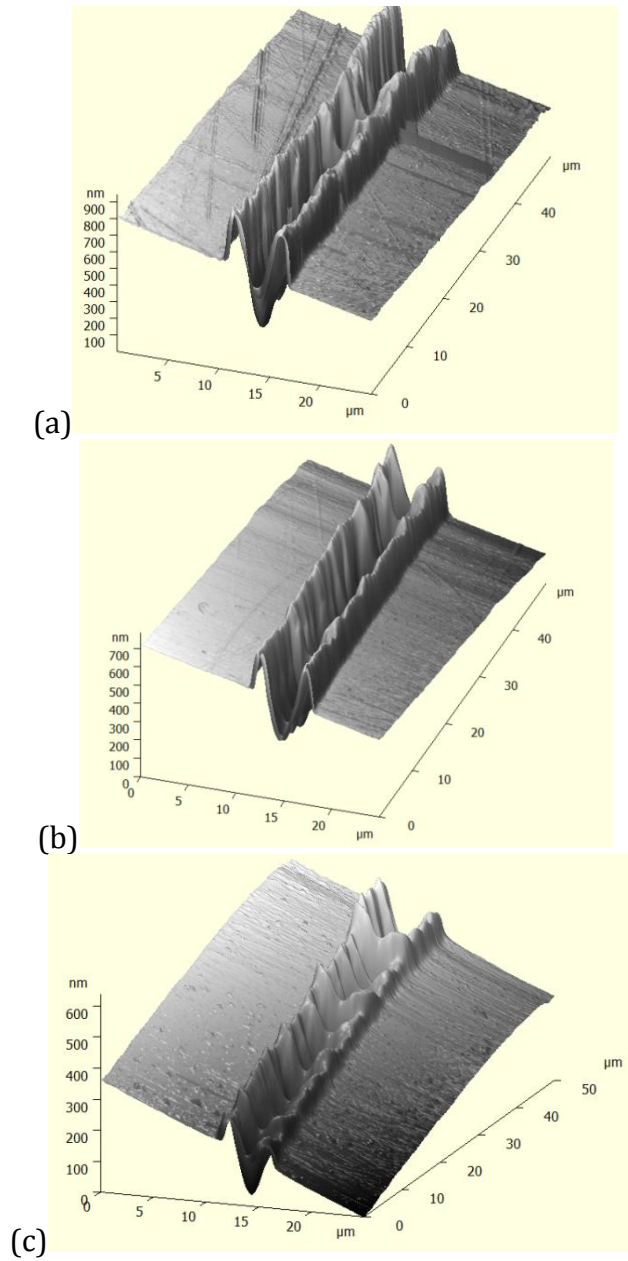


Figure 3.24 AFM images: scratch morphology (a) sample R; (b) sample NS; (c) sample NS-C.

Fig. 3.24a-c shows the AFM images of the scratch. In all the samples two apparent shoulders are recognizable on the sides of the ditch indicating a plastic deformation occurred during the scratch in this first part where the applied forces are very low (around 1 mN). For each sample 10 cross-section profiles along the mar were considered. After enforcing a zero setting, the average heights of the two shoulders and the ditch were calculated and the correspondent areas were found by integration (Fig. 3.25).

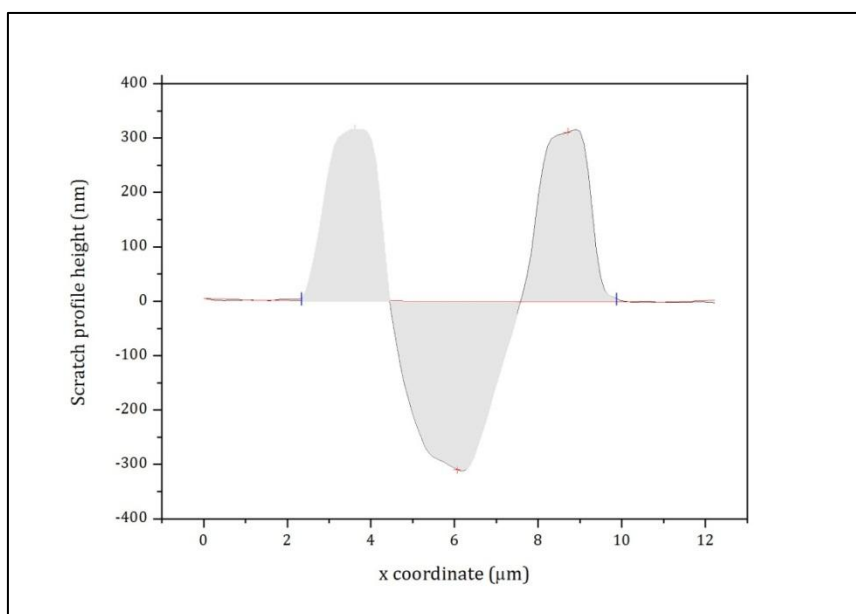


Figure 3.25 Analysis of the cross-section profile: the heights and the areas of the shoulders and the ditch were considered.

Figs. 3.26-3.28 display four example cross-section profiles for each sample. Although the profiles show a certain variability in the height of the shoulders, depth of the ditch and their areas, it is, however, reasonable to conduct a statistical treatment of the data. The differences among the samples R, NS and NS-C are quite apparently visible. The introduction of nano-silica leads to a reduction of the shoulders height and ditch depth, and also the magnitude of the areas is lower. The enhanced crosslinking of sample NS-C produces a further reduction of the abovementioned quantities.

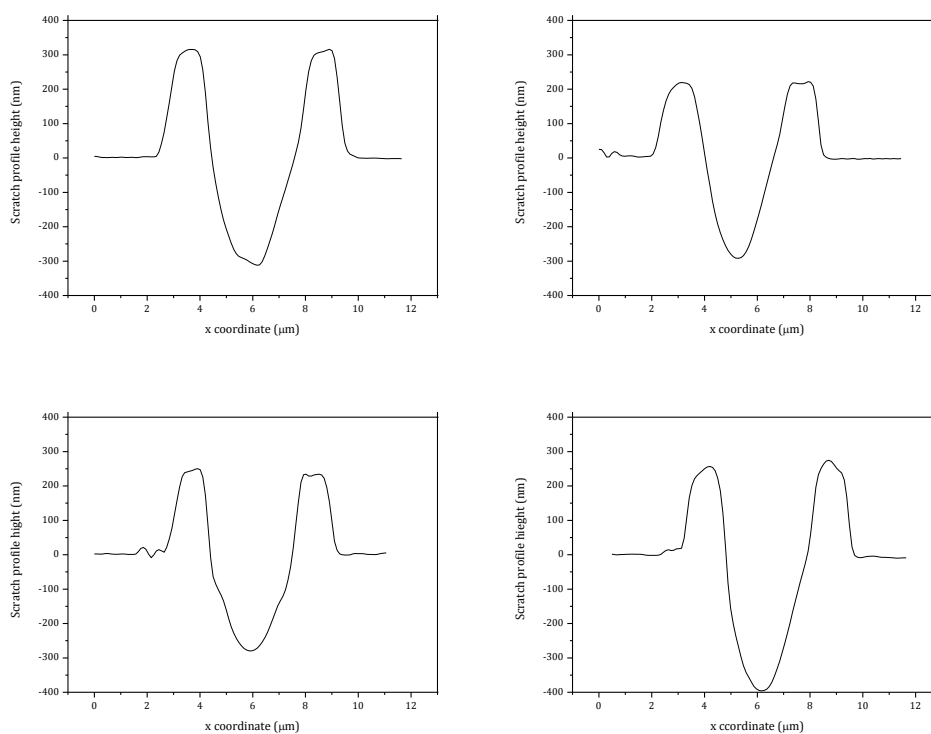


Figure 3.26 Cross-section profiles for sample R.

Chapter 3

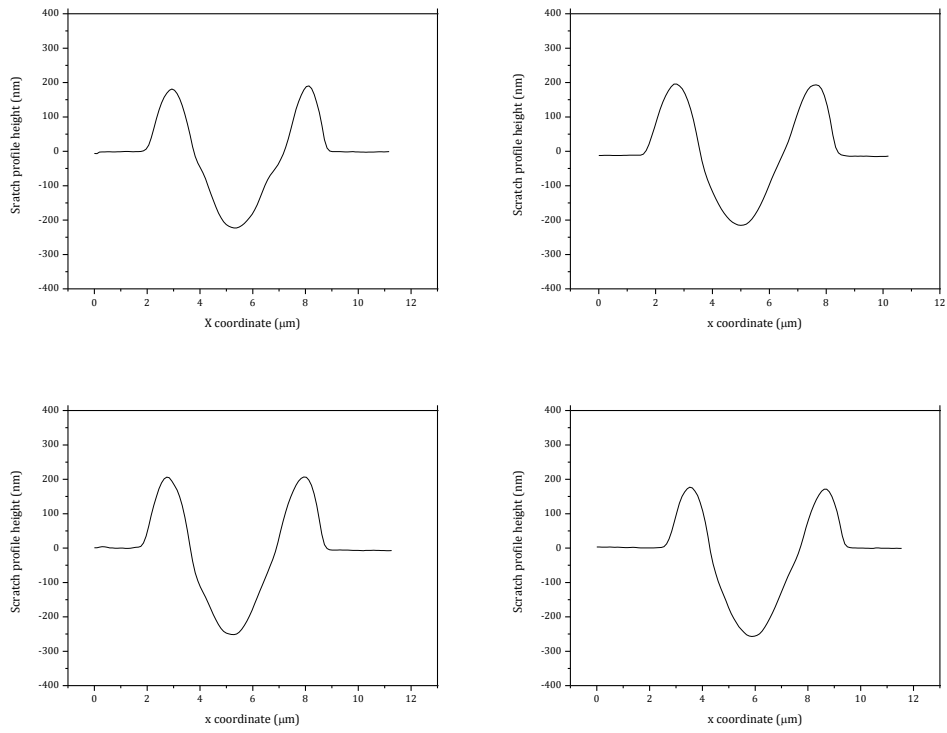


Figure 3.27 Cross-section profiles for sample NS.

Chapter 3

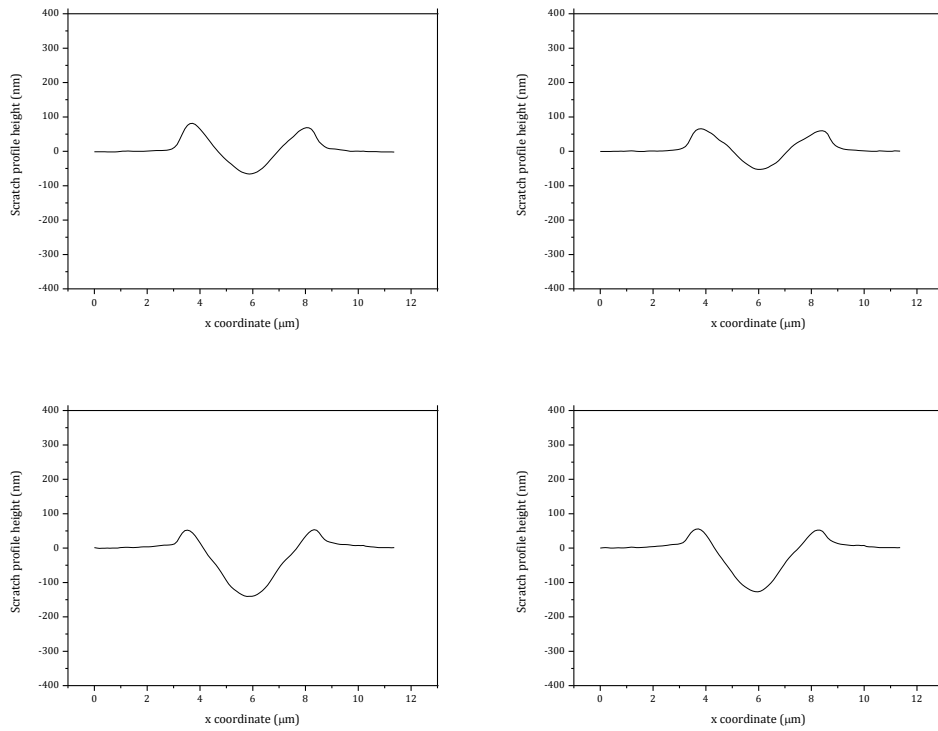


Figure 3.28 Cross-section profiles for sample NS-C.

For a more clear comparison, the average values obtained from the statistical analysis of the considered cross-section profiles are represented in Figs. 3.29-3.30.

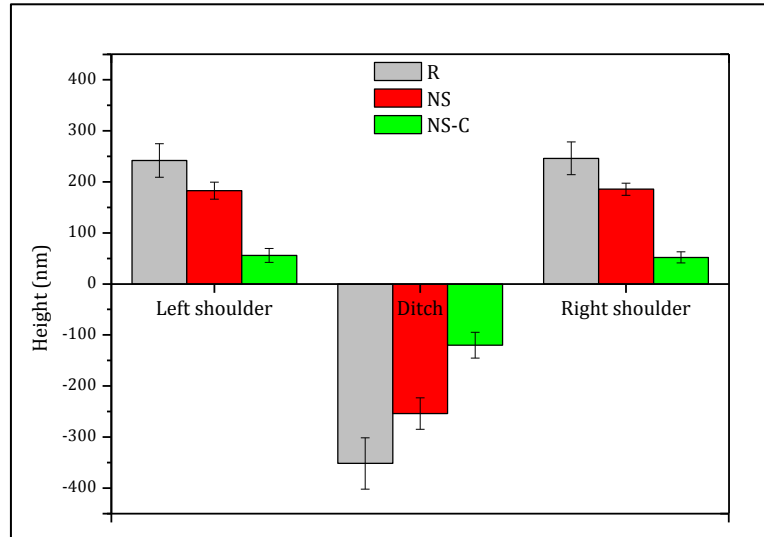


Figure 3.29 Cross-section profiles analysis: average values of shoulders height and ditch depth.

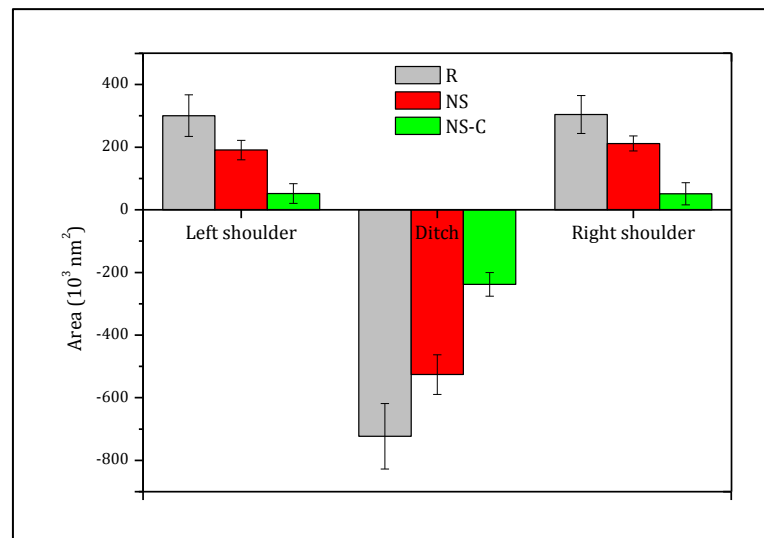


Figure 3.30 Cross-section profiles analysis: average values of shoulders areas and ditch area.

Nano silica containing samples show a decrease in shoulders height of about 25% and in ditch depth of about 28%. NS-C coatings display a further considerable reduction, around 70% for the shoulders and 53% for the ditch with respect to the NS sample. In Fig. 3.30 the areas comparison is reported. The ditch area is plotted in the negative Y half-plane just to distinguish it from the shoulders area. The evaluation of the areas confirms the trend: NS sample shows a reduction of 34% in shoulders area and 27% in ditch area with respect to the R sample; NS-C sample shows a further reduction of 75% in shoulders area and 55% in ditch area with respect to NS sample.

Taber test results

The results obtained by performing nano scratch experiments have been compared with the results of gloss measurements in Taber test and falling abrasive test. In Fig. 3.31 percentage residual gloss as a function of Taber cycles is reported. A clear difference is observable among the three samples. Sample R shows an immediate reduction of gloss after the first 10 cycles, and then a more gradual decrease. Sample NS, but even more sample NS-C, show an apparent improvement in gloss retention. At the end of the test after 50 cycles, samples R, NS and NS-C have a residual gloss of 10%, 42% and 79%, respectively.

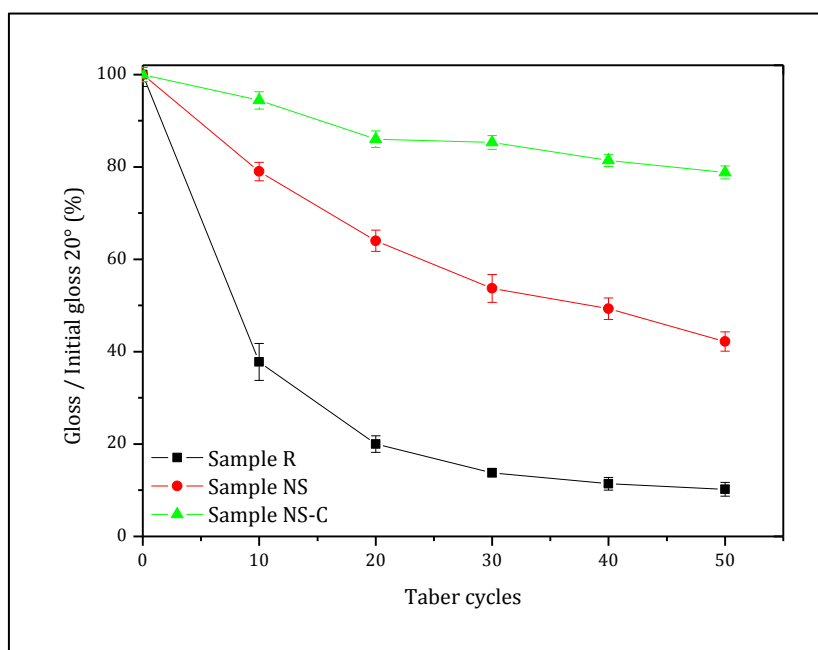


Figure 3.31 Percentage residual 20° gloss during Taber test.

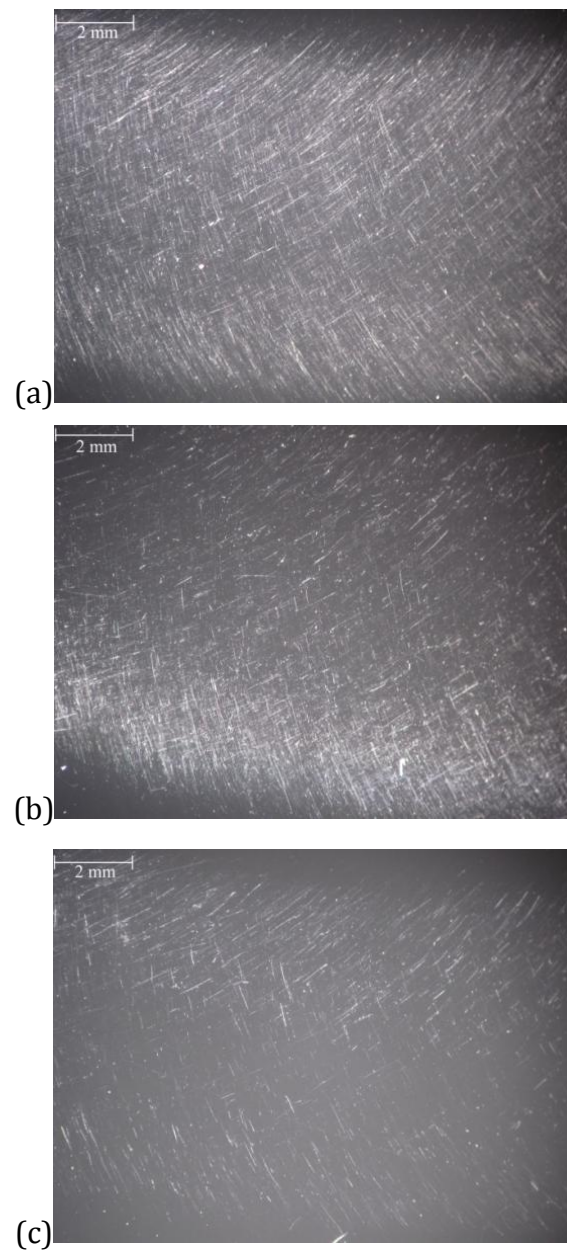


Figure 3.32 Optical micrographs of the abraded surfaces after Taber test (50 cycles):
a) sample R, b) sample NS, c) sample NS-C.

The optical micrographs (Figs. 3.32a-c) of the abraded surfaces after 50 Taber cycles confirm the results obtained by gloss measurements. It is visually appreciable the increasing enhancement in mar resistance from sample R to sample NS-C. The presence of the nano-silica particles in the surface layer increases the scratch hardness with a consequent higher mar resistance. Sample NS-C shows a still less damaged surface with a lower density of defects, thus proving that the enhanced crosslinking level increases further the clearcoat mar resistance.

By observing the damaged surfaces of the three samples by ESEM microscope, it is possible to recognize plastic-type and fracture-type scratches. In Fig. 3.33 ESEM micrographs of sample R are reported as example. The ductile mars (Fig. 3.33a) show the typical smooth edges, whereas the brittle scratches have the characteristic notched edges. The presence of plastic-type mars suggests the potential recovery properties of the material, as it will be shown in the next paragraph.

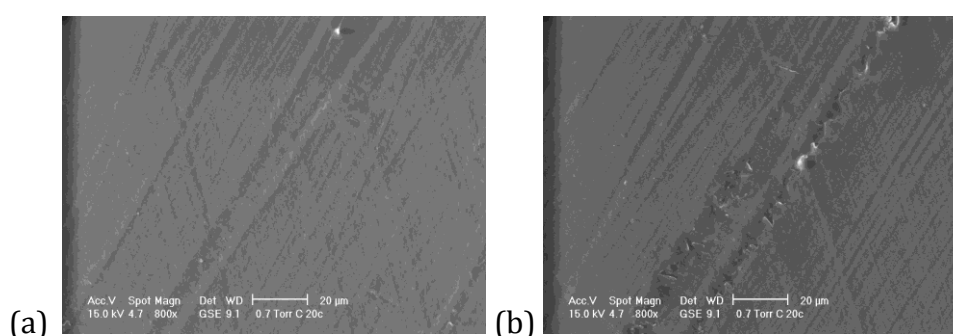


Fig. 3.33 ESEM micrographs of the abraded surface of sample 1 after 20 Taber cycles: a) ductile scratch, b) brittle scratch.

Falling abrasive test results

The falling abrasive test confirms the results obtained in the Taber test. As shown in Fig. 3.34, where the percentage residual gloss is plotted as a function of the amount of fallen abrasive, with respect to the Taber test, the gloss decrease appears to be more gradual, thus revealing the experimental conditions of this test less aggressive in terms of degradation of aesthetic appearance. Sample NS-C shows the highest resistance to the erosion damage: after 100 ml of fallen abrasive the retained gloss is equal to 20% for sample R, is 40% for sample NS, and 66% for sample NS-C.

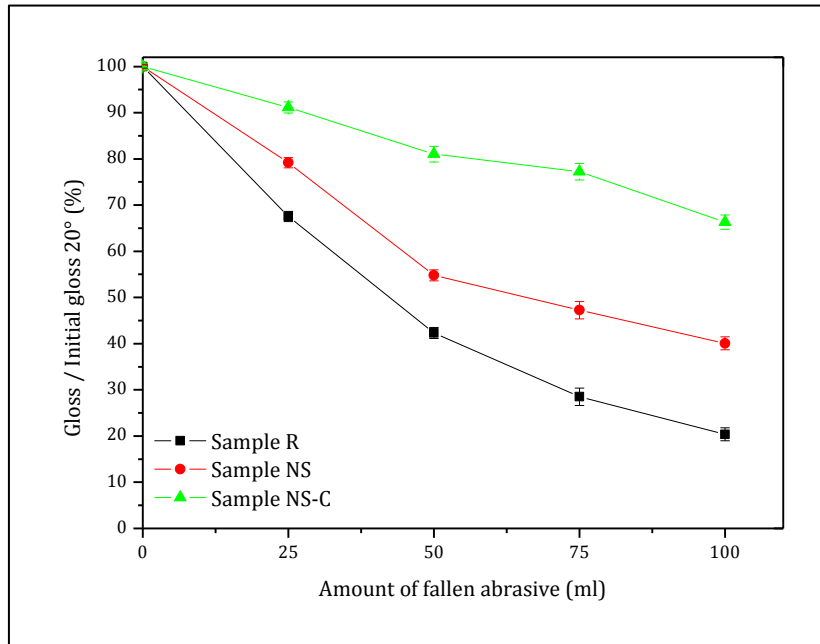


Figure 3.34 Percentage residual 20° gloss during Falling Abrasive test.

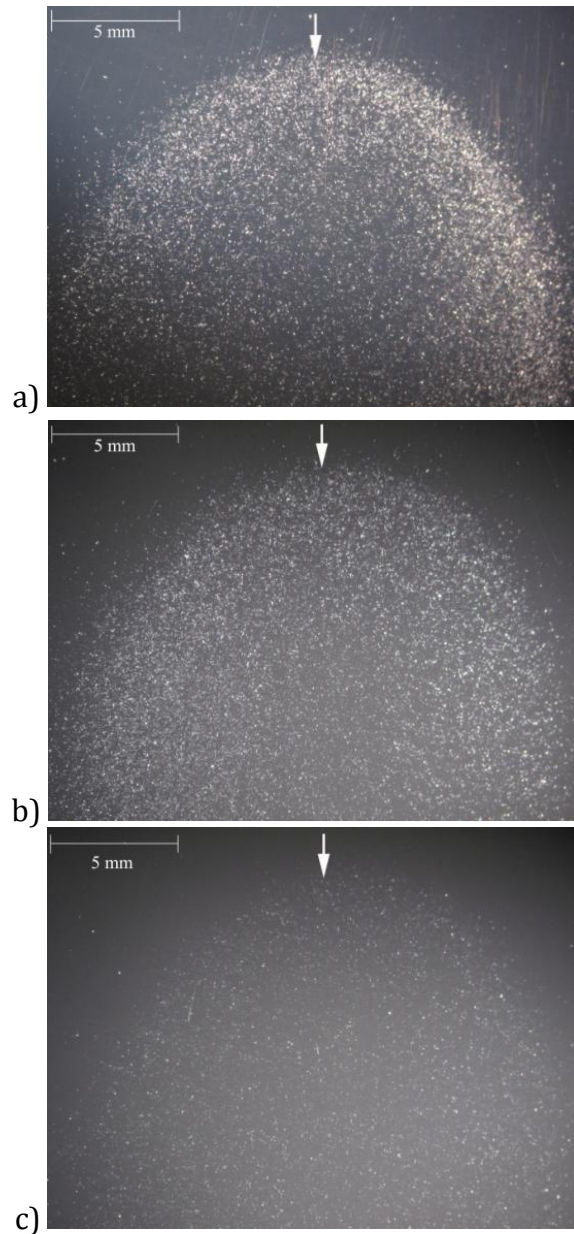


Figure 3.35 Optical micrograph of the abraded surfaces after the falling abrasive test (25 ml): a) sample R, b) sample NS, c) sample NS-C. The arrows indicate the direction of abrasive fall.

The optical micrographs of Figs. 3.35a-c show the damaged surfaces of the samples after 25 ml of fallen abrasive. The small defects produced by the erosion process of the abrasive silica particles are clearly visible, densely crowded in sample R, much less present in sample NS-C.

The results of these field simulation tests highlight the positive role played by the silica nano-particles which, crowded in the first nanometres of the clear coat, increase the hardness, thus enhancing significantly the resistance to mar and erosion damages. The results highlight the further improvement introduced with the innovative clear coat NS-C. The combined action of the nano-particles and the enhanced crosslinking level determines a higher gloss retention in both abrasion tests.

3.4.2 Analysis of the recovery properties

Recovery properties are also investigated in order to get a complete picture of the mechanisms and phenomena involved in mar/scratch damage. The scratches produced in nano scratch experiments and subjected to the thermal treatment are analysed by AFM, the morphology was studied with the same procedure described in the previous paragraph. The 3D images are displayed in Fig. 3.36a-c.

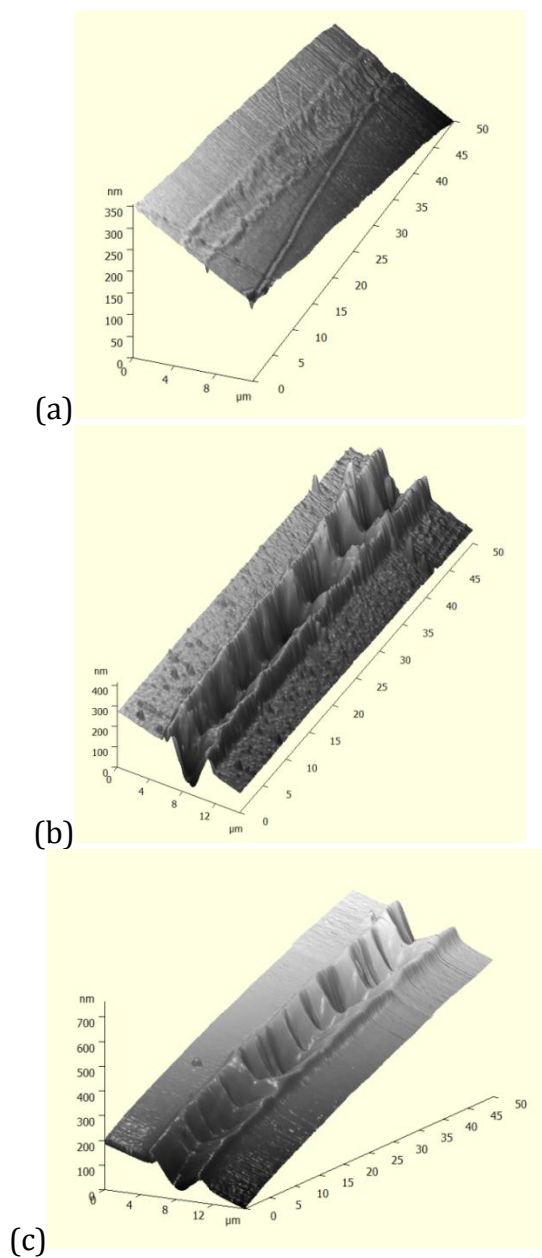


Figure 3.36 AFM images after thermal treatment: (a) sample R; (b) sample NS; (c) sample NS-C.

The high recovery degree of the reference sample R is apparently observable in Fig. 3.36a and in the four examples cross-section profiles in Fig. 3.37. In samples NS and NS-C the extent of the recovery is clearly lower. The differences between these two samples are better appreciable in the statistical analysis of the profiles.

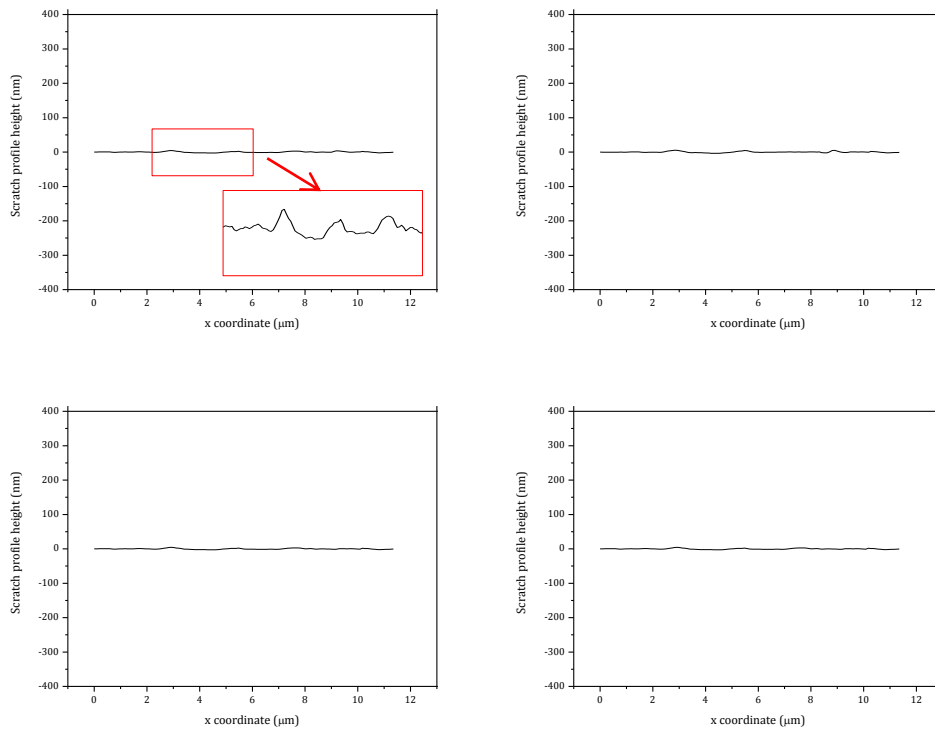


Figure 3.37 Cross-section profiles of sample R after thermal treatment.

As abovementioned, sample R shows an almost complete recovery of the mars (Fig. 3.37). No shoulders or ditches are recognizable in the

Chapter 3

profiles but are become indistinct in the surface roughness profile. From a qualitative investigation of the profiles (Figs. 3.38 and 3.39) samples NS and NS-C present a certain degree of recovery but a more precise and quantitative measurement of the recovery extent can be derived from the analysis of shoulders and ditch heights and areas.

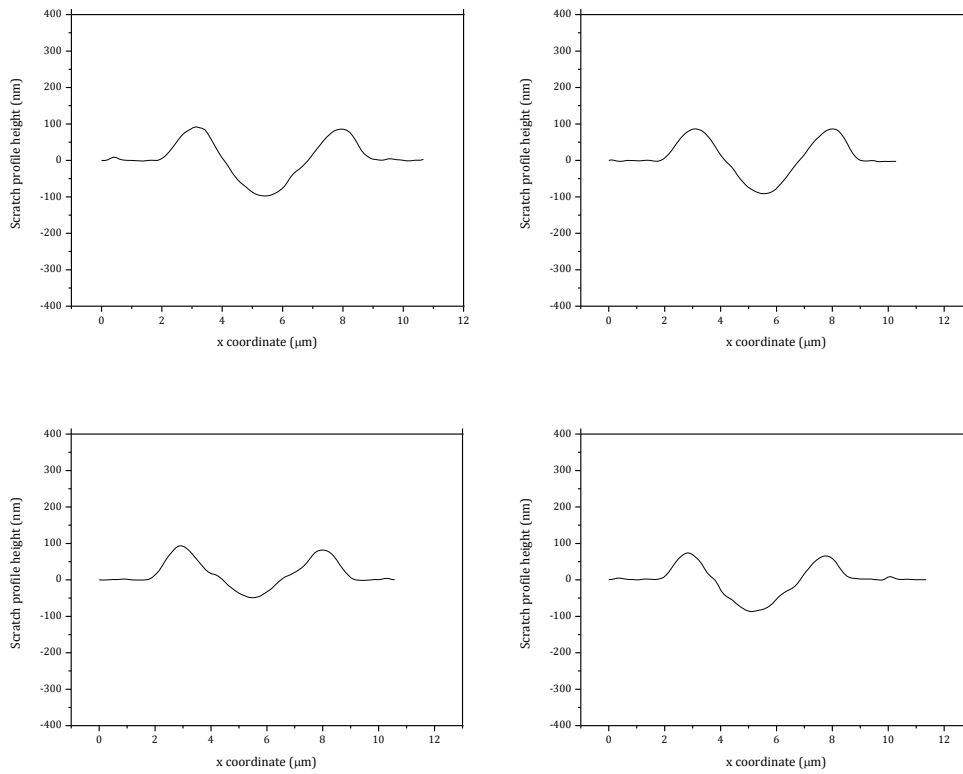


Figure 3.38 Cross-section profiles of sample NS after thermal treatment.

Chapter 3

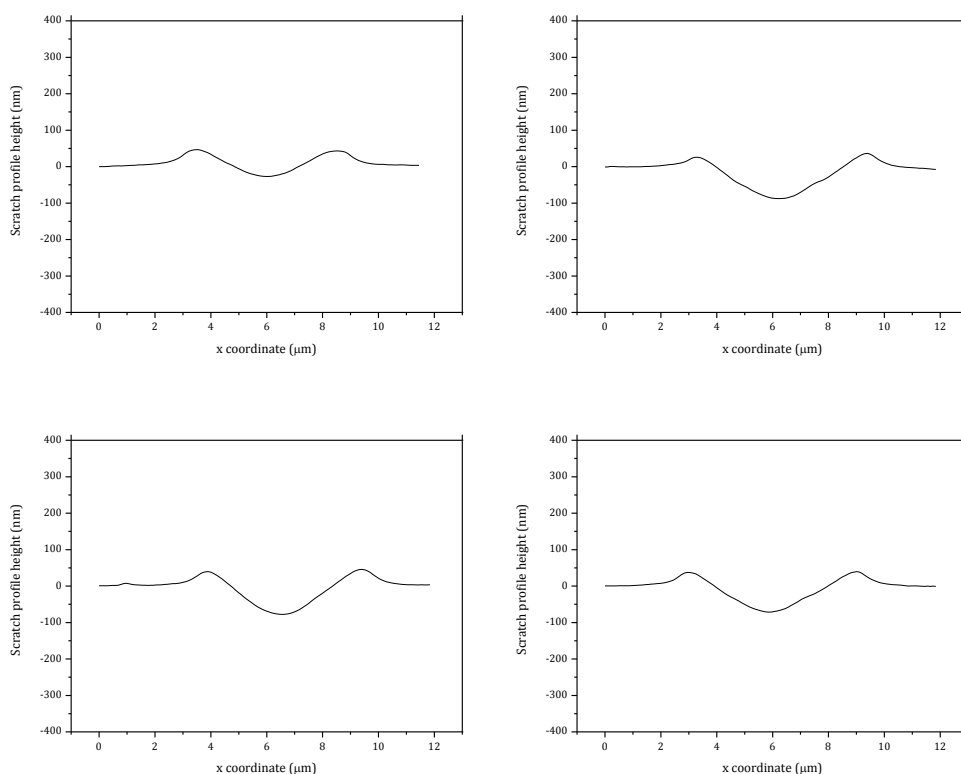


Figure 3.39 Cross-section profiles of sample NS-C after thermal treatment.

In Figs. 3.40 - 3.43 the shoulders height and ditch depth and the correspondent areas are compared before and after the thermal treatment for sample NS and NS-C, respectively. It should be remembered that with respect to the reference sample, the recovery degree of these two samples is much more limited. For this reason only the comparison between sample NS and NS-C is reported. In both cases a certain recovery process occurs, more pronounced in the case of

sample NS. However, in the innovative clear coat the enhanced crosslinking does not inhibit completely the viscoelastic creep phenomena that determine the recovery of the mars.

In Figs. 3.44 and 3.45 the differences between the two samples are summarized. For sample NS the percentage reduction in the shoulders height is approximately of 57% and 65% for the ditch height, whereas for sample NS-C is in average 21% for the shoulders and 37% for the ditch. The differences are more pronounced considering the areas evaluation. In sample NS the shoulders area reduction is of 52% (average of the two shoulders) and 69% for the ditch; in sample NS-C 9% for the shoulders, 25% for the ditch.

Therefore, as regarding the recovery capabilities of the investigated clear coats, it can be observed that the introduction of nano-silica particles determines a remarkable reduction of the recovery degree. The increase in the glass transition temperature in comparison with the reference sample plays a fundamental role in viscoelastic properties of the coating. The temperature of the thermal treatment is 10°C lower than the T_g of sample R, whereas it is around 20°C lower than T_g of sample NS. It should be remembered that the proximity to T_g is one of the parameters determining the mars recovery [4]. Molecular mobility, in fact, is very high above T_g but also below T_g , although less pronounced, it is however present. In the proposed innovative coating, sample NS-C, the recovery processes are slightly decreased but not completely inhibited.

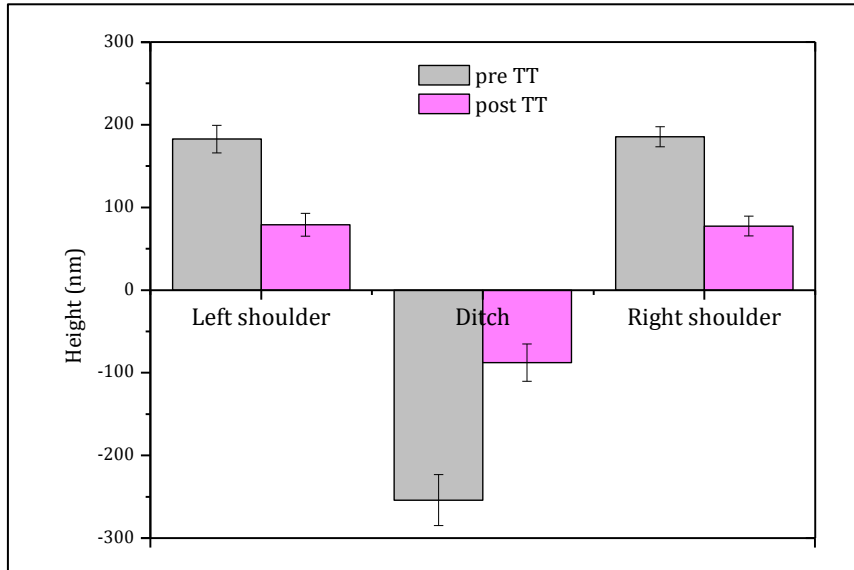


Figure 3.40 Average values of shoulders height and ditch depth before and after the thermal treatment – Sample NS.

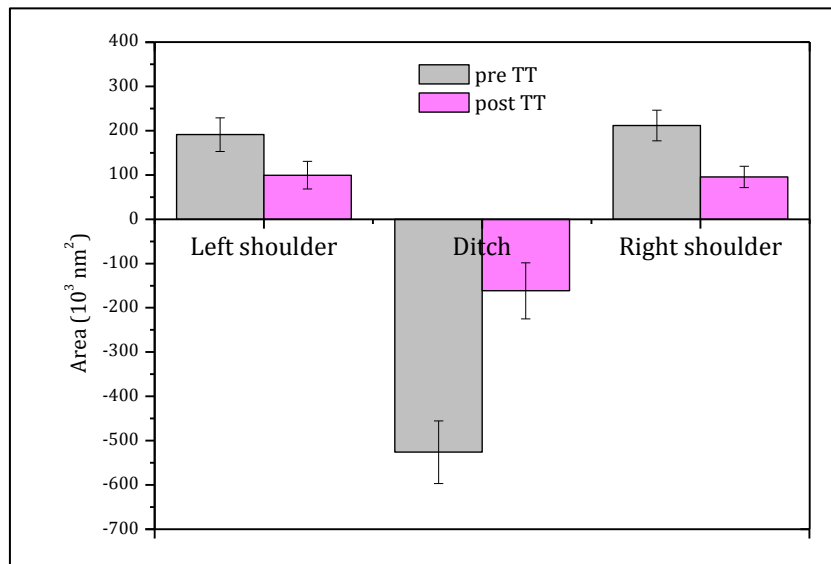


Figure 3.41 Average values of shoulders area and ditch area before and after the thermal treatment – Sample NS.

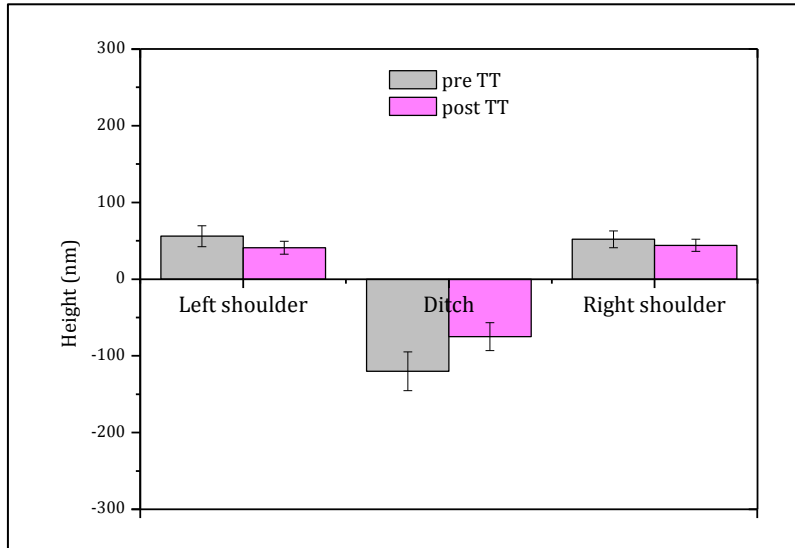


Figure 3.42 Average values of shoulders height and ditch depth before and after the thermal treatment – Sample NS-C.

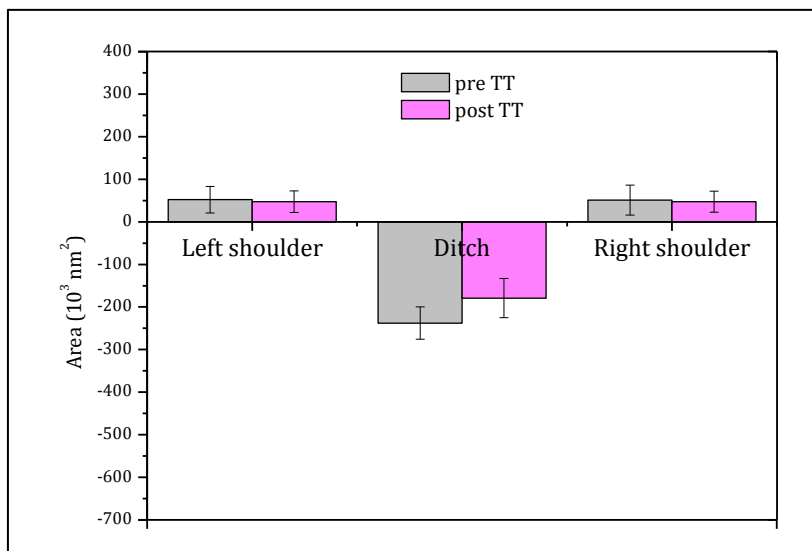


Figure 3.43 Average values of shoulders area and ditch area before and after the thermal treatment – Sample NS-C.

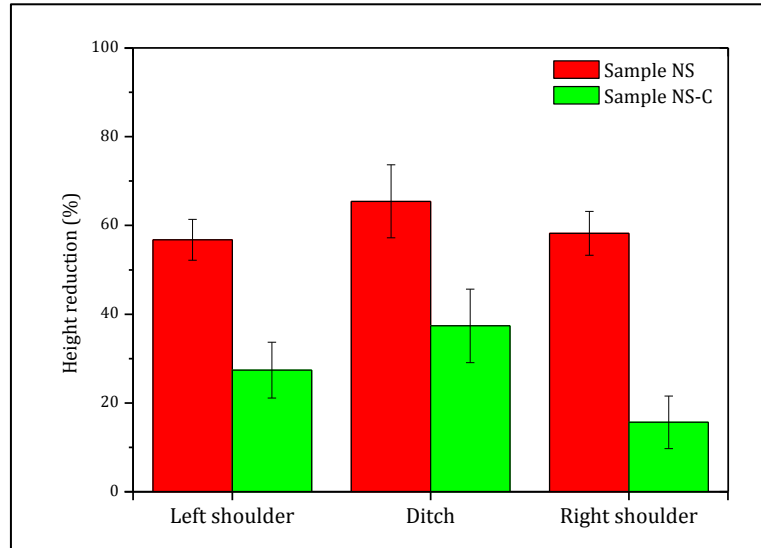


Figure 3.44 Comparison of the percentage height reduction of the shoulders and the ditch after the thermal treatment between sample NS and sample NS-C.

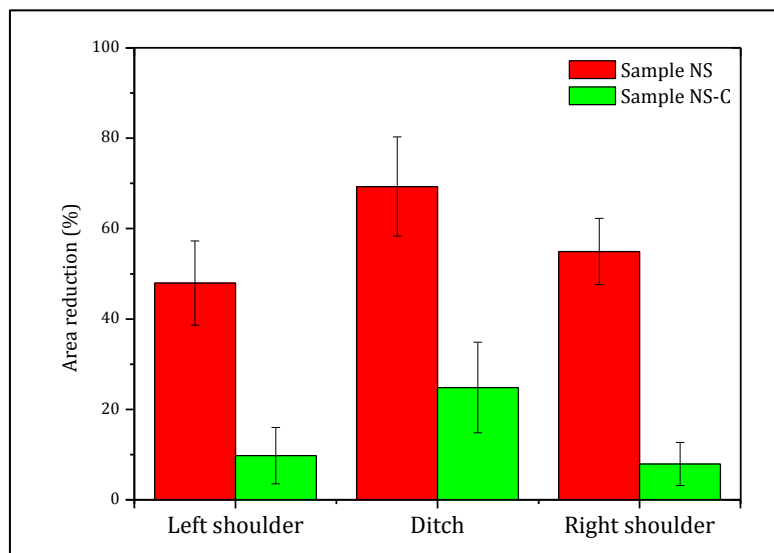


Figure 3.45 Comparison of the percentage area reduction of the shoulders and the ditch after the thermal treatment between sample NS and sample NS-C.

The samples subjected to 20 cycles of Taber test and the fall of 25 ml of abrasive have been thermally treated (2hs at 60°C). Gloss recovery was measured after the treatment. The results are shown in Figs. 3.46 and 3.47 for Taber test and falling abrasive test, respectively. An almost full recovery of the initial value of gloss for the three samples could be observed. After the Taber cycles the residual gloss was equal to 19%, 50% and 91% for sample R, NS and NS-C. After the thermal treatment in all the samples a recovery above 90% of the initial value occurred. As regarding the falling abrasive test (Fig. 3.47), the gloss reduction after the erosion test is less pronounced but also in this case, after the thermal treatment, the gloss values increase to about 90% of the initial value.

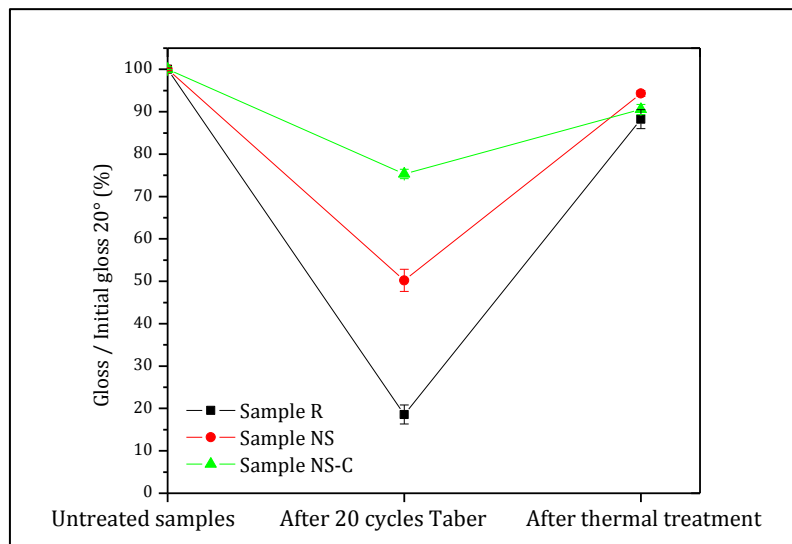


Figure 3.46 Percentage residual gloss of the abraded samples (20 cycles of Taber test) after the thermal treatment.

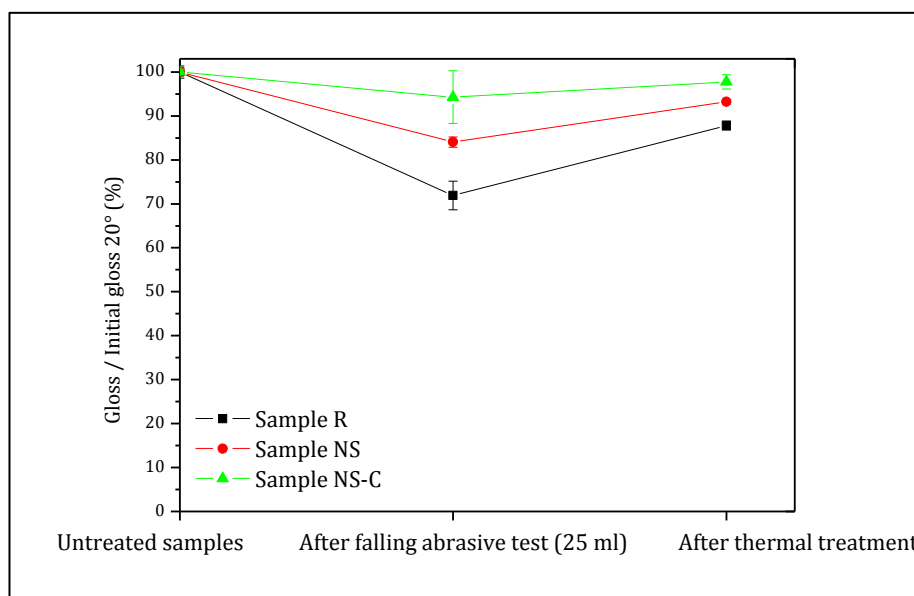


Figure 3.47 Percentage residual gloss of the abraded samples (25 ml of fallen abrasive) after the thermal treatment.

3.4.3 Effects of UV weathering on mar resistance

In this paragraph the results obtained from the study of the UV effect on mar/scratch resistance are discussed. Gloss measurements do not reveal any detectable change in the gloss for all the samples. On the contrary, the mar/scratch resistance undergoes significant variations, as discussed later. In the case of clear coats, gloss changes are not significant until degradation is very high but the decrease in mechanical properties, and, hence, in mar/scratch resistance could be considerable [5, 6, 9].

In Fig. 3.48 the plastic resistance derived from the nano scratch experiments and calculated from the residual depth value at 5 mN is displayed. With respect to the values reported in Fig. 3.22, all the samples show an increase in plastic resistance. In particular, the increase is of 25.7% for sample R, 39.9% for sample NS, and 21.3% for sample NS-C.

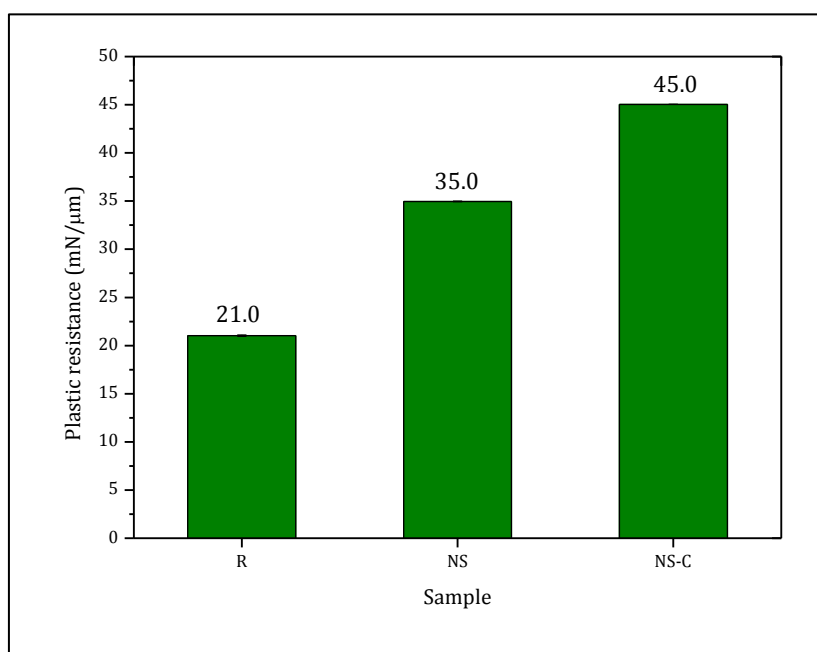


Figure 3.48 Plastic resistance of the samples after UV aging.

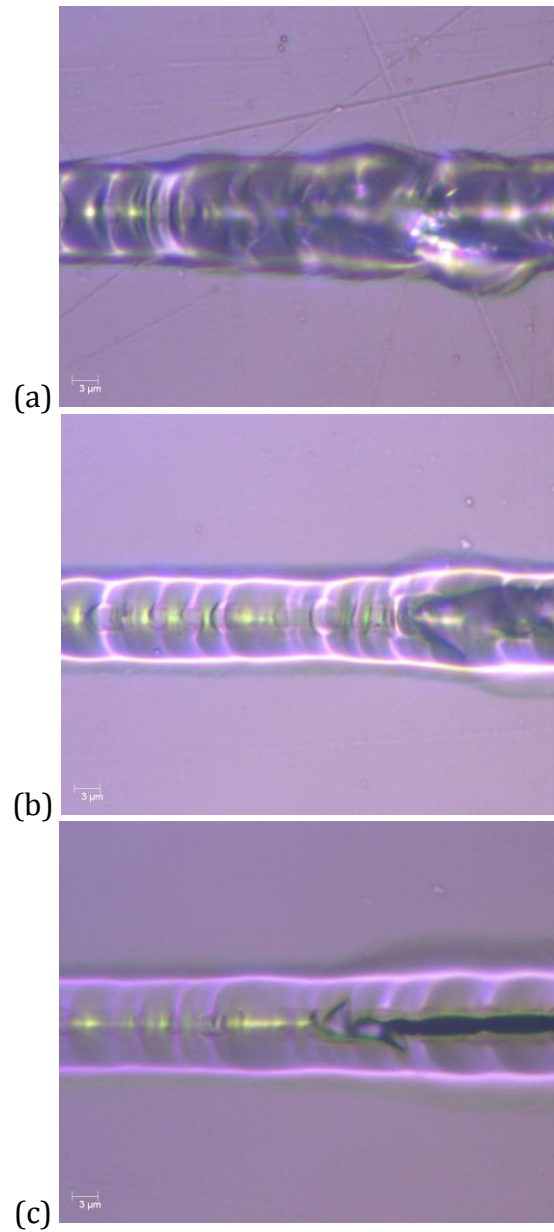


Figure 3.49 *Optical micrographs of the first brittle failure in the UV aged samples: (a) sample R; (b) sample NS; (c) sample NS-C.*

The optical micrographs showing the first fracture occurred are reported in Fig. 3.49a-c. The correspondent critical loads, optically evaluated, are plotted in Fig. 3.50. The UV exposure determines a decrease in the critical load for sample R and NS-C, of 7.8% and 5.6%, respectively. Conversely, for sample NS the weathering test led to an increase of 2.8% in the critical load.

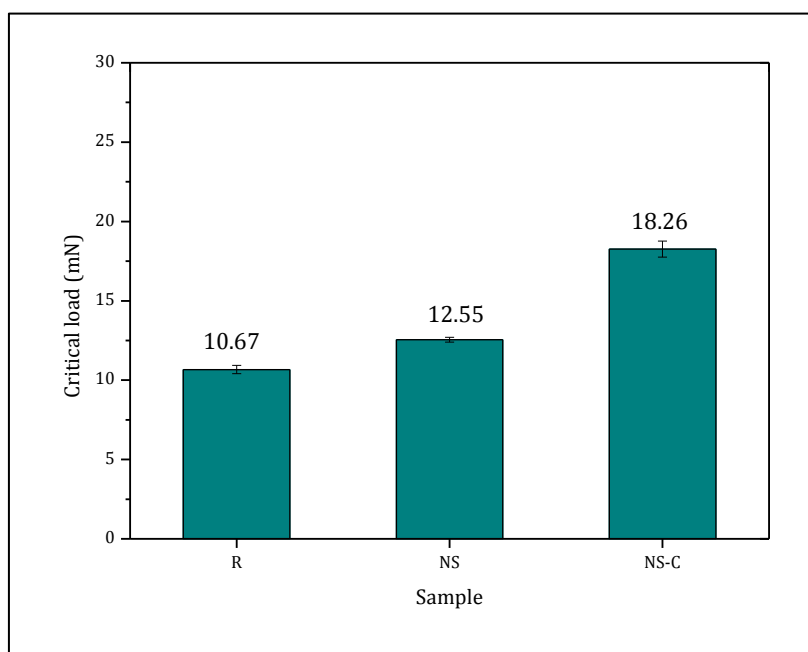


Figure 3.50 Critical load (optically evaluated) after UV exposure.

The results obtained by performing the Taber test after the UV exposure are in agreement with those obtained via nano-scratch experiments. The increase of the plastic resistance finds a confirmation

in an enhanced mar resistance assessed as gloss retention during the Taber test. In Fig. 3.51 the percentage residual gloss as function of Taber cycles is plotted. The increased mar resistance is more evident for sample R, less for sample NS. For the innovative sample NS-C the curves for the aged and no-aged samples are very similar and no appreciable difference is observable.

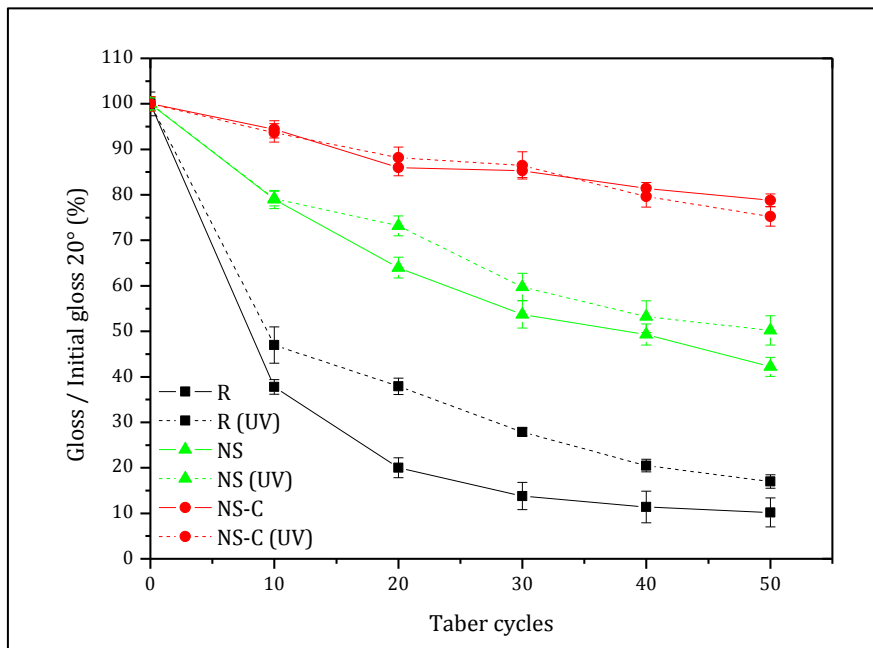


Figure 3.51 Percentage residual gloss during Taber test: comparison between new and UV-aged samples.

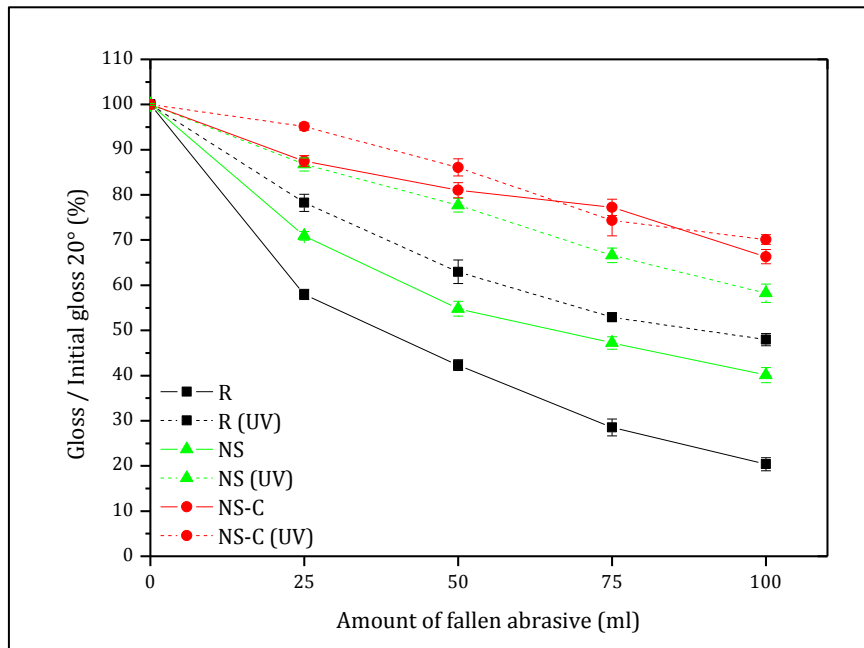


Figure 3.52 Percentage residual gloss during Falling Abrasive Test: comparison between new and UV-aged samples.

The trend found in Taber test is confirmed also by the results obtained in the falling abrasive test, as shown in Fig. 3.52.

Interesting conclusions can be drawn as regarding the effect of the interaction of UV radiation with the investigated clear coats. In all the three samples, UV exposure determines an increased resistance to mar damage demonstrated by higher plastic resistances derived from nano scratch experiments and better gloss retention in Taber test and falling abrasive test. UV action is likely to promote the increase of surface hardness by inducing further crosslinking [5, 9]. As drawback the UV exposure induces a reduction in the critical load, in other words an

embrittlement of the material [9]. This is true for the reference sample and for the innovative proposed clear coat. Conversely, the critical load for sample NS shows a slight increase that could be not much significant, since the critical load before the UV exposure was already much lower than the L_c of the other samples.

3.5 Conclusions

In automotive field the durability of organic coatings properties is of paramount importance. In particular, clear coats play a crucial role in long-term aesthetic performances and one of the key properties to be ensured is the resistance to mar damage. It should not be surprising if new strategies are continuously needed to satisfy increasingly demanding market expectations. Paint systems based on embedding nano-particles are nowadays considered one the most promising ways for improving mar/scratch resistance. In this work, the advantages introduced by nano-silica particles are highlighted. Nano scratch test and field simulation tests, such as Taber test and falling abrasive test have demonstrated an increase in the resistance to plastic deformation. This is due to an increased surface hardness owing to the nano-particles located in the first layers of the clear coat. However, for fully evaluating the mar/scratch behaviour also the resistance to fracture has to be considered. As regarding this parameter, the sample containing nano silica shows a reduction of the critical load having a

more brittle behaviour. For this reason an innovative clear coat with an enhanced crosslinking level was studied. The improvement of the crosslink does not change the glass transition temperature of the clear coat with respect to the nano-silica containing sample, and determines a further increase in the plastic resistance and a remarkable rise in the critical load. Fig. 3.53 clearly shows the enhancement of the main properties governing the mar/scratch behaviour. The innovative sample NS-C displays the best characteristics: the lowest residual depth at the same applied force, i.e. the highest plastic resistance, and the highest critical load.

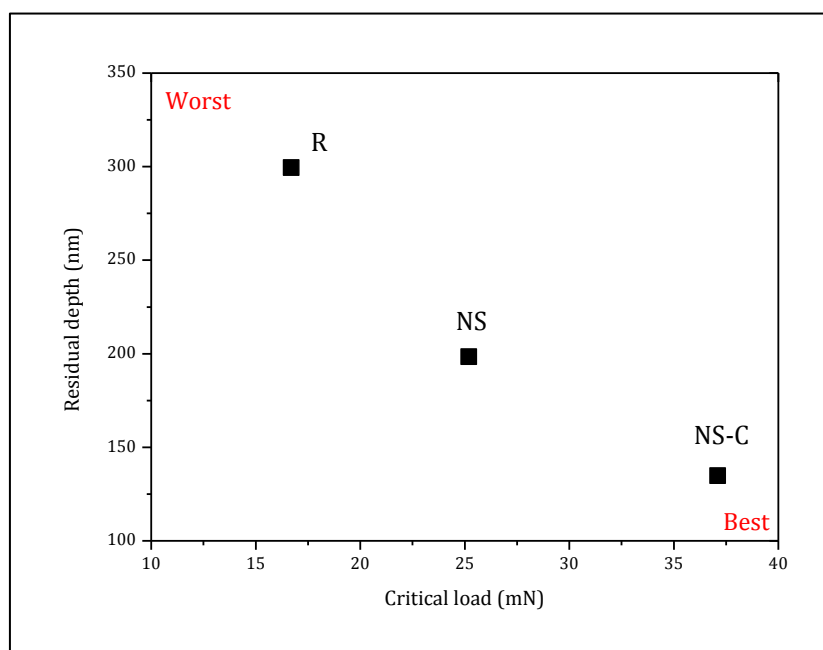


Figure 3.53 Summary of plastic deformation and fracture resistance of the investigated clear coats.

As regarding the recovery properties, the viscoelastic creep phenomena are not completely inhibited in the innovative clear coat, although they are much less present than in the reference sample. However, the benefits deriving from the increase in the resistance to the plastic deformation and fracture make this strategy surely very promising. The effects of the interaction of the UV radiation with the clear coats lead to a higher mar resistance due to an increased surface hardness (induced crosslinking) but also to an embrittlement of the material. In any case, for the NS-C sample the critical load value remains significantly higher if compared to the reference sample and the NS sample.

3.6 References

- [1] R. S. Hunter, *The measurement of appearance*, 2nd ed. New York, NY John Wiley and Sons, 1975.
- [2] M. E. McKnight and J. W. Martin, "Advanced methods and models for describing coating appearance," *Progress in Organic Coatings*, vol. 34, pp. 152-159, 1998.
- [3] J. Markarian, "Additives improve scratch resistance in automotive applications," *Plastics Additives & Compounding*, vol. March/April, pp. 10-15, 2009.
- [4] C. Seubert, *et al.*, "The effect of weathering and thermal treatment on the scratch recovery characteristics of clearcoats," *Journal of Coatings Technology and Research*, vol. 7, pp. 159-166, 2009.

- [5] U. Schulz, *et al.*, "The influence of weathering on scratches and on scratch and mar resistance of automotive coatings," *Progress in Organic Coatings*, vol. 42, pp. 38-48, 2001.
- [6] M. Osterhold, *et al.*, "Effect of weathering on scratch/mar and mechanical behaviour of clearcoats," *Macromolecular Symposia*, vol. 187, pp. 823-834, 2002.
- [7] K. Adamsons, *et al.*, "Oligomers in the evolution of automotive clearcoats: mechanical performance testing as a function of exposure," *Progress in Organic Coatings*, vol. 34, pp. 64-74, 1998.
- [8] H.-J. Streitberger and K.-F. Dössel, *Automotive paints and coatings*, 2nd ed. Weinheim: Wiley-VHC, 2008.
- [9] B. V. Gregorovich, *et al.*, "Scratch and mar and other mechanical properties as a function of chemical structure for automotive refinish coatings," *Progress in Organic Coatings*, vol. 43, pp. 175-187, 2001.
- [10] P. G. Michael Osterhold, "Influence of weathering on physical properties of clearcoats," *Progress in Organic Coatings*, vol. 41, pp. 177-182, 2001.
- [11] C. M. Seubert and M. E. Nichols, "Scaling behavior in the scratching of automotive clearcoats," *Journal of Coatings Technology and Research*, vol. 4, pp. 21-30, 2007.
- [12] J. Zeno W. Wicks, *et al.*, *Organic coatings: science and technology*, 2nd ed. New York, Chichester, Weinheim, Brisbane, Singapore, Toronto: Wiley-Interscience, 1999.
- [13] W. Shen, *et al.*, "A quantitative index for mar and scratch resistance of materials for automotive glazing applications and quantitative evaluation of damages by different scratching modes," *Tribology Letters*, vol. 17, pp. 637-644, 2004.

- [14] V. Jardret, *et al.*, "Scratch Durability of Automotive Clear Coatings: A Quantitative, Reliable and Robust Methodology," *Journal of Coatings Technology*, vol. 72, pp. 79-88, 2000.
- [15] L. Lin, *et al.*, "A new approach to characterize scratch and mar resistance of automotive coatings," *Progress in Organic Coatings*, vol. 40, pp. 85-91, 2000.
- [16] M. Kutschera, *et al.*, "Scratch Resistance of Automobile Clearcoats: Chemistry and Characterization on the Micro- and Nanoscale," *Journal of Coatings Technology and Research*, vol. 3, pp. 91-97, 2006.
- [17] W. Shen, *et al.*, "Use of a Scanning Probe Microscope to Measure Marring Mechanisms and Microhardness of Crosslinked Coatings," *Journal of Coatings Technology* vol. 69, pp. 123-135, 1997.
- [18] F. N. Jones, *et al.*, "Studies of microhardness and mar resistance using a scanning probe microscope," *Progress in Organic Coatings*, vol. 34, pp. 119-129, 1998.
- [19] V. Jardret, *et al.*, "Understanding and quantification of elastic and plastic deformation during a scratch test," *Wear*, vol. 218, pp. 8-14, 1998.
- [20] P. Bertrand-Lambotte, *et al.*, "Understanding of automotive clearcoats scratch resistance," *Thin Solid Films*, vol. 420-421, pp. 281-286, 2002.
- [21] R. A. Ryntz, *et al.*, "Scratch Resistance Behavior of Model Coating Systems," *Journal of Coatings Technology*, vol. 72, pp. 47-53, 2000.
- [22] W. Shen, *et al.*, "Characterization of mar/scratch resistance of coatings with a Nano-indenter and a scanning probe microscope," *Tribology International*, vol. 39, pp. 146-158, 2006.
- [23] M. Groenewolt, "Highly scratch resistant coatings for automotive applications," *Progress in Organic Coatings*, vol. 61, pp. 106-109, 2008.

- [24] M. M. Jalili, *et al.*, "Investigating the variations in properties of 2-pack polyurethane clear coat through separate incorporation of hydrophilic and hydrophobic nano-silica," *Progress in Organic Coatings*, vol. 59, pp. 81-87, 2007.
- [25] Z. Ranjbar and S. Rastegar, "Nano mechanical properties of an automotive clear-coats containing nano silica particles with different surface chemistries," *Progress in Organic Coatings*, vol. 72, pp. 40-43, 2011.
- [26] N. Tahmassebi, *et al.*, "Effect of addition of hydrophobic nano silica on viscoelastic properties and scratch resistance of an acrylic/melamine automotive clearcoat," *Tribology International*, vol. 43, pp. 685-693, 2010.
- [27] S. Zhou, *et al.*, "The change of the properties of acrylic-based polyurethane via addition of nano-silica," *Progress in Organic Coatings* vol. 45, pp. 33-42, 2002.
- [28] B. R. Floryancic, *et al.*, "Effects of Alumina and Silica nanoparticles on Automotive Clear-Coat Properties," in *Smart Coatings II*, T. Provder and J. Baghdachi, Eds., ed Washington, DC: American Chemical Society, 2009, pp. 220-238.
- [29] M. Osterhold and G. Wagner, "Methods for characterizing the mar resistance," *Progress in Organic Coatings*, vol. 45, pp. 365-371, 2002.
- [30] M. R. VanLandingham, "Scratch and Mar Resistance of Polymeric Materials," in *Service Life Prediction-Challenging the Status Quo*, J. W. Martin, *et al.*, Eds., ed: Federation of Societies for Coatings Technology 2005, pp. 349-363.
- [31] G. Wagner and M. Osterhold, "Comparison of different test methods for determining the mar resistance of clearcoats," *Materialwissenschaft und Werkstofftechnik*, vol. 30, pp. 617-622, 1999.
- [32] www.amteckistler.de Access date: October 31 2011.

- [33] www.taberindustries.com Access date: October 31 2011.
- [34] S. Rossi and F. Deflorian, "Mechanical degradation of organic paint coatings," in *High-performances organic coatings*, A. S. Khanna, Ed., ed Boca Raton, Boston, New York, Washington, DC CRC Press, 2008, pp. 123-142.
- [35] S. Rossi, *et al.*, "Comparison of different abrasion mechanisms on aesthetic properties of organic coatings," *Wear*, vol. 267, pp. 1574-1580, 2009.
- [36] S. Rossi, *et al.*, "Reduction of aesthetical properties of organic coatings caused by mechanical damage," *Materials & Design*, vol. 30, pp. 1511-1517, 2009.
- [37] E. Scrinzi, *et al.*, "Effect of slurry mechanical damage on the properties of an organic coating system," *Surface & Coatings Technology*, vol. 203, pp. 2974-2981, 2009.
- [38] I. M. Hutchings, *Tribology Friction and Wear of Engineering Materials*. London: Edward Arnold, Hodder Headline PLC, 1992.
- [39] W. C. Shen, *et al.*, "Measurement of mar resistance and study of marring mechanism of polymeric coatings with scanning probe microscope," *Journal of Coatings Technology*, vol. 72, pp. 89-95, 2000.
- [40] W. Shen, *et al.*, "Methods for Studying the Mechanical and Tribological Properties of Hard and Soft Coatings with a Nano-Indenter," *Journal of Coatings Technology and Research*, vol. 1, pp. 117-125, 2004.
- [41] P. Bertrand-Lambotte, *et al.*, "Nano-indentation, scratching and atomic force microscopy for evaluating the mar resistance of automotive clearcoats: study of the ductile scratches," *Thin Solid Films*, vol. 398-399, pp. 306-312, 2001.
- [42] E. Scrinzi, *et al.*, "Evaluation of durability of nano-silica containing clear coats for automotive applications," *Progress in Organic Coatings*, vol. 71, pp. 384-390, 2011.

CHAPTER 4

Protective properties of advanced polyurethane coatings

In recent years supramolecular chemistry, and in particular hydrogen-bonded polymers synthesis, has aroused great interest leading to significant scientific developments in polymer science, and also technological applications. The introduction of multiple hydrogen bonds provides innovative properties owing to their reversible nature such as self-healing or preemptive healing behaviour. Many different polymeric systems have been studied, both thermo-plastic and thermo-setting, and one of the possible applications could be also in coatings field. The chemical and thermo-mechanical properties of these systems based on self-complementary hydrogen bonds units have been deeply investigated. However, in reference to a potential application as organic coatings, the protection from corrosion phenomena is not fully assessed yet. The present chapter is devoted to explore the effect of a partial substitution of covalent linkages in a polyurethane coating by multiple hydrogen bonds on the protective behaviour.

After a brief introduction about the supramolecular chemistry involving multiple hydrogen bonds and the innovative properties provided by these moieties, the formulation steps of a new polyurethane resin

employing supramolecular cross-links are described. A characterization of the protective behaviour was carried out via electrochemical impedance spectroscopy for different ratios of covalent/hydrogen bonds and the main results are finally reported.

4.1 Introduction

Nowadays, the durability of organic coatings is still regarded one of the most important open issues. The increasing market expectations, and the complexity of the factors involved in coatings' degradation processes represent the driving force from this point of view. Accordingly, products with innovative properties and enhanced durability are continuously demanded and developed.

Many strategies are now available to satisfy this need. From the conceptual point of view, the strategies can be classified into two main groups [1]: *damage prevention* [2] and *damage management* [2-5] approaches. The basic idea behind the *damage prevention* concept foresees the enhancement of the material resistance to degradation processes, as chemical, physical, and mechanical stresses jeopardizing the integrity of the coating. The approaches presented in the previous two chapters for improving the weathering and mar/scratch resistance represent two significant examples of the *damage prevention* philosophy. In the first case (see Ch. 2), the weathering resistance was enhanced simply by modifying the chemical composition of the binder.

In the second case (Ch. 3), mar damage process was bounded by the introduction of nano-silica particles and the increase of the cross-linking level.

Although very good results can be obtained by adopting this approach, it should be remembered that, as the formation of damage during use can never be excluded, these materials invariably need periodic inspection to monitor damage development, thus calling for actions and costs, sooner or later.

Conversely, *damage management* approach is based on the active response of the material to the external chemical, physical, or mechanical stimuli which could affect the coating properties [2]. Active response must be intended both as “removing” or “healing” capabilities offered by the material once the coating has been damaged, and “preemptive healing” by acting against the nucleation of the defect. These *smart materials* are the subject of a huge amount of studies in several research fields. In coatings applications, numerous example can be mentioned and a good survey about these topics can be found in [4]. Healing by microencapsulation [3, 6-9], by reversible covalent networks thermoplastic [3], and by the introduction of hydrogen bonding [3, 10] are some characteristic examples of the damage management strategy.

Fig. 4.1 schematically shows the autonomic healing concept by microencapsulation proposed by White et al. [11] for bulk polymers. A microencapsulated healing agent is embedded in a structural composite matrix containing a catalyst capable of polymerizing the healing

agent. Cracks occurring in the matrix rupture the microcapsules, releasing the healing agent into the crack plane through capillary action; the healing agent contacts the catalyst, triggering polymerization that bonds the crack faces closed.

This concept was adopted for different systems by embedding the microcapsules, and also nanocapsules [12], in structural composite materials [13], elastomers [14], and many other self-healing polymers [15-18].

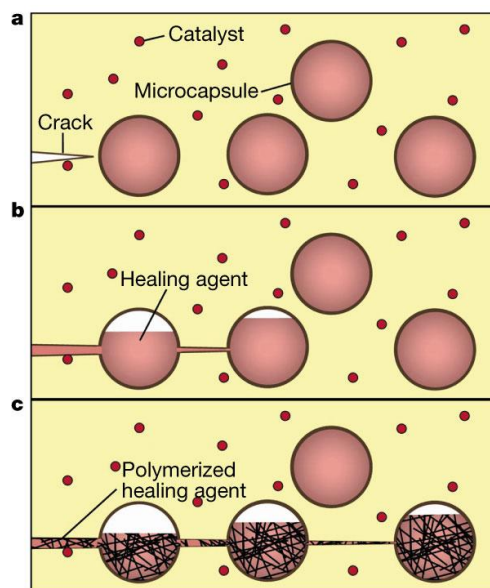


Figure 4.1. Autonomic healing concept by microencapsulation [11].

Similar encapsulation approach has been used also in self-healing coatings [8, 19-22]. The binder of the coating has the role of a passive

matrix, whereas the capsules contain an active material providing a rapid feedback activity (living polymerization) once a crack ruptures the container. In all these cases the healing agent aims to repair the defect by re-establishing the integrity of the film, thus restoring the barrier properties of the coating. In other cases, the microcapsules aim to provide an active corrosion protection [23]. When the barrier represented by the main coating matrix is damaged and the corrosive species come into contact with the metallic substrate, the capsules containing corrosion inhibitors release their content promoting the inhibition of the corrosion process.

The release of the healing agent is triggered by a mechanical damage but other mechanisms may be exploited. The active response can be sensitive to changes in local environment [6, 7]. Depending on the chemical composition of the micro/nano-container shell, different environmental stimuli induce reversible or irreversible changes of the shell permeability, allowing in this way the release of the content. The aforementioned stimuli can be variation of the pH, ionic strength, temperature, ultrasonic treatment, alternating magnetic field, electromagnetic irradiation.

Although this approach has led to several reliable results, it should be taken into account some limitations related to micro/nanocapsules embedment [8]. For such systems, once the healing agent is not more present in the damaged area, the self-healing capability fails. Other issues are related to the long-term stability of the capsules, and the

interface capsule/binder which introduces a discontinuity in the coating matrix with likely weakening effects.

Toohey et al. proposed a bio-inspired system in which the healing agent is delivered to cracks through a microvascular network embedded in the binder instead of capsules [24]. They proved that the resupply of the healing agent is feasible and extended life of the material can be achieved in response to repeated damage.

Another completely different strategy is based on an intrinsically self-healing behaviour of the coating binder (polymer matrix in a more general sense). Reversible polymerization processes are capable to fully restore the original properties of the material, and this process can be repeated many times. Re-mendable polymers belong to this category: after a crack occurred they can be healed by an external intervention owing to a thermal-, photo-, or chemical stimulus. Diels–Alder (DA)-based polymers are an example. The driving force for their repair process is provided by the thermal reversibility of the DA reaction, a process known as the retro-Diels–Alder (RDA) reaction [25]. Polymers based on supramolecular chemistry represent another promising application of this strategy. *Supramolecular chemistry* was defined by the Nobel Prize Jean-Marie Lehn as following: “Beyond molecular chemistry based on covalent bond there lies the field of *supramolecular chemistry* whose goal it is to gain control over the intermolecular bond” [26]. In general, supramolecular chemistry in polymer science

introduces a new approach in the design and synthesis of polymeric materials (Fig. 4.2). The repeating units are held together by non-covalent interactions, such as hydrogen bonds, π - π interactions, metal coordination, van der Waals forces.

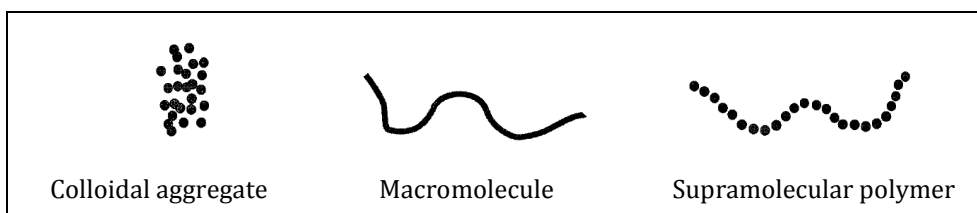


Figure 4.2 *Supramolecular polymers concept (compared to Staudinger's macromolecular concept) [27].*

These highly directional secondary interactions assembling the units provide novel properties essentially owing to the reversibility of this kind of linkages. Consequently, the response of the material to external stimuli is significantly different from that one of traditional macromolecules based on covalent bonds [27-31].

One of the most promising systems concerns supramolecular polymers is based on hydrogen bonding [32, 33]. This kind of chemistry was the subject of the experimental analysis aimed to develop a new binder for organic coatings applications. A more detailed description is reported in the next chapters.

Many of the abovementioned strategies aimed to endow the material with an active responsive behaviour for improving its durability have

been developed for bulk polymer materials. Some considerations must be stressed for following the same approaches in coatings applications. The main differences between polymer coatings and bulk polymers [3] are:

- coatings show a higher ratio interface area/polymer matrix volume;
- three main interfaces are present (coating-substrate, coating-air, binder-filler);
- most polymer coatings are thermosetting in order to have higher chemical and mechanical resistance, whereas most of bulk polymers are thermoplastic;
- in thermosetting, material transport is limited by the network of crosslinks;
- different functional requirements for the two systems.

In particular, organic coatings are required to have a suitable mix of functional properties. The most important functions are decoration and protection by providing an attractive appearance (gloss properties, colour perception, hiding power), and protecting the substrate from the environmental influences [3, 34]. With regard to this aspect, corrosion protection is one of fundamental function that must be ensured. The optimization of the active response of the material to mechanical damage or other external stresses should not compromise other functional properties such as protective behaviour. The experimental activity carried out in this Ph.D. work aimed to give a contribution in

this direction. Many efforts have been spent in defining the *smart* behaviour in response to mechanical damage but the actual corrosion protection properties of these coatings are not fully assessed.

The research topic was the investigation of the protective properties of a new polyurethane coating in which the covalent bonds are partially substituted with hydrogen bonds. Similar systems were already studied by Wietor et al. and Dimopoulos et al. [35, 36] proving preemptive healing properties related to the supramolecular networks. More detailed description is reported in Paragraph 4.2.3. However, in these contributions the barrier properties of this kind of coatings were not taken into account. From this point of view, the water uptake plays a fundamental role. A moisture absorption mechanism in the pyridine ring was studied by Chen et al. [37] and in the multiple hydrogen-bonded complexes based on 2-Ureido-4[1H]-pyrimidinone by Sun et al. [38]. In Fig. 4.3 the scheme proposed for the pyridine ring is represented. The stimulus of water produces the replacement of the N–H...N–Py hydrogen bond in the dried state by more adaptive hydrogen bonding. The pyridine ring tends to be protonated by H₂O (O–H...N–Py) or linked via hydrogen bonds of bridging H₂O molecules (Py–N–H...O–H–O...H–N–Py), which has a long bond distance. The authors reported that the interaction gets weaker, thus resulting in a decrease in the stiffness or modulus of the polymer as moisture absorption increases [37]. Sun et al. reported that water molecules may interact with the

donor or acceptor sites and hence disrupt the hydrogen bonds of 2-Ureido-4[1H]-pyrimidinone (UPy) dimers [38].

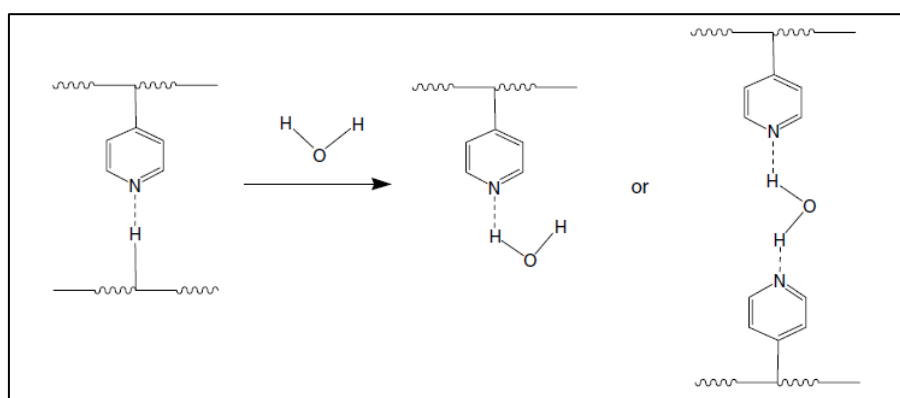


Figure 4.3 *Moisture absorption mechanism in the pyridine ring* [37].

In this work the water uptake was investigated by electrochemical impedance spectroscopy (EIS) in order to study the protective properties of a polyurethane coating modified by the introduction of UPy units. Moreover, the behaviour in terms of corrosion properties in presence of an artificial defect was investigated.

4.2 Supramolecular polymers based on multiple hydrogen bonding units

The use of non-covalent, reversible bonds allowed to open new ways in formulating materials with novel properties [39, 40]. In particular, the behaviour of this kind of materials is similar to crosslinked systems at room temperature but it responds strongly to a change in temperature for example. It may become “self-healing” at elevated temperatures without the need of reforming covalent bonds by chemical reactions.

Hydrogen bonds linking neutral organic molecules do not show the highest strength among the non-covalent bonds but they are very effective in comparison with other intermolecular forces owing to their versatility and directionality [39]. They have been shown to allow the tuning of association constant between several M^{-1} up to $10^7 M^{-1}$ by use of a specific hydrogen-bond matching pair [40]. Recently building blocks associated via five to ten hydrogen bonds have been developed with binding constants larger than $10^9 M^{-1}$ [33]. In general the multiple hydrogen-bonding motifs are classified in two families [31, 41]: complementary (CMHB) and self-complementary systems (SCMHB). In the former the two dissimilar complements containing complementary donor and acceptor sites must be present to form the hydrogen-bonds through self-recognition, in the latter the hydrogen-bonds are automatically established between two identical complements.

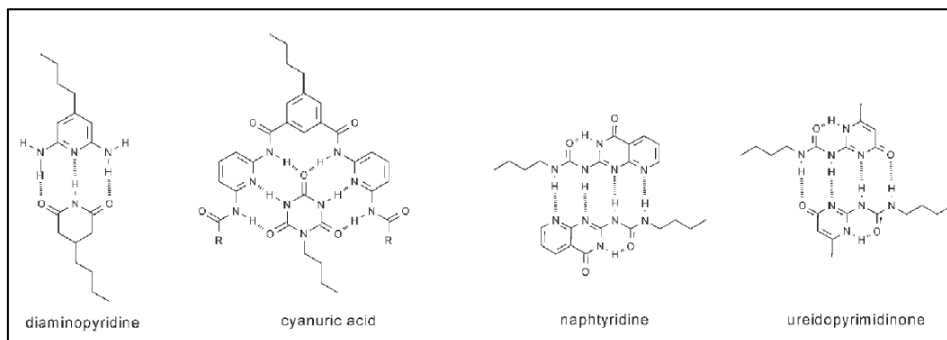


Figure 4.4 Schematic representation of typical multiple hydrogen-bonding moieties [31].

In Fig. 4.4 some different hydrogen-bonding motifs employed in the design of supramolecular polymers are schematically displayed.

Meijer, Sijbesma et al. first described the potential of SCMHB between 2-ureido-4[1H]-pyrimidinone (UPy) units, which strongly self-dimerize through four hydrogen bonds arranged in donor-donor-acceptor-acceptor (DDAA) sites, as shown in Fig. 4.5 [10, 42]. The advantages provided by this quadruple hydrogen-bonding motif are deeply described in the next paragraph.

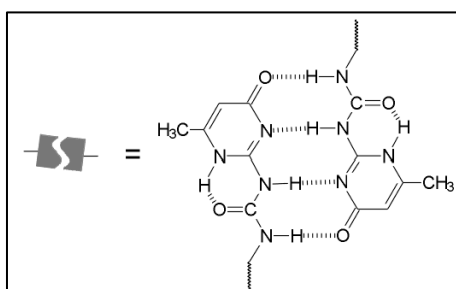


Figure 4.5 Self-complementary quadruple hydrogen bonds unit [43].

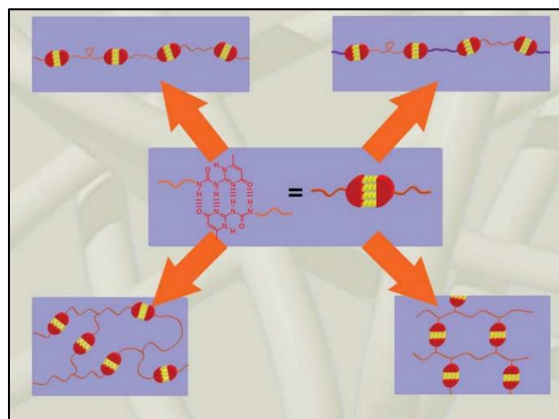


Figure 4.6 Different architectures for supramolecular polymers [30].

Many different architectures are possible in the design of a supramolecular polymer based on multiple hydrogen bonds units, as shown in Fig. 4.6: linear supramolecular polymer or block-copolymer and supramolecular networks via branching or grafting [30].

4.2.1 2-Ureidopyrimidin-4-one (UPy) dimer

The basic idea of the multiple hydrogen bonding units is the *cooperativity* principle, which states that “1+1 is more than 2”. By using this concept, several chemically stable structures have been developed based on the reversible formation of multiple hydrogen bonds [32].

Some advantages make quadruple hydrogen bonding units one of the most promising motif to be used in the design of supramolecular polymers. As displayed in Fig. 4.7, they show the best trade-off between the association constant and the synthetic accessibility. In fact, they

show a dimerization constant $K_{\text{dim}} > 10^6 \text{ M}^{-1}$ in chloroform [10] and an ease of synthesis thus making them available on large scale [44]. Moreover, UPy have higher strength in comparison with most of the non-covalent bonds [10, 42]. Considering the number of repulsive secondary interactions this DDAA dimer is proved to be more stable than DADA dimer, as explained in Fig. 4.8. While both dimers have four primary attractive hydrogen bonds, the DADA dimer has six repulsive secondary interactions, whereas the DDAA dimer has two repulsive and four attractive secondary interactions [42].

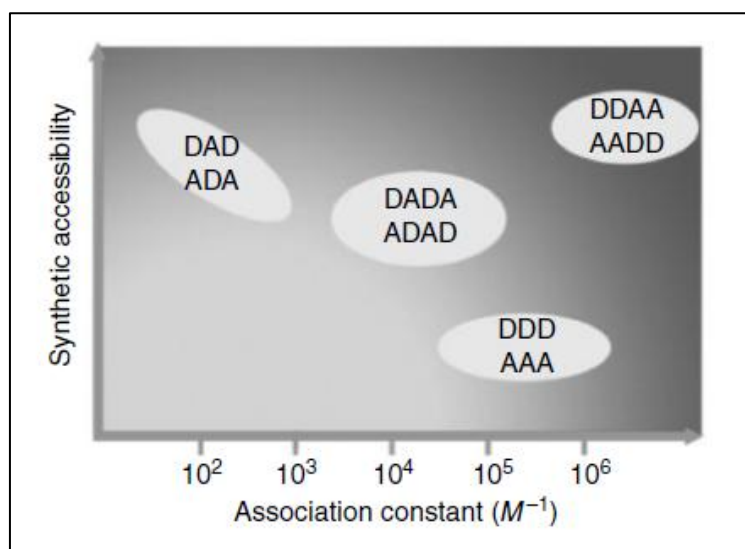


Figure 4.7 Multiple hydrogen-bonding units synthetic accessibility vs. association constant [33].

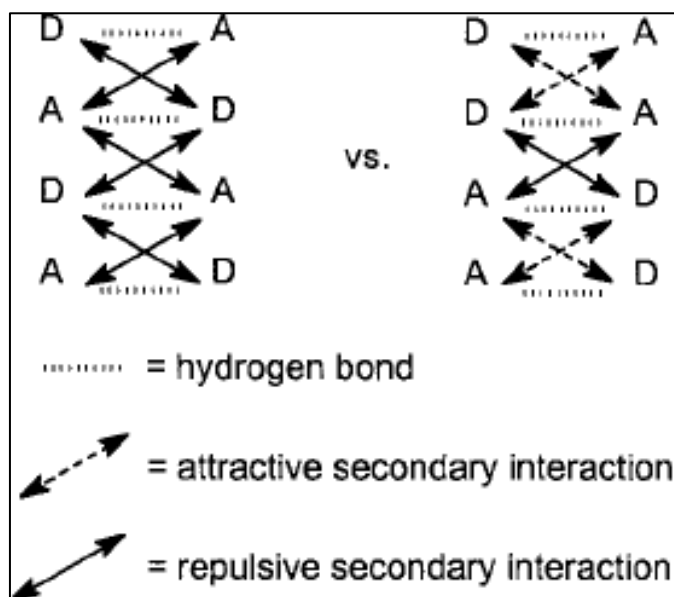


Figure 4.8 Interactions in DADA and DDAA dimers [42].

4.2.2 UPy applications

The quadruple hydrogen-bonding motif has been employed in the formulation of a great variety of polymers with different architectures [41, 43-48]. Some examples are briefly described.

Functionalization of hydroxyl telechelic polymers by UPy units produce a dramatic change in the mechanical properties of the starting material [33]. Poly(ethylene butylene) is a viscous liquid, if modified with UPy it becomes a rubber-like material [43, 44], as clearly shown in Fig. 4.9.

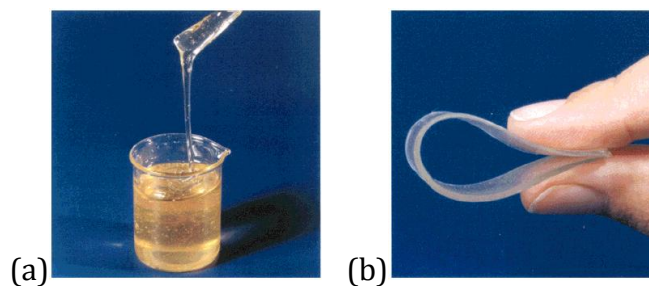


Figure 4.9 Poly(ethylene/butylene) with OH end groups (a), poly(ethylene/butylene) functionalized with UPy units (b) [43].

Examples in self-healing materials are the modification with UPy of hydrogenated polybutadiene or telechelic polydimethylsiloxanes [39, 45]. In these cases the self-healing behaviour is triggered by the heat treatment (see Fig. 4.10).

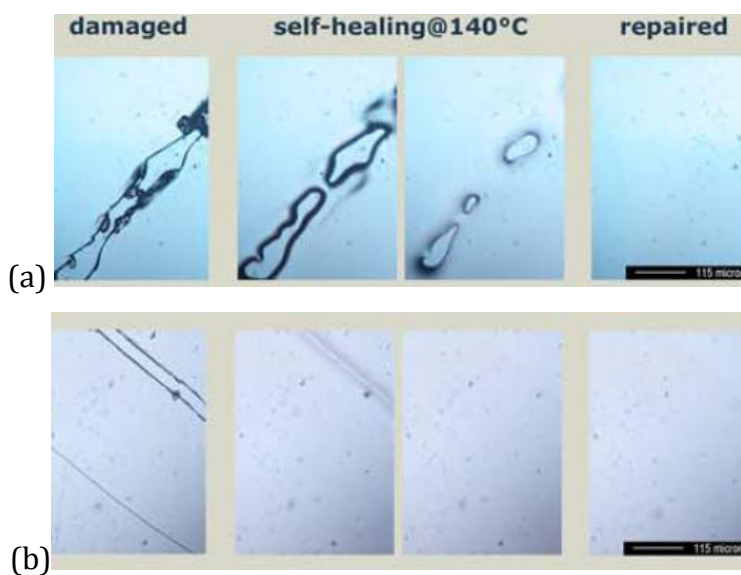


Figure 4.10 Heat triggered self-healing behaviour of UPy modified hydrogenated polybutadiene (a) and polydimethylsiloxane (b) [39].

4.2.3 UPy introduction in crosslinked coatings

Quadruple hydrogen-bonding ureidopyrimidinone (UPy) moieties can be a promising tool also in cross-linked systems which applications can be in coatings field. Generally, highly cross-linked thermoset materials have a limited stress relaxation behaviour above or just below the glass transition temperature. Wietor et al. and Diamopoulos et al. [35, 36] investigated a system based on ϵ -caprolactone and L-lactic acid crosslinked partially with a commercial diisocyanate and partially with dimers of UPy units, according to the scheme represented in Fig. 4.11.

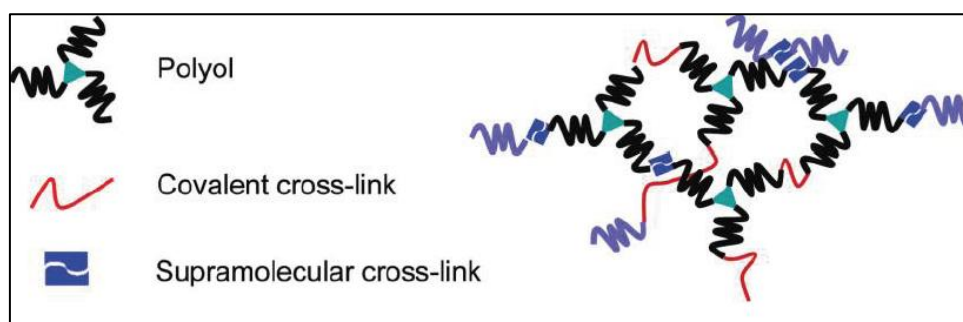


Figure 4.11 *Cross-linked network with covalent and non-covalent cross-links [35].*

The main results obtained by the introduction of reversible cross-links consist of a better relaxation of stresses also below T_g . The dissociation of UPy dimers in the networks provides an additional relaxation mechanism. Moreover, the UPy dynamic properties determine a slow stress relaxation at lower temperatures, thus reducing the stresses related to the application of the coating on a metallic substrate with

different thermal expansion coefficient. This ability of pre-emptive stress relaxation can be considered a sort of preemptive healing. This concept can be clarified by the schemes represented in Figs. 4.12 and 4.13. Fig. 4.12 describes the evolution of the damage process from a microscopic level to a macroscopic level, involving different phenomena at different scales. The macroscopic damage is always associated with a damage at microscopic level.

Scale	Descriptors	Phenomena
Micro	Molecules Polymers	Dissociation Bond breakage
↓		↓
Meso	Networks Interfaces	Microcracks Cavitation, crazing
↓		↓
Macro	Coating Film	Rupture Delamination

Figure 4.12 *Evolution of damage processes from microscopic level to macroscopic one [3].*

Many kinds of stresses may affect the eventual macroscopic damage [3]:

- internal stresses due to formation of networks (crosslinking reactions);
- internal stresses in the coating and interfacial stresses at the substrate interface due to the different thermal expansion

between the coating and the substrate and the thermal history of the entire system;

- effects of previous external stresses not revealed at macroscopic level.

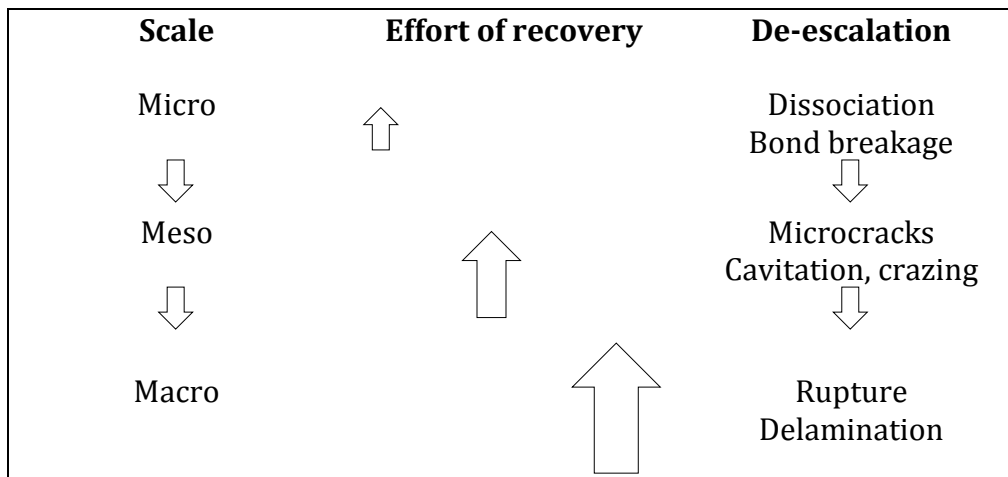


Figure 4.13 *Damage recovery and pre-emptive de-escalation [3].*

In damage recovery processes the same sequence has to be kept in mind (Fig. 4.13). Damage recovery is mainly based upon material transport phenomena in organic polymer coatings. Material transport can take place within the bulk or close to the substrate, air, and filler interfaces, and can involve either individual motion of small molecules or collective motions. However, it should be remembered that material transport is rather limited in cross-linked networks. It is apparent that crack filling (macroscopic scale) needs for large amounts of material

transport than that required for stopping the crack growth or initiation (meso- and microscopic scales). Consequently, it is more effective if the recourse to the material transport is limited in the self-healing process as much as possible.

In this framework, the ability of relaxing stresses pre-emptively before the build-up of stresses, and the consequent mechanical failure, acquires a fundamental role.

4.2.4 Synthesis of UPy unit

One of the positive features of the UPy unit is its ease of synthesis from available commercial reagents. The procedure described in [43, 44] was followed in this thesis work.

The 2 - (6 - isocyanatohexylaminocarbonylamino) - 6 - methyl - [1H] pyrimidinone is obtained from 2-amino-4-hydroxy-6-methylpyrimidine using six-fold excess of hexyldiisocyanate (as shown in Fig. 4.14).

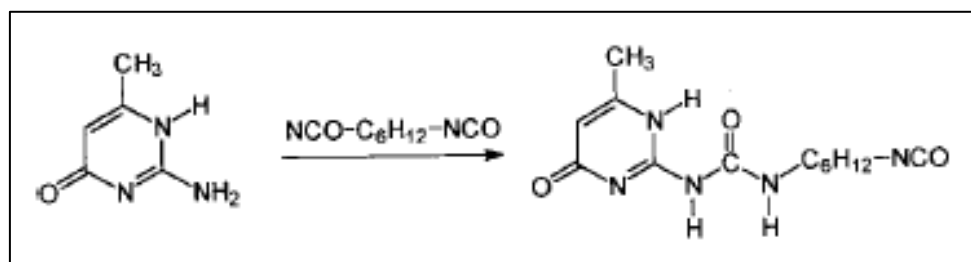


Figure 4.14 Synthesis of 2-(6-isocyanatohexylaminocarbonylamino)-6-methyl-[1H]pyrimidinone [43].

With the addition of pentane, the product precipitates, then it is filtered and washed with some more pentane. The obtained white powder is dried under reduced pressure. The excess of hexyldiisocyanate is recovered by distillation.

4.3 Materials and experimental procedures

The details of experimental investigation aimed at determining the role played by quadruple hydrogen bonds in the barrier properties of a novel coating are reported in the present paragraph. The survey was carried out on a polyurethane resin containing UPy moieties.

Based on the results obtained by Wietor et al and Diamopoulos et al. [35, 36], the synthesis of the novel binder was achieved according to the following steps:

1. synthesis of 2(6-isocyanatohexylaminocarbonylamino)-6-methyl-[1H]pyrimidinone;
2. functionalization of acrylic polyol with 2(6-isocyanatohexylaminocarbonylamino)-6-methyl-[1H]pyrimidinone;
3. extension with hexyldiisocyanate of the product.

The first step concerns the production of the self-complementary unit providing quadruple hydrogen bonds (Fig. 4.5). This unit was obtained by linking a 2-ureido-4[1H]-pyrimidinone unit to a reactive isocyanate group (Fig. 4.14).

The synthesis of 2(6-isocyanatohexylaminocarbonylamino) - 6 - methyl - [1H] pyrimidinone was carried out according to the procedure of the Eindhoven's group [43, 44]. The reagents (2-amino-4-hydroxy-6-methylpyrimidine and hexyldiisocyanate) were provided by Sigma Aldrich. In Table 4.1 the amounts of reagents for step 1 are reported. The batch size was 25 g.

Table 4.1 Amount of reagents step 1

	Molecular weight	Used amount (mol)	Used amount (g)
2-amino-4-hydroxy-6-methylpyrimidine	168.19	0.70	2.47
Hexyldiisocyanate	125.13	4.75	22.53

The solution was heated at 100°C for 16 h using oil bath to maintain a constant temperature. The batch was continuously stirred by magnetic stirring, and the reaction was carried out under nitrogen flow. After 16-18 hours pentane was added and the product settled. The liquid was removed and new pentane was added. The operation was repeated 4 times to eliminate the pentane and the excess of isocyanate in it. The product was then filtered and put under vacuum at 100°C over night. The success of the reaction was checked by NMR analysis. The spectra were recorded on a Bruker Avance 400 MHz instrument at a constant temperature of 298K. Deuterated chloroform (CDCl₃) was used as reference for both ¹H (CHCl₃ at 7.260 ppm) and ¹³C-NMR (CHCl₃ at

Chapter 4

77.00 ppm). In Figs. 4.15 and 4.16 ^1H -NMR and ^{13}C -NMR spectra are reported. Good agreement with the data available in literature [43, 44] were found.

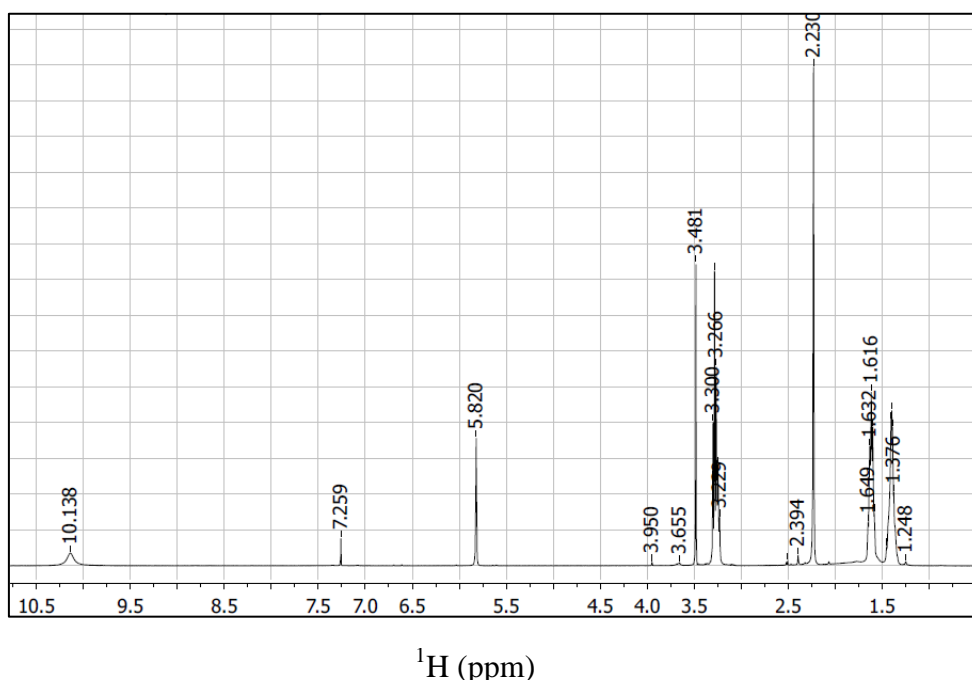
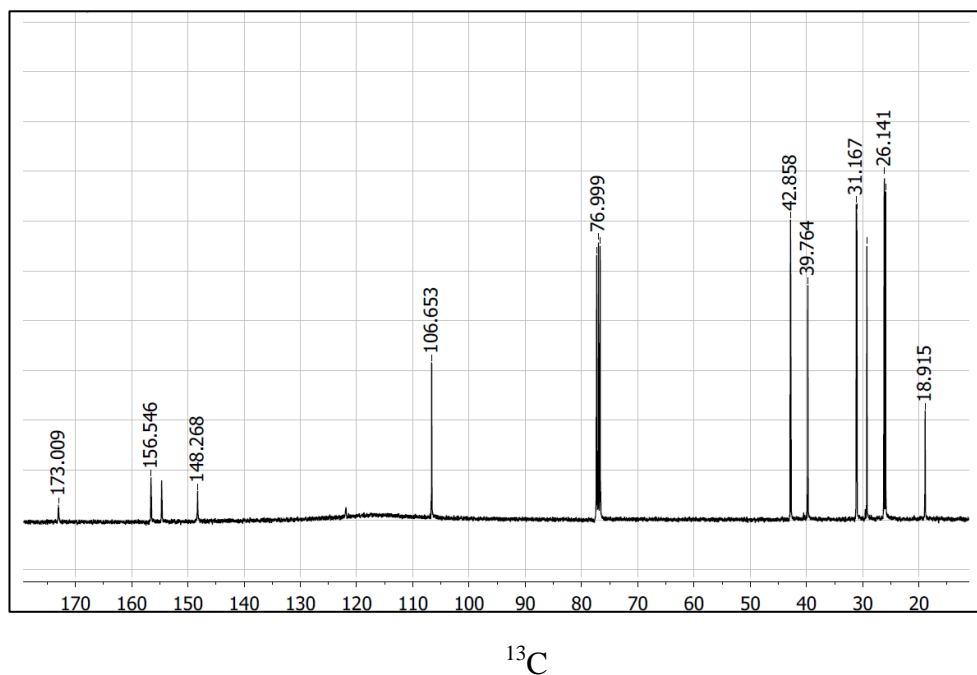


Figure 4.15 ^1H -NMR spectrum.

Figure 4.16 ^{13}C -NMR spectra.

In the second step, an acrylic polyol, commonly used in the formulation of commercial polyurethane coatings, was functionalized with the 2 (6 - isocyanatohexylaminocarbonylamino)- 6 - methyl - [1H] pyrimidinone. A defined number of OH groups pending from the backbone of the polyol reacts with NCO group of the UPy units, according to the cartoon represented in Fig. 4.17.

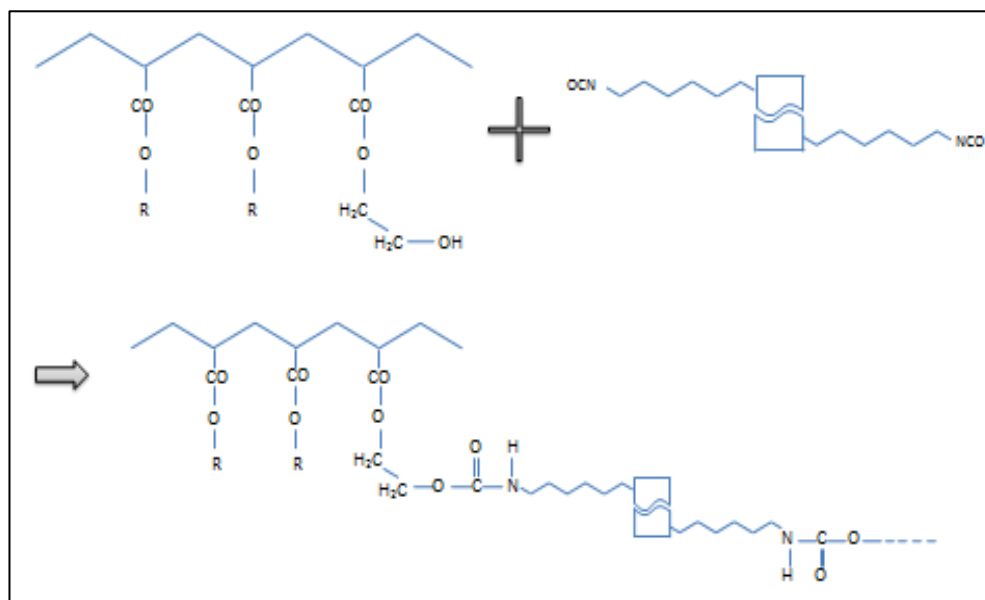


Figure 4.17 Scheme of the step 2.

In Table 4.2 the properties of the acrylic polyol Joncryl 910 (BASF) used in the second formulation step are summarized.

Table 4.3 Physical properties of Joncryl 910

Physical characteristic	
Solids, % by weight	71
Solids, % by volume (calculated)	63
Solvent	Methyl n-Amyl Ketone
Viscosity	7,000 cps
Density as Supplied	1.04 g/mL
Density of Solids	1.17 g/mL
Hydroxyl Number of solids	94
Equivalent Weight as supplied	845
Measured T _g	9 °C

The product obtained from the step 1 was added in a round flask to the acrylic polyol, anhydrous chloroform (Sigma Aldrich) was used as solvent (boiling point 61°C), dibutyltindilaurate (Sigma Aldrich) as catalyst. The batch was maintained at 60°C for 24 hours using an oil bath, under magnetic stirring, and nitrogen flow. A condenser was used to collect the evaporating solvent.

The completeness of the reaction was checked by Fourier Transform Infrared Spectroscopy (FTIR) performed with Varian 4100 instrument, Excalibur Series. The presence of NCO group peak (2270 cm^{-1}) was monitored until its disappearance was registered.

The remaining OH groups of the acrylic polyol were reacted with NCO groups supplied by hexyldiisocyanate (HDI) (Sigma Aldrich). dibutyltindilaurate (Sigma Aldrich) was used again as catalyst.

The amount of reagents were calculated on the base of equivalent weights in order to obtain different ratio between covalent bonds and multiple hydrogen bonds. In Table 4.3 the equivalent weights of the reagents used in the formulation steps are reported.

Table 4.3 Equivalent weights of reagents

Raw materials	Eq-wt
Joncryn 910	597
UPy	293
HDI	84

Both in the second step and in the third one the reactions were performed with a slight excess of NCO containing reagent (NCO/OH = 1.05), a common practice in polyurethane coatings formulation which takes into account the likelihood that NCO functional groups react with moisture [49].

In Table 4.4 the amounts of reagents used in step 2 and 3 are reported. The quantities of this samples were calculated to obtain 0% (U0), 10% (U10) 25% (U25), 35% (U35), 50% (U50) and 100% (U100) of OH groups of the acrylic polyol reacted.

Table 4.4 Amounts of reagents in steps 2 and 3

Reagent	U0	U10	U25	U35	U50	U100
Joncryl 910 (g)	36.029	12.261	10.936	11.235	20.539	11.855
UPy unit (g)	-	0.642	1.144	1.568	3.947	4.551
HDI (g)	3.960	1.164	0.874	0.786	1.129	-
Chloroform (ml)	20	100	150	150	200	250
DBTDL (drops)	2	2 (step 2) 2 (step 3)				

Just after the addition of HDI in step 3 the coating was applied on steel Q-panels by an adjustable film applicator. The average thickness of the films was $60 \pm 10 \mu\text{m}$. The samples were dried at room temperature for one week before testing.

To establish the role played by the number of hydrogen bonds in the thermal behaviour of the new resin, Differential Scanning Calorimetry (DSC) tests were performed. The measurements were carried out by using a Mettler DSC30 instrument. The two thermal cycles cover the

temperature range from -20°C to 200°C under a nitrogen flow of 100 ml min^{-1} , at a heating rate of $10^{\circ}\text{C min}^{-1}$. Before the measurements, the samples were put in a vacuum oven at 60°C for 24 hours to eliminate the presence of residual solvent. After the first heating the samples was weighted to check any weight loss due to solvent evaporation. A second scan was therefore performed.

The protective properties were investigated via Electrochemical Impedance Spectroscopy (EIS). The measurements were performed on potentiostat equipped with a Frequency Response Analyser PARSTAT2273. The swept frequency range was from 10^5 to 10^{-2} Hz, the voltage signal amplitude 20 mV. 3 electrodes set-up was used, Ag/AgCl as reference electrode, and platinum as counter-electrode. The cell area was 15.9 cm^2 . The EIS tests were carried out on the samples monitoring their behaviour during 24 hours of immersion in 0.3%wt Na_2SO_4 aqueous solution. The raw EIS data were fitted by using ZSimpWin 3.22 Software.

Some EIS measurements were also performed on to samples with an artificial defect (a hole of $50\text{ }\mu\text{m}$) produced using a dentist drill bit, before and after a thermal treatment (1 hour at 60°C) to explore any damage recovery phenomena. The defects have been observed before and after the thermal treatment by an environmental scanning electron microscope TMP ESEM FEI (back scattering images obtained in low vacuum mode) (ESEM Philips XL30).

4.4 Results and discussion

Figs. 4.18a-b display the DSC curves during the first and second heating, respectively. With respect to the base material (U0), the introduction of UPy units clearly modifies the thermal response of the material. The introduction of the UPy units modifies the DSC curves shape at the first heating above the glass transition temperature. A more and more pronounced broad peak can be easily recognized with increasing UPy content. Since these peaks are no longer present in the second heating DSC curves, they could be associated to residual crosslinking reactions. This finding is also corroborated by the increasing of glass transition temperature T_g derived from the second heating curves. Greater UPy units percentage higher T_g (Fig. 4.19).

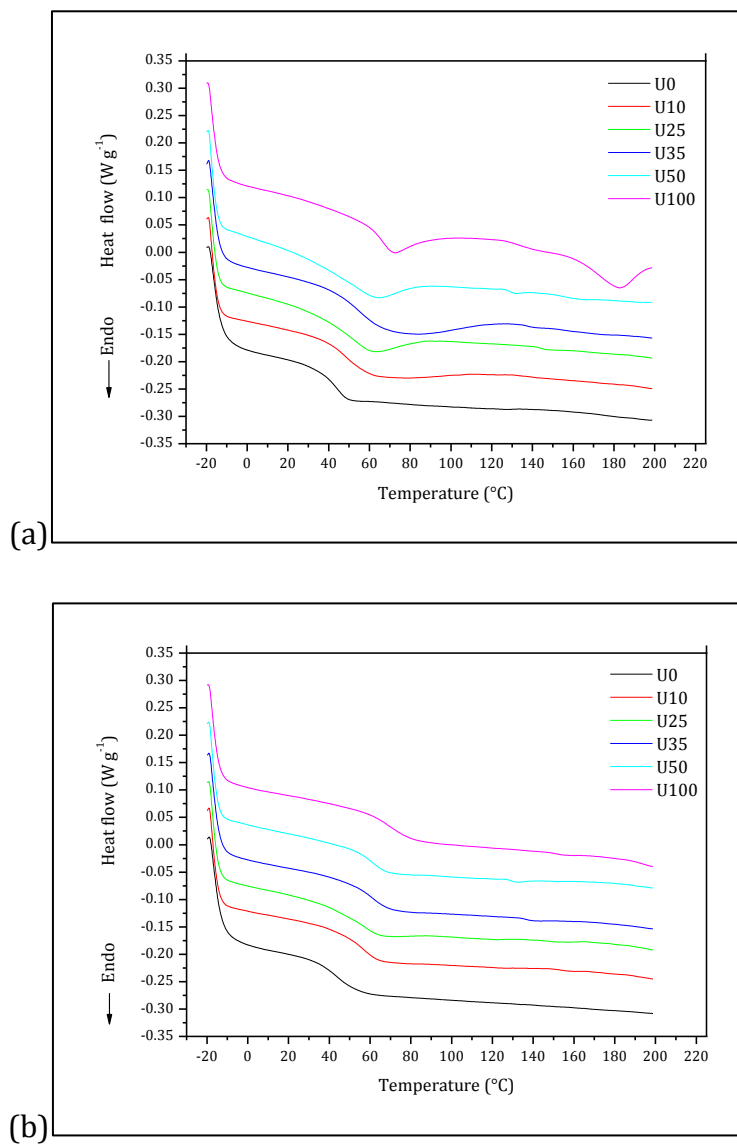


Figure 4.18 Effects of sample composition onto the DSC curve:
 (a) first heating and (b) second heating.

As revealed by Fig. 4.19, the increment in T_g does not vary linearly with the UPy units percentage. The effects appear more evident at low percentages of UPy units, while a trend toward a saturation seems to characterize the global response of the material.

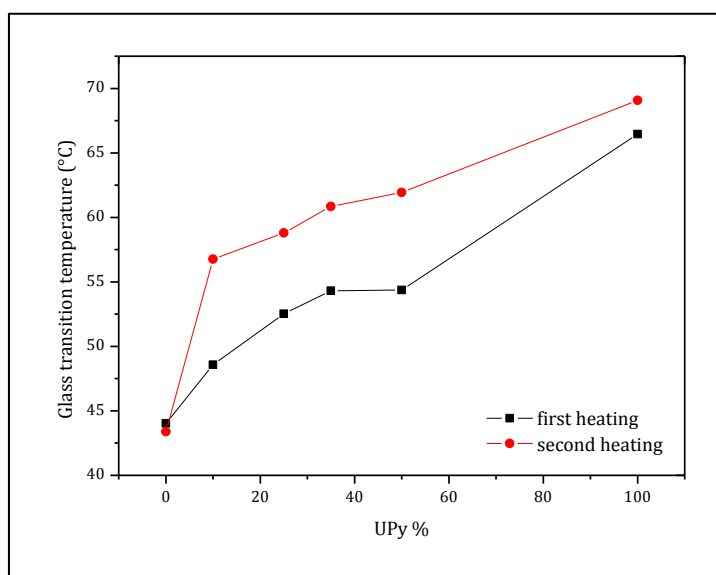


Figure 4.19 Glass transition temperature as a function of the sample formulation.

The EIS results were performed onto the samples until 25% of OH groups reacted with UPy units because for higher percentages the application of the film was found to be difficult due to the brittle behaviour of the coating. Similar findings were observed by the Eindhoven's groups [36].

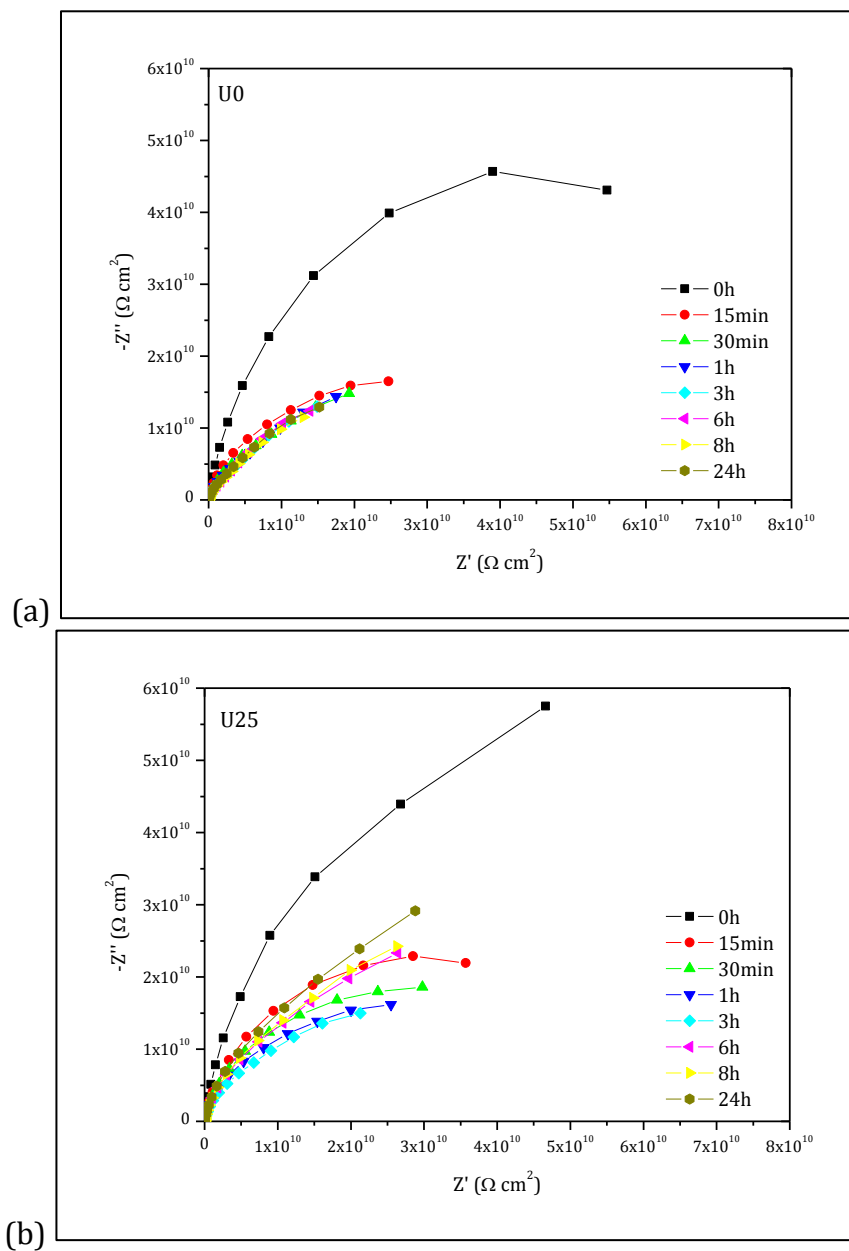


Figure 4.20 Nyquist plot of EIS data as a function of immersion time (a) for the reference sample U0 and (b) sample U25.

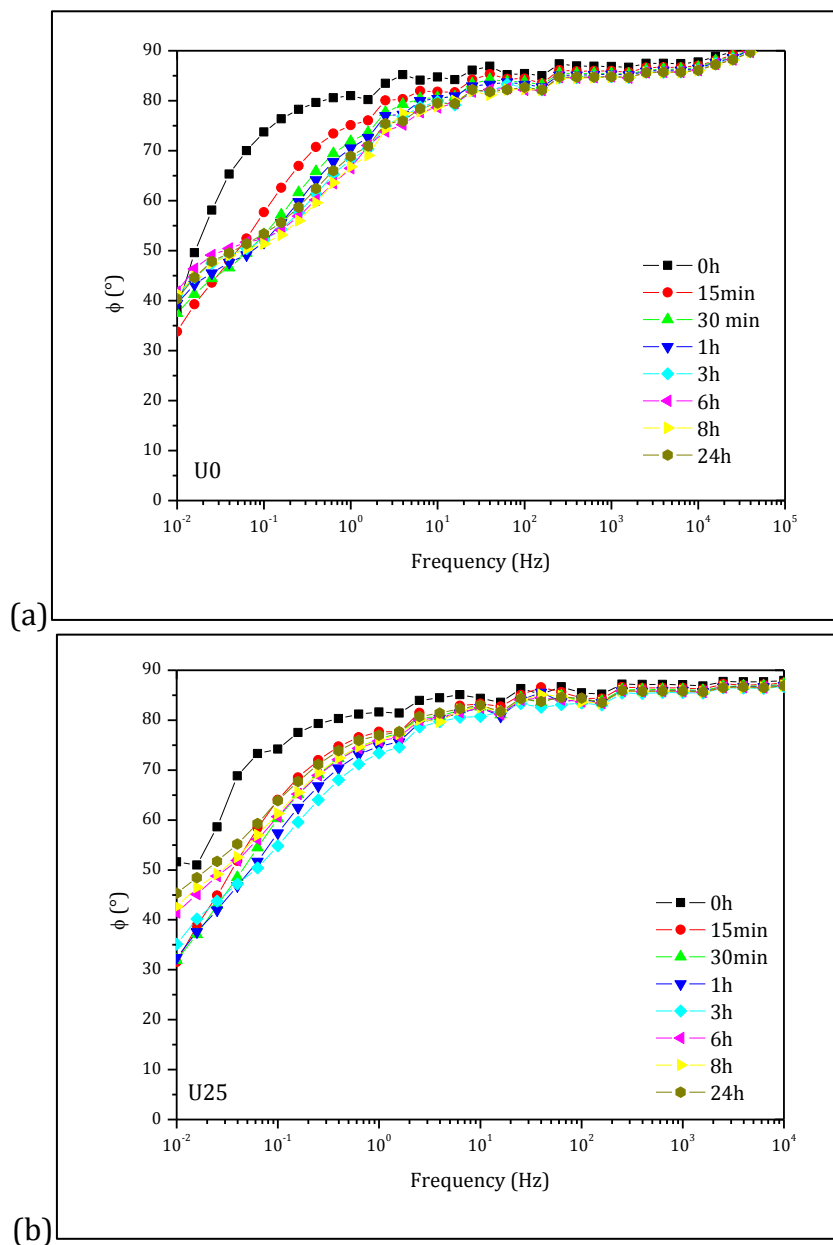


Figure 4.21 EIS phase (Bode plot) as a function of immersion time (a) for the reference sample U0 and (b) sample U25.

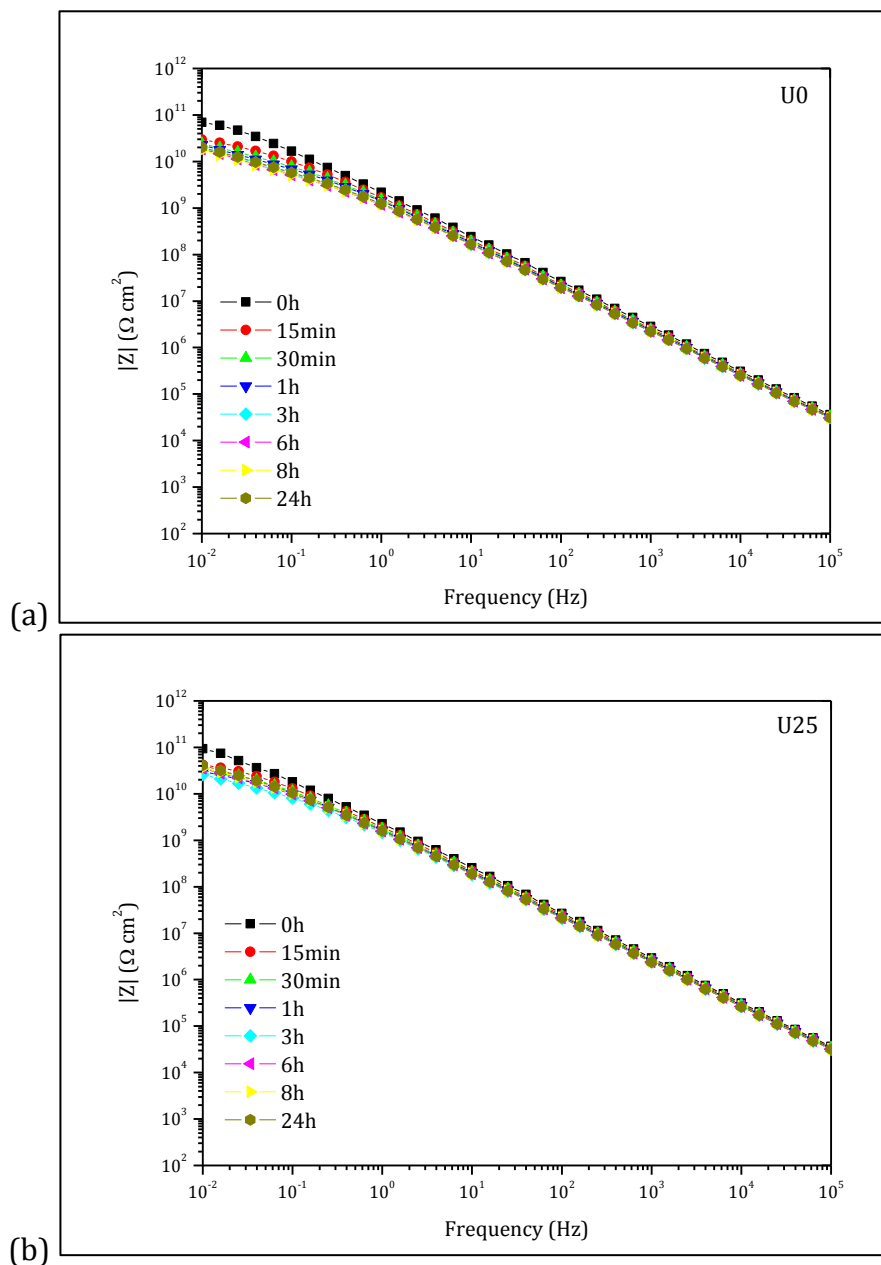


Figure 4.22 EIS modulus (Bode plot) as a function of immersion time (a) for the reference sample U0 and (b) sample U25.

The results obtained for sample U25 compared to the reference sample U0 are reported as example in Figs. 4.20-4.22. The figures display the Nyquist and Bode plots of the EIS spectra measured during 24 hours of immersion in sulphate aqueous solution. From the analysis of these data, the introduction of hydrogen bonds does not modify significantly the electrochemical response of the coating, in particular the total impedance of the systems at the beginning of immersion time is quite similar. As it can be drawn from the experimental data, small but appreciable differences between the reference and modified material can be detected especially at longer time of immersion. A significant decrease in the coating resistance (Fig. 4.20) characterizes the response during the first stages of immersion in both cases, but the amount of the drop does not seem to be dependent upon the coating chemical composition. The effects of the presence of hydrogen bonds are conversely recognizable, as the time of immersion increases. For more than 6 hours the trend of Nyquist curves reveals an increase of the coating resistance in the modified material.

From the Bode phase plots (Fig. 4.21), two time constants can be recognized in the curves in both cases. This means that a slight interaction of the electrolyte solution with the substrate occurs at the interface. For this reason the raw data have been fitted using the equivalent electric circuit represented in Fig. 4.23 [50].

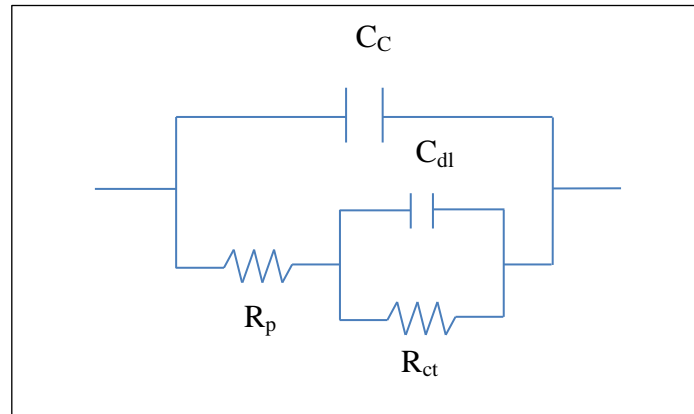


Figure 4.23 Equivalent electrical circuit used for fitting the EIS data.

One time constant is related to the coating characteristics (C_c is coating capacitance, R_p the pore resistance), the second one to the Faradaic phenomenon at the interface coating/substrate (C_{dl} the double-layer capacitance and R_{ct} the charge transfer resistance). The electrolyte resistance is not represented here.

Some considerations about the coating water uptake can be drawn from the trend of the coating capacitance derived from the data fitting. The coating capacitance C_c is given by the formula expressed in Eqn. 4.1:

$$C_c = \frac{\varepsilon_0 A}{d} \quad (4.1)$$

where ε is the dielectric constant of the coating, ε_0 is the permittivity of vacuum, A is the tested area, d is the thickness of the coating. From the increase in the coating capacitance, a numerical value

for the water uptake is computable by using Brasher and Kingsbury equation [51]:

$$X_V = \frac{\log\left(\frac{C_c}{C_0}\right)}{\log \epsilon_w} \quad (4.2)$$

where X_V is the water uptake volume fraction, C_0 is the initial coating capacitance, C_c is the coating capacitance at a generic time and ϵ_w is the dielectric constant of water (=80). In fact the water penetration inside the coating causes a detectable increase in the capacitance due to a higher dielectric constant respect to the dielectric constant of the coating (80 vs. 3-4).

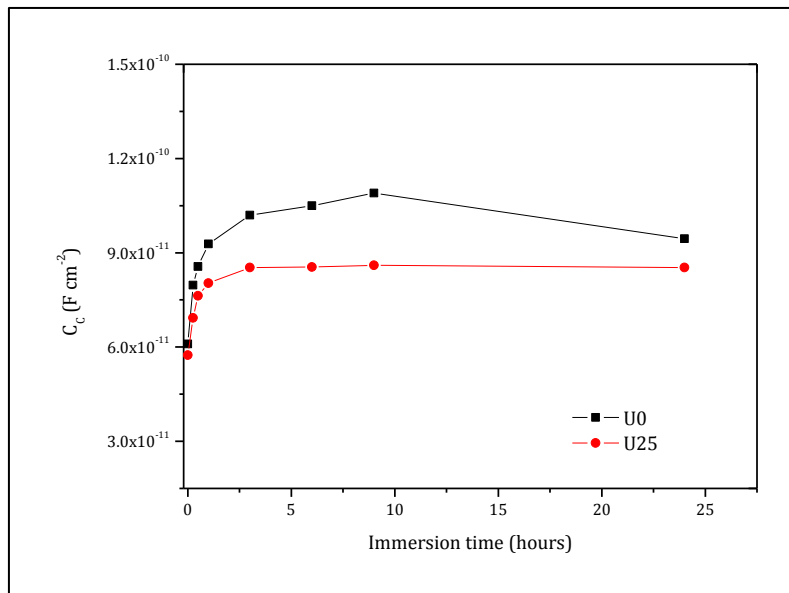


Figure 4.24 Coating capacitance trend vs. immersion time.

As shown in Fig. 4.24, in both the samples the coating capacitance increases during immersion time. The C_c values are very similar at the beginning of the test but they reach higher values for the reference sample. From Brasher and Kingsbury equation (considering as C_c the values after 6 hours of immersion) the derived water uptake values expressed as volume fraction are 12% for the reference sample and 9% for the modified material. From these results it is possible to conclude that the introduction of UPy moieties has a slight but appreciable positive effect on the barrier properties of the coating.

The results of the EIS measurements performed on the samples with an artificial defect are reported in Fig. 4.25 (sample U25).

As shown in the Nyquist and phase plots, after creating the artificial defect the second loop corresponding to the Faradaic process is clearly recognizable. The thermal treatment does not seem to produce any detectable change in EIS response.

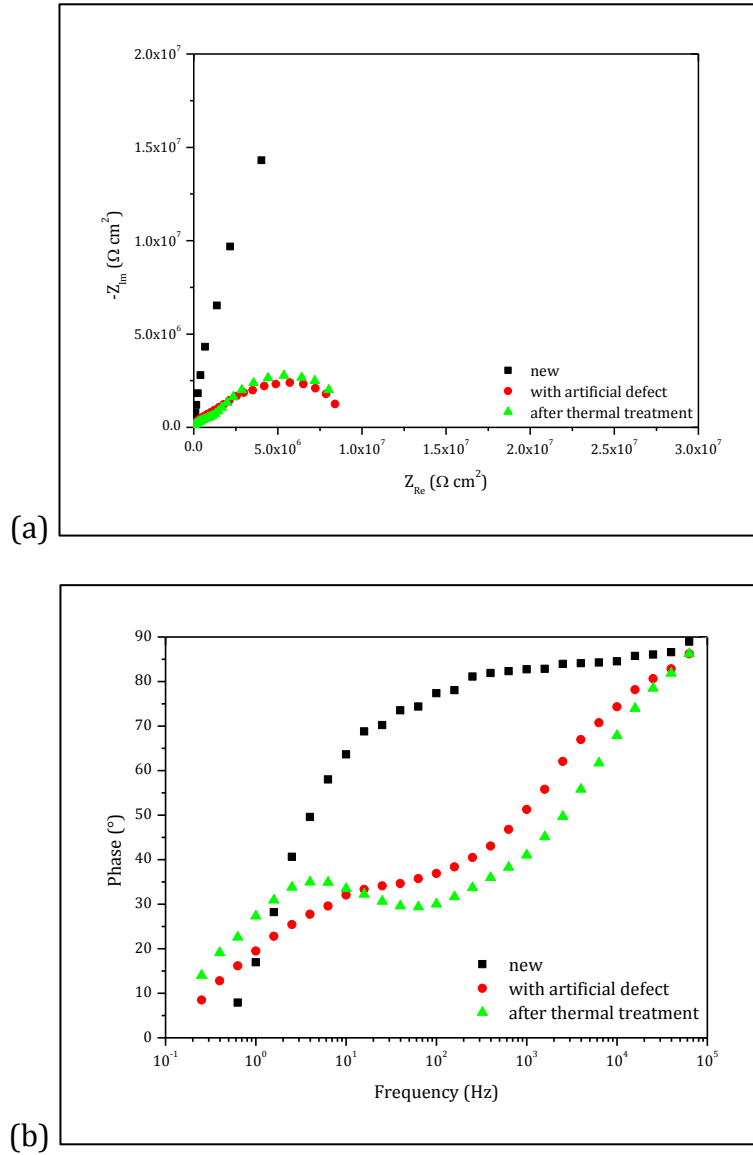


Figure 4.25 EIS data (a) Nyquist plot and (b) Bode phase plot of sample U25: new, with an artificial defect and after the thermal treatment.

The electronic micrographs displayed in Fig. 4.26 before and after the heat treatment show a partial damage recovery but not sufficient to reclose the defect, and consequently having any effect on the EIS response.

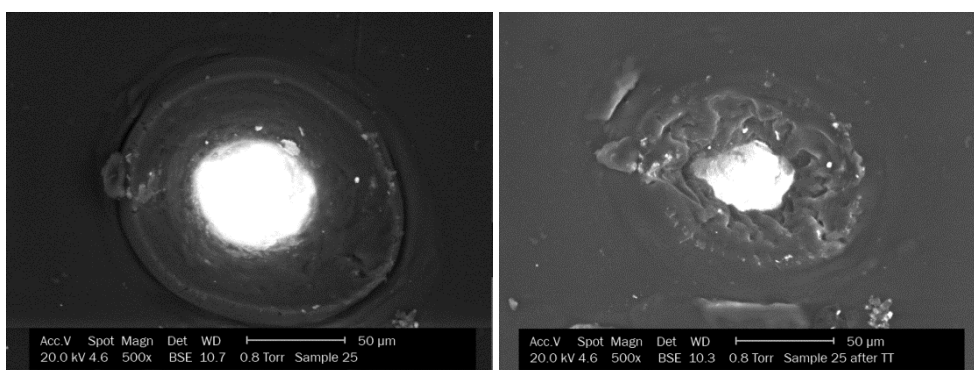


Figure 4.26 *The artificial defect before and after the thermal treatment.*

4.5 Conclusions

Damage management could be regarded an effective strategy for developing high performance organic coatings. In this framework, several innovative solutions have been proposed in the last two decades, but hydrogen bonding supramolecular chemistry surely represents one of the most promising and challenging approaches. The developed solutions are able to promote damage recovery, once a defect is created (self-healing) or to prevent defects nucleation by self relaxation phenomena (self-preemptive healing). It is now well-established that hydrogen bonding may promote preemptive healing

phenomena in polyurethane coatings. However, a lack of knowledge still remains about the role of hydrogen bonding in the water absorption characteristics, namely in the coating barrier properties. It should be remembered that protective properties against corrosion phenomena must be always ensured in any organic coating applied on metallic substrates, otherwise the application field results very limited. From the *damage management* point of view, the development of organic coatings having simultaneously self-healing and protective properties appears to be of paramount importance. All strategies aiming to repair and/or prevent any damage jeopardizing the integrity of coatings, must ensure, at the same time, an improvement or at least a maintenance of the protective properties. This topic has not deeply analysed yet, even if the developed self-preemptive healing polyurethane coatings represent a very good starting point for obtaining an effective combination of the above mentioned properties. In order to assess the effects of hydrogen bonding in the barrier properties of thermosetting polyurethane resins, a new polyurethane binder employing supramolecular cross-links was firstly produced. A characterization of the protective behaviour was then carried out via Electrochemical Impedance Spectroscopy for different ratios of covalent/hydrogen bonds.

The present survey probes that the partial replacement of covalent bonds with hydrogen bonds does not negatively affect the barrier properties of the investigated thermosetting polyurethane resin.

Barrier properties appear to be mainly defined by the covalent bonds networks in this class of materials, at least for percentages of hydrogen bonds replacement till to 25%. Although higher hydrogen bonding replacement percentages are theoretically possible, it should be kept in mind that the correspondent coatings result too stiff and brittle, thus making it impossible to use them in real applications. The present work demonstrates that the potential of multiple-hydrogen bonds can be effectively exploited in coatings applications owing to the combination of improved damage response behaviour and protection from corrosion phenomena. Even if the presented experimental survey is a preliminary analysis in this field, it opens the way for further investigations on the challenging subject of the coatings durability.

4.6 References

- [1] S. v. d. Zwaag, "An Introduction to Material Design Principles: Damage Prevention versus Damage Management," in *Self Healing Materials. An Alternative Approach to 20 Centuries of Materials Science*, S. v. d. Zwaag, Ed., ed Dordrecht, The Netherlands: Springer, 2007, pp. 1-18.
- [2] S. v. d. Zwaag, *Self healing materials: an alternative approach to 20 centuries of materials science*. Dordrecht, The Netherlands: Springer, 2007.
- [3] R. A. T. M. v. Benthem, *et al.*, "Self Healing Polymer Coatings," in *Self Healing Materials. An Alternative Approach to 20 Centuries of Materials Science*, S. v. d. Zwaag, Ed., ed Dordrecht, The Netherlands: Springer, 2007, pp. 139-159.

- [4] W. Feng, *et al.*, "Smart polymeric coatings—recent advances," *Advances in Polymer Technology*, vol. 26, pp. 1-13, 2007.
- [5] S. K. Ghosh, *Self-healing materials: fundamentals, design strategies, and applications*. Weinheim; Chichester: Wiley-VCH; John Wiley, 2009.
- [6] D. Andreeva and D. Shchukin, "Smart self-repairing protective coatings," *Materials Today*, vol. 11, pp. 24-30, 2008.
- [7] D.G. Shchukin and M. Helmuth, "Self-Repairing Coatings Containing Active Nanoreservoirs," *Small*, vol. 3, pp. 926-943, 2007.
- [8] M. Samadzadeh, *et al.*, "A review on self-healing coatings based on micro/nanocapsules," *Progress in Organic Coatings*, vol. 68, pp. 159-164, 2010.
- [9] H. M. Andersson, *et al.*, "Self Healing Polymers and Composites," in *Self Healing Materials. An Alternative Approach to 20 Centuries of Materials Science*, S. v. d. Zwaag, Ed., ed Dordrecht, The Netherlands: Springer, 2007, pp. 19-44.
- [10] R.P. Sijbesma, *et al.*, "Reversible Polymers Formed from Self-Complementary Monomers Using Quadruple Hydrogen Bonding," *Science*, vol. 278, pp. 1601-1604, 1997.
- [11] S. R. White, *et al.*, "Autonomic healing of polymer composites," *Nature* vol. 409, pp. 794-797 2001.
- [12] B. Blaiszik, *et al.*, "Nanocapsules for self-healing materials," *Composites Science and Technology*, vol. 68, pp. 978-986, 2008.
- [13] M. Kessler, *et al.*, "Self-healing structural composite materials," *Composites Part A: Applied Science and Manufacturing*, vol. 34, pp. 743-753, 2003.
- [14] M. W. Keller, *et al.*, "A Self-Healing Poly(Dimethyl Siloxane) Elastomer," *Advanced Functional Materials*, vol. 17, pp. 2399-2404, 2007.

- [15] L. Yuan, *et al.*, "Synthesis and characterization of microencapsulated dicyclopentadiene with melamine-formaldehyde resins," *Colloid and Polymer Science*, vol. 285, pp. 781-791, 2007.
- [16] J. Yang, *et al.*, "Microencapsulation of Isocyanates for Self-Healing Polymers," *Macromolecules*, vol. 41, pp. 9650-9655, 2008.
- [17] S. Park, "Preparation and Characterization of Microcapsules Containing Lemon Oil," *Journal of Colloid and Interface Science*, vol. 241, pp. 502-508, 2001.
- [18] B. J. Blaiszik, *et al.*, "Microcapsules filled with reactive solutions for self-healing materials," *Polymer*, vol. 50, pp. 990-997, 2009.
- [19] B. E. Koene, *et al.*, "Self healing coatings for corrosion control," in *First International Conference on Self Healing Materials*, Noordwijk aan Zee, The Netherlands, 2007.
- [20] A. Kumar, *et al.*, "Self-healing coatings for steel," *Progress in Organic Coatings*, vol. 55, pp. 244-253, 2006.
- [21] S. H. Cho, *et al.*, "Self-Healing Polymer Coatings," *Advanced Materials*, vol. 21, pp. 645-649, 2009.
- [22] C. Suryanarayana, *et al.*, "Preparation and characterization of microcapsules containing linseed oil and its use in self-healing coatings," *Progress in Organic Coatings*, vol. 63, pp. 72-78, 2008.
- [23] M. Zheludkevich, *et al.*, "On the application of electrochemical impedance spectroscopy to study the self-healing properties of protective coatings," *Electrochemistry Communications*, vol. 9, pp. 2622-2628, 2007.
- [24] K. S. Toohey, *et al.*, "Characterization of Microvascular-Based Self-healing Coatings," *Experimental Mechanics*, vol. 49, pp. 707-717, 2008.
- [25] S. D. Bergman and F. Wudl, "Re-Mendable Polymers," in *Self Healing Materials. An Alternative Approach to 20 Centuries of Materials Science*, S. v. d. Zwaag, Ed., ed Dordrecht, The Netherlands: Springer, 2007, pp. 45-68.

- [26] J.-M. Lehn, *Supramolecular chemistry: concepts and perspectives*. Weinheim: VCH, 1995.
- [27] A. W. Bosman, *et al.*, "Supramolecular polymers: from scientific curiosity to technological reality," *Macromolecular Symposia*, vol. 201, pp. 143-154, 2003.
- [28] L. Brunsveld, *et al.*, "Supramolecular Polymers," *Chemical Reviews*, vol. 101, pp. 4071-4097, 2001.
- [29] J.-M. Lehn, "Review Supramolecular polymer chemistry-scope and perspectives," *Polymer International*, vol. 51, pp. 825-839, 2002.
- [30] A.W. Bosman, *et al.*, "Supramolecular polymers at work," *MaterialsToday*, pp. 34-39, April 2004.
- [31] H. Hofmeier and U. S. Schubert, "Combination of orthogonal supramolecular interactions in polymeric architectures," *Chemical Communications*, pp. 2423-2432, 2005.
- [32] L.J. Prins, *et al.*, "Noncovalent Synthesis Using Hydrogen Bonding," *Angewandte Chemie International Edition*, vol. 40, pp. 2382-2426, 2001.
- [33] A. W. Bosman and R. P. Sijbesma, "Supramolecular Polymers in Action," in *Supramolecular Polymers*, A. Ciferri, Ed., ed Boca Raton, London, New York, Singapore: CRC Press Taylor & Francis Group, 2005.
- [34] J. Zeno W. Wicks, *et al.*, *Organic coatings: science and technology*, 2nd ed. New York, Chichester, Weinheim, Brisbane, Singapore, Toronto: Wiley-Interscience, 1999.
- [35] A. Dimopoulos, *et al.*, "Enhanced Mechanical Relaxation below the Glass Transition Temperature in Partially Supramolecular Networks," *Macromolecules*, vol. 43, pp. 8664-8669, 2010.
- [36] J.-L. Wietor, *et al.*, "Preemptive Healing through Supramolecular Cross-Links," *Macromolecules*, vol. 42, pp. 6640-6646, 2009.

- [37] S. Chen, *et al.*, "Fourier transform infrared study of supramolecular polyurethane networks containing pyridine moieties for shape memory materials," *Polymer International*, vol. 59, pp. 529-538, 2010.
- [38] H. Sun, *et al.*, "Multiple Hydrogen-Bonded Complexes Based on 2-Ureido-4[1H]-pyrimidinone: A Theoretical Study," *Journal of Physical Chemistry B*, vol. 115, pp. 11053-11062, 2011.
- [39] A. W. Bosman, "Self healing in action," in *First International Conference on Self Healing Materials*, Noordwijk aan Zee, The Netherlands, 2007.
- [40] D. Farnik, *et al.*, "Synthesis and Self assembly of Hydrogen-Bonded Supramolecular Polymers," *Macromolecular Symposia*, vol. 217, pp. 247-266, 2004.
- [41] K. Yamauchi, *et al.*, "Synthesis and Characterization of Novel Complementary Multiple-Hydrogen Bonded (CMHB) Macromolecules via a Michael Addition," *Macromolecules* vol. 35, pp. 8745-8750, 2002.
- [42] F. H. Beijer, *et al.*, "Strong Dimerization of Ureidopyrimidones via Quadruple Hydrogen Bonding," *Journal of the American Chemical Society*, vol. 120, pp. 6761-6769, 1998.
- [43] B. J. B. Folmer, *et al.*, "Supramolecular Polymer Materials Chain Extension of Telechelic Polymers Using a Reactive Hydrogen-Bonding Synthron," *Advanced Materials*, vol. 12, pp. 874-878, 2000.
- [44] H. M. Keizer, *et al.*, "Scale-up of the synthesis of ureidopyrimidinone functionalized telechelic poly(ethylenebutylene)," *Polymer*, vol. 44, pp. 5505-5511, 2003.
- [45] J. H. K. K. Hirschberg, *et al.*, "Supramolecular Polymers from Linear Telechelic Siloxanes with Quadruple-Hydrogen-Bonded Units," *Macromolecules*, vol. 32, pp. 2696-2705, 1999.

- [46] J. L. Wietor and R. P. Sijbesma, "A Self-Healing Elastomer," *Angewandte Chemie International Edition*, vol. 47, pp. 8161-8163, 2008.
- [47] S. H. M. Söntjens, *et al.*, "Thermoplastic Elastomers Based on Strong and Well-Defined Hydrogen-Bonding Interactions," *Macromolecules*, vol. 41, pp. 5703-5708, 2008.
- [48] D. J. M. v. Beek, *et al.*, "Supramolecular Copolyesters with Tunable Properties," *Macromolecules*, vol. 40, pp. 6340-6348, 2007.
- [49] B. Müller and U. Poth, *Coatings formulation: an international textbook* Hannover, Germany: Vincentz, 2006.
- [50] A. Amirudin and D. Thierry, "Application of electrochemical impedance spectroscopy to the degradation of polymer-coated metals," *Progress in Organic Coatings*, vol. 26, pp. 1-28, 1995.
- [51] D. M. Brasher and A. H. Kingsbury, "Electrical measurements in the study of immersed paint coatings on metal. I. Comparison between capacitance and gravimetric methods of estimating water-uptake," *Journal of Applied Chemistry*, vol. 4, pp. 62-72, 1954.

CHAPTER 5

Concluding remarks and future work

Owing to the capabilities of satisfying the wide-ranging demands, organic coatings are nowadays used in a large number of areas such as automotive, appliances, furniture, architecture, and the like. Although the remarkable success of the paint systems may suggest that organic coatings are able to meet any kind of requirements, the advent of new driving factors, such as market expectations, cost effectiveness, and environment concerning issues is providing hard challenges even for this class of materials. This is especially true from the durability point of view. As known, durability involves many different factors simultaneously, and it is claimed to ensure the integrity of a mix of properties, involving both the aesthetic and protective perspectives. In this varying scenario, the development of high performance coatings and, more in general, novel design strategies for enhancing the durability of existing products are needed. The abovementioned aims represent the final goals of this doctoral dissertation. Automotive and architecture can be surely considered two of the most important and challenging application fields where organic coatings are claimed to overcome hurdles and satisfy increasing expectations. The development of novel design strategies for optimizing the durability was

consequently focused in these two fields and represents the subject of the first part of the investigation. In order to validate the proposed strategies, the research was carried out in collaboration with industrial partners operating in these areas, thus making it possible to produce and test real organic coatings.

Architectural organic coatings durability is handled in Chapter 2. Degradation phenomena concern both the aesthetic properties and corrosion protection in metallic structures, and are mainly related to the weathering stresses. The investigation, carried out in collaboration with Akzo Nobel Coatings, concerned polyester powder coatings with different pigments applied onto pre-treated (chromate conversion) and untreated aluminium alloy substrates. Two different binders were especially considered: polyesters based on terephthalic-isophthalic acid and polyesters based solely on isophthalic acid. The experimental campaign was carried out for determining the decrease in aesthetic attributes during artificial weathering tests, and the reduction in the protective properties via electrochemical techniques and standard artificial accelerated corrosion tests. The results confirmed that the chromate conversion surface pre-treatment allows to obtain a very high durability level which is barely influenced by the formulation of the coating. However, it was also probed that chromate conversion makes hard to highlight the contributions of the organic coating in the protective capabilities of the coating-substrate system. Experimental findings obtained for the untreated samples revealed that the

formulation parameters related to the aesthetic properties (pigments) noticeably affect the barrier properties of the coating, and thus the corrosion protection. The negative/positive contributions in the protective properties depend on the coating constituents: pigments, binder, additives and all the formulation parameters related to a particular pigment system. This investigation suggests that proper binder/pigments/additives combinations have to be designed for obtaining high performance durability organic coatings. These results take a different meaning in the current scenario. Environmental restrictions do not allow the recourse to chromate conversion for surface pre-treating. Unfortunately, chromate conversion alternative surface treatments do not still provide the same effectiveness in terms of durability. From this point of view, organic coatings having enhanced durability must be developed for attaining the durability levels correspondent of coating-chromate converted metallic substrates. It is apparent that the development of novel formulation inspired by this strategy could represent the main topic of future works.

The issues inherent the organic coatings durability in automotive industry are addressed in Chapter 3. Multilayer coating systems are typically used to ensure the protection from corrosion and provide the final appearance. It is needless to highlight that the aesthetic perception is of paramount importance in automotive market. In multilayer coating systems the mar resistance of clear-coats plays a key role in the appearance durability. Strategies for improving this property usually

foresee the introduction of inorganic fillers as nano-silica particles, although it is believed that further enhancement may be attained if a proper combination of cross-linked binder-inorganic fillers is selected. Chapter 3 provides new insights in this direction. In collaboration with PPG Industries, the mar behaviour of a 2-component polyurethane coating and a nano-silica filled polyurethane coating was firstly investigated via single-probe scratching and field simulation tests. Nano scratch test, Taber test and falling abrasive test confirmed that embedding nano-silica particles into the coating causes an increase in the surface hardness. However, it also produces a reduction in the characteristic critical load, namely in the fracture resistance. Coating embrittlement can be also promoted if crosslinking is not properly designed. The experimental evidences display that higher plastic resistance and higher critical loads can be gained if a secondary crosslinking aimed at creating a secondary structure is introduced into the clear-coats. In addition, the secondary crosslinking does not significantly alter the recovery properties of the protective layer with respect to the nano-silica filled clear-coats. In this novel class of clear-coats, UV effects are also less invasive with respect to the other classes of existing products. The overall benefits make this strategy surely very promising and represent an excellent starting point for obtaining future improvements in the recovery properties and UV resistance.

Considering the last main topic of this doctoral dissertation exploring the corrosion protection capabilities of preemptive healing

polyurethane coatings, important concluding remarks can be drawn. The partial replacement of covalent bonds with hydrogen bonds does not negatively affect the barrier properties of the investigated thermosetting polyurethane resin. Barrier properties appear to be mainly defined by the covalent bonds networks. The present work demonstrates that the potential of multiple-hydrogen bonds can be effectively exploited in coatings applications owing to the combination of improved damage response behaviour and protection from corrosion phenomena. Even if the presented experimental survey has to be considered a preliminary analysis in this field, it opens the way for further investigations on the challenging subject of the coatings based on supramolecular chemistry in order to obtain enhanced performances and higher durability.